THE UNIVERSITY *of* EDINBURGH

Biophysical modelling of bacterial colonisation of urinary catheters

Freya Bull

Doctor of Philosophy
The University of Edinburgh
May 2023

Abstract

I developed the first mathematical model for the infection dynamics of a urinary catheter. Urinary catheters are thin tubes which are inserted into the urethra to drain the bladder. They are commonly used for patients undergoing surgery under anaesthesia, or for elderly patients in long term care facilities. Unfortunately, urinary catheters develop bacterial infections at rates up to 5% per catheter day, with potential complications including catheter blockage, bladder damage, and kidney infections. Attempts to prevent or mitigate infections have been largely ineffective, and through mathematical modelling I seek to understand why.

The primary aim of my PhD was to uncover routes by which techniques and approaches from physics can contribute to tackling catheter-associated urinary tract infections (CAUTI). I have provided new clinical insight by developing a novel population dynamics model and applying it to reveal the key factors determining how, why, and when catheters get infected.

CAUTI are complex phenomena, involving the host physiology in the urethra and bladder, multiple catheter surfaces, urine flow dynamics within the catheter lumen (the inner channel), and bacterial growth and behaviour. Guided by discussions with clinical collaborators, I considered this system (of catheter, host, and colonising bacteria) as a set of smaller subsystems. I divided the model into 4 subsystems, in which bacteria first grow and colonise the extraluminal surface (the outside of the catheter), before spreading into the bladder. The bacteria grow in the urine in the bladder, and then are swept down through the catheter lumen, where finally some adhere on the intraluminal surface. I then identified suitable mathematical descriptions for the change in the bacterial populations. These descriptions take the form of Fisher, logistic growth, and convection-diffusion equations, which, using insight from clinicians, I coupled together.

I implemented this model computationally by developing code (in C++ and

Python) to numerically solve the coupled equations, applying this to explore the effects of varying the properties of the catheter, host, and bacteria. I found the rate of urine production by the kidneys to be critical in determining the outcome of bacterial infection, as it governs a transition between a high bacterial density state in the bladder and a 'washed-out' state whereby bacteria may grow on the catheter surfaces, but there is no bacteriuria (no bacterial growth in the urine). These results are highly significant for the prevention and mitigation of CAUTI, as they imply that increasing fluid intake may reduce the likelihood of bacteriuria. I also discovered that the urethral length determines the timescale over which infection may occur, giving important insight into observed gendered differences in infection rates in short-term catheterisation. Finally, my model suggests an avenue for future work to investigate the origin of infections, by studying bacterial distributions across the catheter surface, and comparing with modelled distributions to determine the initial conditions.

I interpreted the model predictions in the context of clinical data, finding new perspectives on both *in vitro* and *in vivo* previous studies. By considering how clinical interventions correspond to changes in model parameters, I classified clinical interventions as postponement, mitigation, or prevention, and discussed the contexts in which those interventions might be effective. I applied the model to predict the outcome of a clinical trial of catheter interventions, showing that the model provides quantitatively better fits to clinical data than previous fits applied in the literature, and successfully qualitatively predicted trial outcomes, including identifying an outcome (reduced incidence of bacteriuria associated with the use of silver-alloy catheters in males) that was present in the study dataset, but not discussed in the original study.

My work suggests physical mechanisms that explain clinical observations, demonstrating how from basic assumptions many complex phenomena emerge. Through the development of a population dynamics model with direct clinical implications, I applied physics to make an important contribution to CAUTI research.

Lay summary

Urinary catheters – thin tubes which are used to drain the bladder – are unfortunately prone to developing infections due to bacterial colonisation. I developed the first mathematical model for bacterial colonisation of a catheter and applied it to reveal the key factors determining how, why, and when catheters get infected. My model is a mathematical implementation of a clinical 'narrative', describing how bacteria grow and colonise the external (extraluminal) surface of the catheter, ascend into the bladder and grow there, then are swept down the inside of the catheter (the lumen) by the urine flow, with some bacteria then adhering to the internal (intraluminal) surface of the catheter.

I implemented my model computationally, numerically solving the model equations, and explored the effects of varying the properties of the catheter, patient, and bacteria. I found that the rate of urine production by the kidneys (directly related to the fluid intake of a patient) determines the outcome of an infection, as when the urine rate is high, bacteria are diluted out of the bladder faster than they can grow (wash-out). Additionally, I found that urethral length determines the timescale over which infection may occur, as bacteria must first ascend the catheter (up the length of the urethra) before they can grow in the bladder.

I then applied my model to reinterpret the results and data of previous work, from both controlled laboratory experiments (*in vitro*) and clinical studies (*in vivo*). My model was able to predict the outcome of a large clinical study of different types of catheters, correctly identifying that antimicrobial catheters are more effective in reducing bacteriuria (the presence of bacteria in the urine) in males undergoing short-term ($\lesssim$ 14 days) catheterisation than in females. My model predicted that this was due to the differing urethral lengths (males have much longer urethral lengths than females), and this prediction led to quantitatively much better fits to the data for incidence of bacteriuria than previous models (which did not consider urethral length).

Declaration

I declare that this thesis was composed by myself, that the work contained herein is my own except where explicitly stated otherwise in the text, and that this work has not been submitted for any other degree or professional qualification except as specified.

Parts of this work are available as a preprint in [12].

(*Freya Bull, May 2023*)

Acknowledgements

We often say it takes a village to raise a child – this thesis took a village of its own, and I am very grateful to all who contributed.

My thanks first to Rosalind Allen, without whom this thesis would not have been possible – your guidance and support has been invaluable. My further thanks to Chris Brackley and Sharareh Tavaddod, who joined in my supervision wholeheartedly, and perhaps ended up learning far more about the mathematics of urinary catheters than they had ever wanted. Although not my supervisors, Richard Blythe, Paul Clegg, Ines Foidl, and Cait MacPhee all provided me with support, guidance, and mentoring, for which I am very grateful.

For helpful discussions and contributions, I thank all my colleagues, collaborators, and co-authors: Balagardash Bashirov, Nick Bommer, Craig Breheny, Aidan Brown, Rory Claydon, Susana Direito, Voula Granitsiotis, Gail McConnell, Meghan Perry, Liam Rooney, Patrick Sinclair, Bartlomiej Waclaw, and Ellen Young.

The clinical data analysed in Chapter 8 is a subset of the CATHETER trial (Pickard et al., 2012; [91]). I am very grateful to Graeme MacLennan for facilitating my access to the trial data, and to all the authors of the study.

I cannot thank everybody individually for their support and helpful comments without fear I will miss someone, so I must now thank many groups: the members of the group of Rosalind Allen, past and present; the statistical physics theory group here in Edinburgh; the students and staff of the CM-CDT; my officemates, past and present; the students and speakers of the Boulder summer school (2022); and all of the regular lunch group of JCMB.

Outside of the academic environment, I am very grateful to all my friends, flatmates, and family. My thanks to Matilda and Zachary, whose faith in me has never wavered; Rachel, who still remembers what I do; Karina, who would love me even more if I were a worm; Jackie, who has been there for the beginning, the end, and everything in between; and Chris, who hasn't dropped me yet. And above all, thanks to Clement, who held onto my sanity when I had long since lost my grasp; and Andrew, whose patience with this thesis is matched only by his kindness and care.

Contents

List of Figures

List of Tables

Glossary

backflow the reversal of the normal (outwards) direction of urine flow in a catheter. 13

bacteriuria the presence of bacteria in the urine. 1, 6, 9, 77, 80, 93, 109

biofilm bacteria adhered to a surface and to each other, producing a structural matrix formed of extracellular polymers. 7, 9, 51, 82

CAUTI catheter-associated urinary tract infection. 1

CFU colony forming units. 12, 82

chemostat a device in which bacteria grow under conditions of continuous dilution. 41

crawling the active motion of bacteria on a surface. 30

epifluorescence microscopy a form of optical microscopy, whereby light at a specific wavelength from the microscope excites fluorophores in the sample, which then emit light at a different wavelength. 27

epithelial cells the cells of a mucous membrane. 8, 12

extraluminal outside of a tube. 12, 20, 27

fibrinogen a protein that is released by the body as an immune response to a urinary catheter. 11, 15, 27

flagella tail-like appendages, used for bacterial motion. 7

hydrogel a material that holds water within its (hydrophilic) structure. 14, 104

incidence rate rate of new infections per population-time. 1, 6, 9

intracellular bacterial communities bacterial colonies within the epithelial cells that line the bladder. 8, 12

intraluminal inside the internal passage of a tube. 11, 12, 21, 51

lumen the internal passage of a tube. 4, 51

micturition urination. 15, 40, 44, 77

pathogen a microorganism that causes disease. 7

pili tiny hair-like filaments on the bacterial surface. 7

polymicrobial involving more than one microbial species. 7

poor growth media media lacking some or all amino acids requisite for bacterial growth, such that bacterial cells must synthesize these nutrients for growth. 25

randomised control trial a prospective clinical study that evaluate the effectiveness of an intervention by randomly assigning patients to treatment or control groups. 109

Reynolds number the ratio of inertial forces to viscous forces. 4, 54

rich growth medium a medium where the exact chemical composition is unknown, containing everything required for many different bacterial species to grow. 12

swarming flagella-powered motility of multicellular 'rafts' of bacteria. 30, 107

swimming the active motion of bacteria in a liquid media. 30

urethra the passage connecting the bladder to the skin. 2

urinary catheter a thin tube used to drain the bladder. 1

uropathogenic causing disease in the urinary tract. 7

virulence factor a bacterial trait that specifically contributes to the bacterial strain's ability to cause disease. 7

washout in continuous culture, a non-zero bacterial population can be sustained only for dilution rates lower than the bacterial growth rate. 42, 77

Chapter 1

Introduction

Urinary catheters – thin tubes which are used to drain the bladder – are commonly used for patients with a wide range of urological[1] issues, in intensive care units and long-term care facilities [68, 95]. Bacterial colonisation of the catheter, leading to bacteriuria (bacteria in the urine) is almost universal in long-term catheterised patients. While asymptomatic[2] bacteriuria does not require treatment, bacterial colonisation can also lead to symptomatic catheter-associated urinary tract infections (CAUTI) with incidence rates[3] estimated at up to 0.3 – 0.7% per catheter day [18, 82], with potential complications including catheter blockage, bladder damage, and kidney infections. CAUTI account for up to 40% of hospital acquired infections [48, 68, 74, 82, 105, 115, 128], with vast financial and societal costs [31]. Despite the importance of this topic, there is limited understanding of the role of different factors in CAUTI development [44, 48, 71, 78, 82, 99], why some patients are plagued by recurrent CAUTI while others are hardly troubled [42], and why some infections develop far more rapidly than others [67]. Better understanding could lead to more effective strategies to prevent or mitigate CAUTI [25]. Bacterial colonisation of the catheter is clearly a crucial step in CAUTI development, yet to date there have been no predictive mathematical models for bacterial colonisation of a urinary catheter.

[1] *urology* – the study of urine [88]

[2] *asymptomatic* – occurring without symptoms [88]

[3] *incidence rate* – "the rate of new cases or events over a specified period for the population at risk for the event" [113]. In urinary catheter studies this is typically calculated by dividing the total recorded number of new infections in the study population by the total number of catheter days in the study (the sum over all patients of the number of days a catheter was in place).

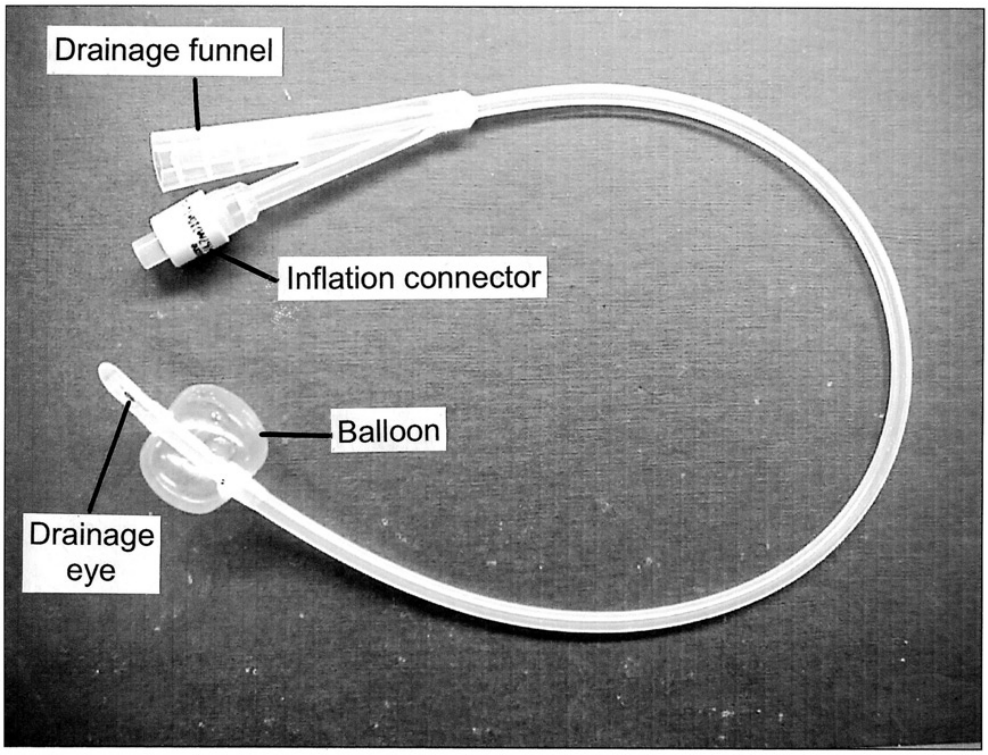

Figure 1.1 *A Foley catheter. The balloon is inflated with sterile water after insertion, holding the catheter in place. Image reproduced from Feneley et al. (2015; [31]).*

Mathematical models provide a context, and framework, through which we can better understand observations and measurements [108]. A mathematical model for bacterial colonisation of urinary catheters could provide new insights into the key factors determining how, why, and when catheters get infected. Additionally, the modelling process could highlight where gaps in the current understanding exist, providing guidance for future investigation. In this respect, physics might be viewed as a lens through which we can search for new insight into a clinical phenomenon.

1.1 Urinary catheters

A urinary catheter is a tube that is used to drain urine from the bladder into a drainage bag. Catheterisation can be intermittent (i.e., the catheter is removed immediately after drainage), but this work focuses on longer-term catheterisation, where the catheter is indwelling (i.e., the catheter remains in the bladder). An indwelling catheter is inserted into the bladder through the urethra (the passage

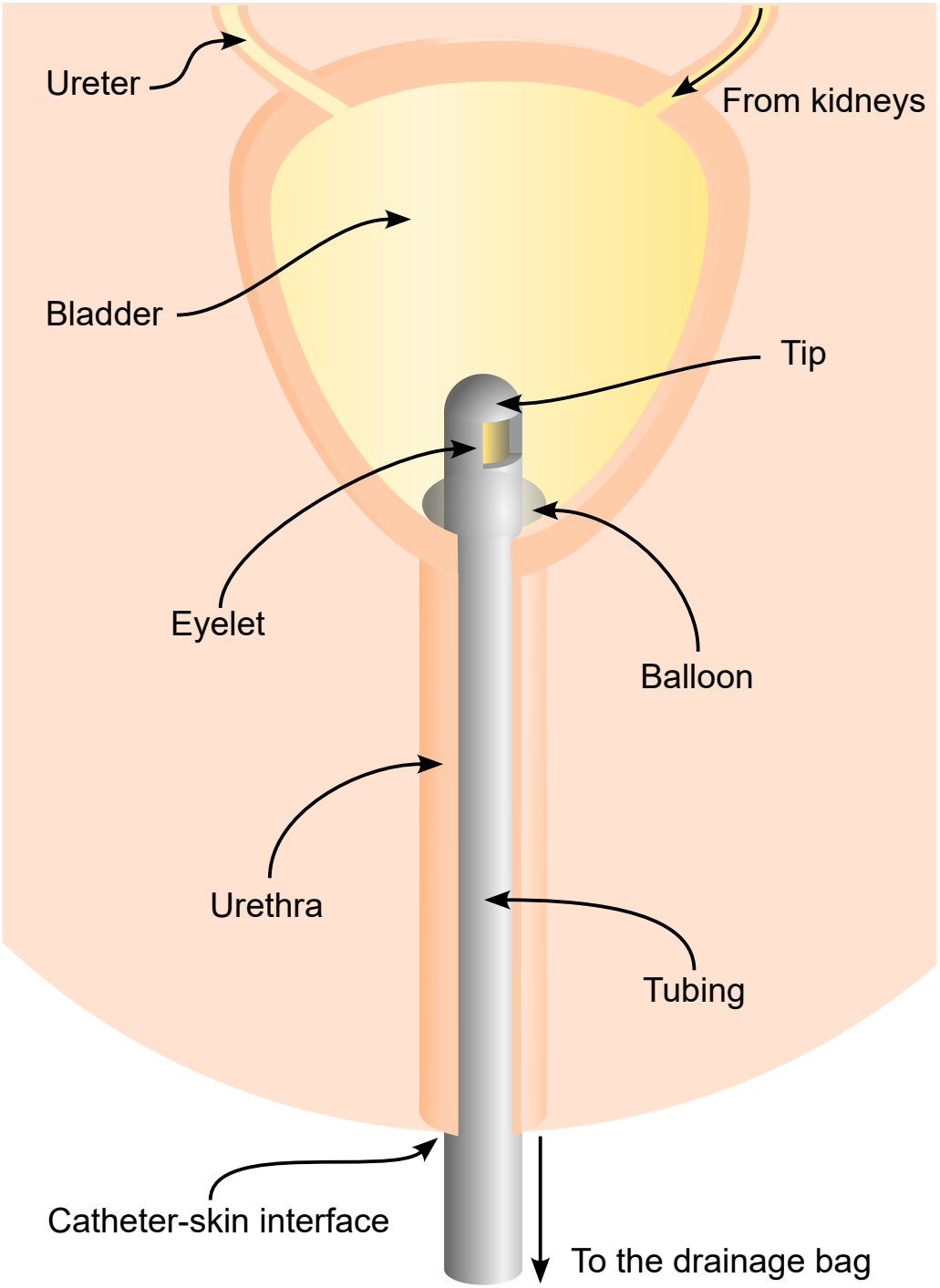

Figure 1.2 *When a Foley catheter is placed in a patient, the catheter tubing passes through the urethra, from the bladder, where an inflatable balloon anchors the tip in place, and terminates in an external drainage bag.*

connecting the bladder to the skin), or through a hole in the abdomen (suprapubic catheter). This can occur in a hospital setting, commonly during and after surgery, or in a long-term care setting. Catheterisation is extremely common: over 90,000 people live with an indwelling catheter in the United Kingdom [38], and 30 million urinary catheters are used annually in the USA [68].

In this thesis, we focus on the indwelling Foley catheter (Figure 1.1). This type of catheter is a flexible tube that is inserted into the bladder via the urethra. The tube contains two lumens[4]. Sterile water is injected into one of the lumens after insertion, to inflate a balloon just below the catheter tip. This balloon sits within the bladder and holds the catheter in place. The other lumen is used to drain urine. It has holes (eyelets) close to the catheter tip (Figure 1.2) through which urine passes from the bladder, before flowing through the lumen into a drainage bag outside the body. Typical flow rates for urine passing through the catheter are 1 mL min^{-1} [31] (controlled by the rate at which urine is made by the kidneys). Catheter lengths range from 40 mm for women up to 160 mm, or greater, for men (since in the men the urethra is longer than in women), with the balloon having a volume of 10 mL [31]. Modern catheters are typically made of latex or silicone, with external cross-sectional diameters of 4.0 – 5.3 mm (catheters are generally sized in French gauge, where 3 Fr = 1 mm; typical catheters are sized between 12 and 16 Fr) [31]. The Foley catheter remains close to its original 1930s design, although a closed drainage system (to reduce contamination from the drainage bag) was successfully introduced in the 1960s [64, 111].

Hydrodynamics of a catheter

Urine flow through a Foley catheter is an example of pipe flow. The hydrodynamics of flow through a pipe is well-established, with its properties being determined by the Reynolds number [118]. The Reynolds number is the ratio of inertial forces to viscous forces,

$$Re = \frac{LU\rho}{\mu}, \tag{1.1}$$

where L is a characteristic length, U a velocity, ρ is the fluid density, and μ is the (dynamic) viscosity. When the Reynolds number is small, $Re \ll 1$, viscous forces dominate, whereas for large values of the Reynolds number, $Re \gg 1$, the inertial forces are stronger. For flow through pipes, when the Reynolds number is 'low', $Re < 2000$, then flow is laminar. For higher Reynolds number, $Re > 4000$,

[4] *lumen* – an opening, passage, or canal [88]

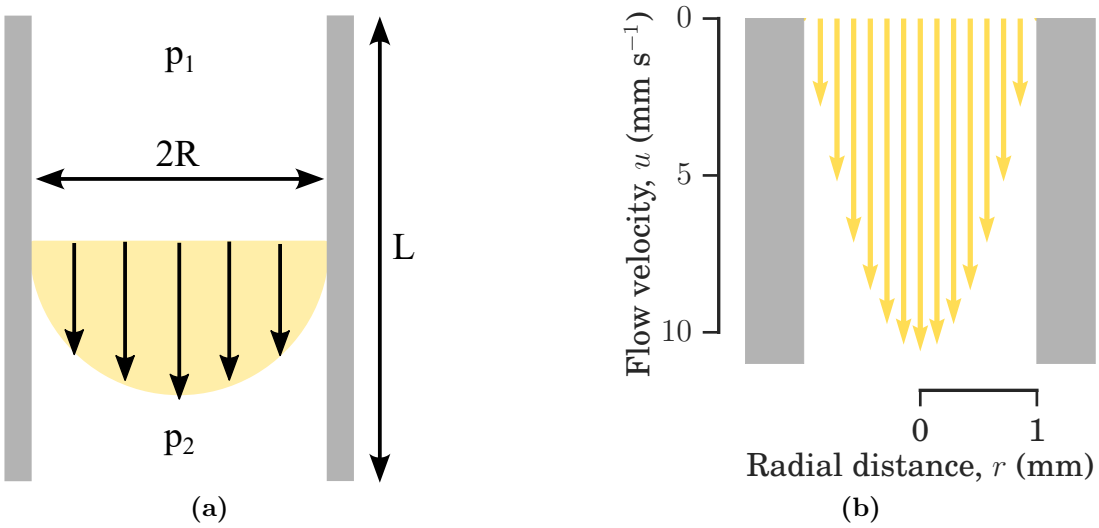

Figure 1.3 *(a) Cross section of laminar flow within a pipe of length L and radius R. The pressure difference driving the flow is $\Delta p = p_1 - p_2$. (b) The flow of urine through the catheter is parabolic and described by $u(r) = \frac{2\lambda}{\pi R^4}\left(R^2 - r^2\right)$. Here, $\lambda = 16.7\ mm^3\ s^{-1}$, and $R = 1\ mm$.*

the flow becomes turbulent [118]. We can calculate the Reynolds number for a 'typical' catheter of radius $R = 1$ mm, and urine flow rate of $\lambda = 1$ mL min^{-1}:

$$Re = \frac{\lambda}{\pi R \nu} = \frac{\frac{1}{60}10^{-6}}{\pi 10^{-3} \cdot 0.83 \cdot 10^{-6}} \approx 6 \tag{1.2}$$

where $\nu = 0.83$ mm^{2}s^{-1} is the kinematic viscosity[5] of urine at 37 °C [51]. Clearly, we are in the 'low' Reynolds number regime, $Re < 2000$, for which flow is laminar.

Laminar flow is illustrated in Figure 1.3a: in this regime, fluid flows in smooth orderly layers without eddies or mixing. At the pipe surface the no-slip boundary condition (arising from the fluid viscosity) means that the velocity must be zero. We can write down the velocity as a function of the radial distance from the centre of the pipe [118]:

$$u(r) = \frac{\Delta p}{4\mu L}\left(R^2 - r^2\right), \tag{1.3}$$

where $\Delta p = p_1 - p_2$ is the pressure differential driving the flow, μ is the viscosity, L is the length of the pipe, R is the radius of the pipe, and r is our radial coordinate. We can rewrite Eq. 1.3 in terms of parameters that are more easily physically measurable, as

$$u(r) = \frac{2\lambda}{\pi R^4}\left(R^2 - r^2\right) \tag{1.4}$$

[5]The kinematic viscosity is defined by $\nu = \mu/\rho$.

where λ is the (volume) rate of fluid flow, R is the internal radius of the catheter, and r is our radial coordinate. The rate of fluid flow is $\lambda = \Delta p \pi R^4 / 8\mu L$ – for a catheter this is equal to the rate of urine production by the kidneys, as the pressure driving the flow arises from gravity acting on the urine that is within the bladder.[6] This results in the parabolic, Poiseuille flow profile for urine flow within a urinary catheter that is shown in Figure 1.3b.

1.2 A clinical problem

Catheter-associated urinary tract infection (CAUTI)

Urinary catheters are prone to colonisation by bacteria. When this leads to symptoms such as fever, pain, or inflammation, it is known as a catheter associated urinary tract infection (CAUTI). CAUTI is unfortunately a regular occurrence for patients with long-term indwelling catheters, with some studies finding incidence rates of symptomatic episodes as high as 1.1 per 100 catheterised patient-days [48] (i.e., an incidence rate of 1.1% per catheter-day). CAUTI is also prevalent in hospital settings: in fact, CAUTI accounts for up to 40% of hospital acquired infections [48, 68, 74, 82, 105, 115, 128]. CAUTI incurs huge economic costs; for example, it is estimated to cost the United Kingdom between £1.0 and £2.5 billion annually [31]. If bacterial colonisation of the bladder occurs without clinical symptoms, it is known as asymptomatic bacteriuria (see below, §Bacteriuria).

Despite the prevalence of CAUTI, there is still limited understanding of the role of different factors in the development of infection [44, 48, 71, 78, 82]. Understanding these factors and the pathways to bacterial colonisation of urinary catheters may be a key step in reducing the impact of CAUTI [25]. Known risk factors for CAUTI include the duration of catheterisation [48, 71, 99]; biological sex, with prevalence of CAUTI significantly higher in female hospital patients than males [93, 99]; and dehydration [5, 111].

[6] This is a result of the elasticity of the bladder. If, for example, the pressure at the catheter drainage bag rises, (due to the bag being raised, or the bag filling) then the volume of residual urine in the bladder will also increase (thus raising the pressure at the bladder). This will occur until the flow of urine through the bladder is balanced, with volume flow of urine out of the bladder equal to the volume flow in from the kidneys (λ).

Pathogens causing CAUTI

The bacterial pathogens[7] most commonly associated with CAUTI overlap substantially with those that cause urinary tract infections more generally. With or without a catheter, infections are primarily associated with uropathogenic[8] *Escherichia coli* (UPEC), which is present in 75% of uncatheterised urinary tract infections [34], and in 40 – 70% of CAUTI [82]. Other bacteria commonly isolated from CAUTI include *Klebsiella* spp, *Enterococcus* spp, *Proteus mirabilis*, and *Pseudomonas aeruginosa*. *P. mirabilis* has been the focus of attention in the context of CAUTI because of its tendency to form crystalline biofilms in the catheter lumen (see below, §Catheter blockage). CAUTI can also be caused by the yeast *Candida* spp [82]. A notable difference between CAUTI and uncatheterised UTI is the prevalence of polymicrobial infections, or infections that involve more than one microbial species. Polymicrobial infections are uncommon in uncatheterised UTI but are increasingly likely to occur with duration of catheterisation, with up to 95% of bacteriuria in long-term catheterised patients being polymicrobial [123].

Uropathogenic E. coli

E. coli is frequently considered as a model bacterium in microbiology and bacterial physics [7]. Uropathogenic strains of *E. coli* have been found to be present in up to 70% of CAUTI [82]. *E. coli* cells are rod-shaped, with dimensions around 2.5 μm by 0.8 μm [7], and have several flagella (tail-like appendages), each up to 20 μm in length [50] (Figure 1.4a). Uropathogenic *E. coli* (UPEC) is generally associated with uncomplicated UTI, where it has been identified in up to 90% of infections [36, 52]. The *E. coli* strains that cause CAUTI typically do not possess the full set of virulence factors (bacterial traits that specifically contribute to the strain's ability to cause disease in the human bladder or urethra) expressed by UPEC [52]. UPEC strains are typically very sticky (expressing many adhesins, most commonly P fimbriae – tiny hair-like filaments on the bacterial surface, known as pili), highly motile (due to the bacterial flagella), resistant to the host immune system, and can easily form biofilms within the urinary tract. Comparatively, *E. coli* strains associated with CAUTI are less sticky (have a reduction in expression of P fimbriae), and may also be less

[7] *pathogen* – a microorganism that causes disease [88]

[8] *uropathogen* – a microorganism that causes disease in the urinary tract

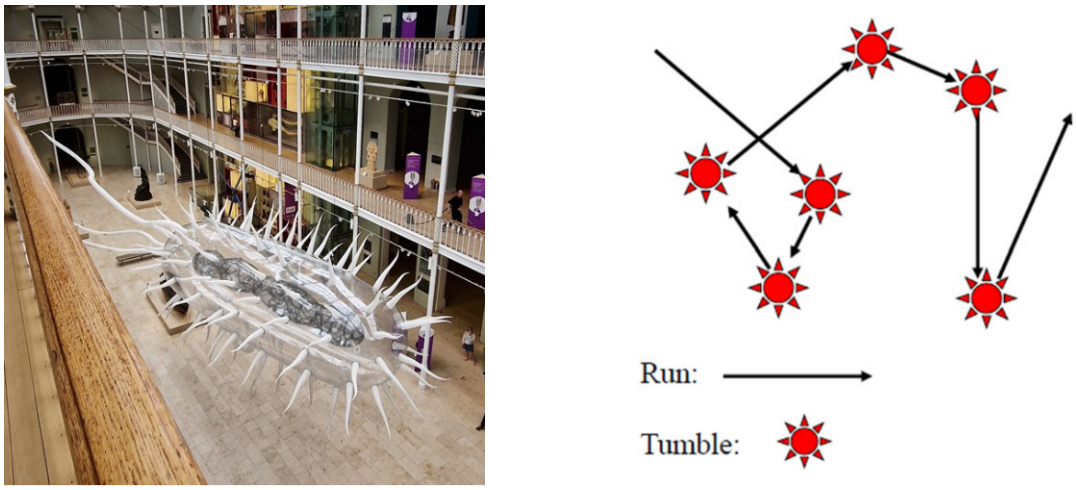

(a) **(b)**

Figure 1.4 *(a) A 90 ft inflatable sculpture of an E. coli cell, as displayed in the National Museum of Scotland. Note the rod-shape, with a long tail-like flagella (left), and covering by smaller hair-like pili (all-over). Image reproduced from National Museum of Scotland (E. coli by Luke Jerram, National Museum of Scotland, 2022; [53]). (b) E. coli cells swim with characteristic run-and-tumble dynamics, schematised here. Figure reproduced from Cates (2012; [15]).*

resistant to the host immune system [52]. *E. coli* cells can form intracellular bacterial communities, whereby *E. coli* invades the epithelial cells[9], which make up the lining of the bladder, and colonises them [52]. These intracellular bacteria communities protect bacteria from both the host immune response, and from antibiotics. They may also contribute to the recurrence of infections, providing a reservoir for reinfection [83].

The motility of *E. coli* plays a key role in colonisation of urinary catheters, as we shall see later in this thesis. Motility of *E. coli in vitro*[10] has been extensively characterised by biophysicists. *E. coli* cells swim in liquid media by rotating their (helical) flagella together [15], which generate an anisotropic[11] frictional force, propelling the cells forwards [27]. *E. coli* has a characteristic 'run-and-tumble' style of motion (Figure 1.4b), as cells periodically reverse the direction of some of their flagella, disrupting the rotation, and reorienting the cell to swim in a different direction [72]. At long length- and time-scales, this run-and-tumble motion is the statistical physics random walker [15], characterised by an active diffusion coefficient – $D \sim 100\ \mu\text{m}^2\text{s}^{-1}$ [100]. The motility of *E. coli* on or near

[9] *epithelium* – the tissue forming the mucous membrane [88]
[10] *in vitro* – in laboratory conditions [88]
[11] *anisotropy* – having different properties depending on direction

surfaces is more complicated, and in general is less well-characterised (we discuss this further in Chapter 3). We will however discuss one phenomenon arising when *E. coli* swim close to a surface within a fluid flow in §1.3.

Bacteriuria

It is important to clarify the difference between CAUTI and asymptomatic bacteriuria. CAUTI is defined as a bacterial infection accompanied by symptoms (inflammation, fever, pain etc), whereas bacteriuria is the presence of bacteria within urine, which can occur without symptoms [48]. Bacteriuria is extremely prevalent, occurring at an incidence rate of $3-7\%$ per catheter day [71], and hence long-term catheterisation almost always leads to bacteriuria [123]. In the models we will develop in this thesis we do not include the response of the human host, and therefore we cannot predict the presence or absence of clinical symptoms, such as fever. Therefore, our work can predict the occurrence of bacteriuria, but it cannot distinguish between CAUTI and asymptomatic bacteriuria.

Catheter blockage

CAUTI is not merely an unpleasant inconvenience for sufferers; it also brings risk of serious consequences, including kidney infections, bloodstream infections and tissue damage within the bladder [23, 36]. A common consequence of CAUTI is blockage of the catheter (up to 50% of catheterised patients will experience blockages [124]), which will, at best, result in urine bypassing the catheter, and at worst can lead to the backflow of infected urine into the kidneys [34].

Catheter blockage is sometimes due to the formation of a thick biofilm by bacteria such as *P. aeruginosa* [9]: in fact, when bacteria grow on catheters, many species, including *E. coli* form biofilms [111]. In a biofilm, bacteria adhere to a surface and to each other, producing extracellular polymers that form a structural matrix [9, 25]. These biofilms are known to provide protection for bacteria from both antimicrobial defences and host defences [9, 82], as well as reducing the rate at which cells are dislodged by flow [58]. For the biophysicist, biofilms are an interesting example of a non-equilibrium self-assembly process, with many models developed to account for biofilm emergent phenomena such as quorum-sensing (interbacterial communication via the release and detection of small signal molecules) and antimicrobial tolerance [58]. The binding of bacterial biofilms to

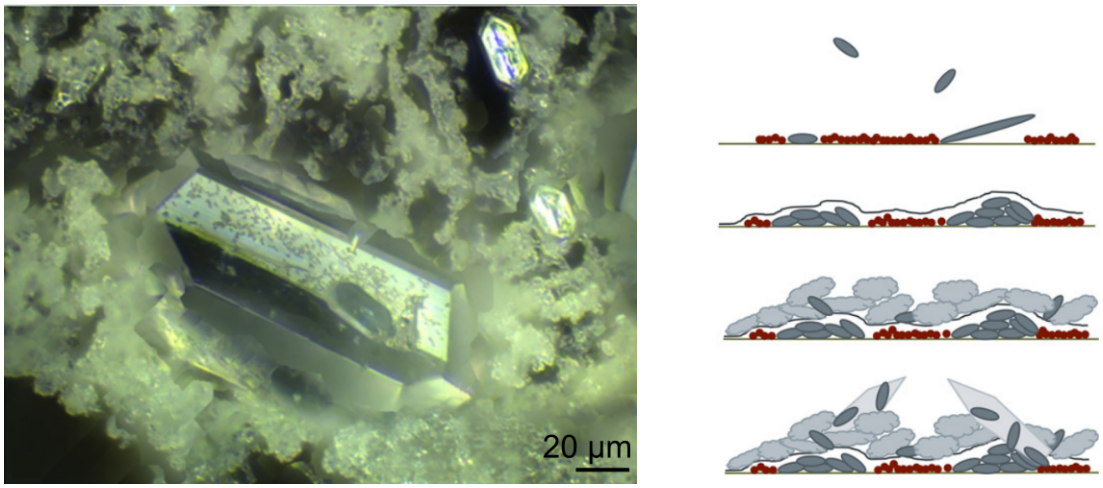

(a) **(b)**

Figure 1.5 *P. mirabilis mediates crystalline biofilm formation. (a) Struvite crystals embedded in diffuse crystalline material on a silicone catheter, following 20 days of exposure to P. mirabilis. Image modified from Wilks et al. (Figure 4d, 2015; [124]). (b) Schematic representation of the four stages of crystalline biofilm development by P. mirabilis. 1. Individual cells attach to a polysaccharride-based foundation layer. 2. A micro-crystalline sheet forms above. 3. Diffuse crystalline material accumulates. 4. Defined crystals form, bacteria swarm on the surfaces. Figure modified from Wilks et al. (Figure 7, 2015; [124]).*

a catheter is known to be aided by the accumulation of fibrinogen; fibrinogen is a protein in the blood, generally mediating clotting, which is produced and released by the body as an immune response to the catheter [34, 120].

However, the more common cause of catheter blockage is crystalline biofilms formed by the bacterium *P. mirabilis* [11, 52]. *P. mirabilis* hydrolyses urea (through the production of urease [83]), producing ammonia, which increases the alkalinity of the urine, leading to precipitation of crystals of struvite and apatite [5, 11, 52]. Wilks et al. [124] investigated the development of *P. mirabilis*-mediated crystalline biofilms through high-magnification microscopy imaging (Figure 1.5a), defining the biofilm in four components (Figure 1.5b). In earlier work, Band et al. [5] developed a mathematical model for the chemical physics of the aggregation and deposition of crystals on urinary catheters. Band et al. [5] modelled the bladder as a well-mixed constant-volume reservoir, and the catheter as a rigid channel, with small crystal particles entering the bladder from the ureters at a constant rate and aggregating within the bladder and catheter channel (modelled with Becker-Döring coagulation theory), with some crystals being deposited on the catheter surface, where they permanently adhere. Band et al. [5] modelled the urine flow through the catheter as Poiseuille, in the same manner as we discussed previously (§1.1). Band et al. [5] did not consider the action of bacteria within their model, and concluded that their model predicts crystalline aggregation will be greatest in the region closest to the catheter eyelets (i.e. the 'top' of the catheter; Figure 1.2) – we will see later (Figure 7.5) that our model mirrors this prediction for bacterial deposition on the intraluminal[12] catheter surface.

1.3 Bacterial colonisation of urinary catheters

Several different factors contribute to the vulnerability of catheterised patients to CAUTI infections. The catheter surface provides a direct pathway for bacteria to enter the body, by harbouring biofilms and providing access to the bladder. The catheter surface is particularly vulnerable to contamination at the meatus (the urethra-skin interface; Figure 1.2), potentially by gut bacteria. Moreover, the presence of a foreign object (the catheter) in the urethra and bladder can cause trauma to the tissues there, which in turn increases their susceptibility to

[12] *intraluminal* – within the lumen [88]

infection. [30, 31, 82, 111]. The port connecting the catheter to the drainage bag also constitutes a potential point of vulnerability to infection. Although the port is theoretically sterile, the need to regularly replace the drainage bag exposes it to possible contamination, particularly for catheterised patients in the community (i.e., outside hospitals).

Catheterisation also changes the characteristics of the bladder as a site of infection. Even in the absence of a catheter, the bladder is known to retain a small volume of urine [43]; this is a rich growth medium[13] [111] that can support high bacterial densities: up to 10^8 CFU g^{-1} (CFU = colony forming units; an experimental estimate for the number of viable cells in a sample), with doubling times as fast as 30 mins for *E. coli* [35]. With indwelling catherisation, the volume of this residual sump is increased due to a combination of factors including the location of the catheter balloon and inlets, the cessation of tidal drainage (i.e., periodic urination) in favour of continuous drainage, and hydrostatic pressure differentials, particularly as a result of kinks in the catheter tubing [40]. The prevention of tidal drainage also disrupts the self-cleaning nature of the bladder and urethra, preventing the regular flushing out of bacteria [31, 68]. It is likely that the epithelial cells that line the bladder walls also have a role to play in infections. Some patients experience recurrent urinary tract infections due to persistent intracellular bacterial communities in the epithelial cells [83]; the same mechanism could also cause recurrent CAUTI [52]. Thus, the catheter can act as a reservoir for bacteria to spread into the bladder, but so too can the residual urine within the bladder act as a reservoir from which the catheter can become infected.

Upstream swimming and catheters

Biophysicists are prone to become particularly excited by the discussion of the intraluminal ascension of swimming bacteria (a separate phenomenon to the ascension of bacteria on the extraluminal surface that we discussed above). The hydrodynamics of a micro-swimmer (such as a bacterial cell) can be calculated close to a surface (such as a catheter), and often differs significantly from the far-field hydrodynamics [109]. Hill et al. [47] demonstrated experimentally that close to a surface *E. coli* consistently swims upstream. Hill et al. [47] showed that this effect is due to the local shear rate at the surface, causing cells to pivot and

[13] *rich (complex) growth medium* – "containing ingredients whose exact chemical composition is unknown" [89]. These media often support growth by a wide variety of bacterial strains.

orient to point into the flow. Hill et al. [47] suggested in their conclusions that this phenomenon of upstream swimming may be relevant to the transport of *E. coli* in the upper urinary tract, or to the development of infection in catheterised patients. Since then, many physicists have studied upstream swimming, for example Nash et al. [80], Shen et al. [104], and Kaya and Koser [55]. In particular, Kaya and Koser [55] directly discussed their results in the context of the Foley catheter, estimating an upstream bacterial velocity of 20 μms^{-1}, resulting in a suggestion that *E. coli* might ascend the distance from the drainage bag to the bladder in ~ 5 hrs. Kaya and Koser [55] comment that this calculation neglects the (potentially much larger) issue of backflow – the gravity driven nature of catheter drainage means that if the drainage bag is elevated above the bladder (as may happen overnight) then the direction of urine flow is reversed. If bacteria are present in the drainage bag, then backflow virtually guarantees the bacteria will eventually be present in the bladder.

In assessing this literature in the context of urinary catheters, we should note a few things, starting with the observation that, although bacteriuria is indeed common, it does not typically occur within ~ 5 hrs of catheterisation, as the work of Kaya and Koser [55] predicts, but rather over a timescale of days (around $\sim 25\%$ of patients are bacteriuric within 2 weeks [52]). One factor in this is likely to be the neglect of bacterial adhesion in all work investigating upstream swimming: recall that uropathogenic strains of *E. coli* are much 'stickier' than laboratory strains of *E. coli* (§Uropathogenic *E. coli*), as well as the rapid formation of a highly 'sticky' conditioning layer on the catheter surface following catheterisation (§Catheter blockage). Additionally, and more significantly: since the introduction of a closed drainage system, bacterial contamination of the drainage bag is a comparatively rare event, so that upstream bacterial ascension from the drainage bag is not the main pathway of infection. It has been established that around two thirds of catheter-associated infections are in fact extraluminal, i.e., originate from bacterial growth on the outside of the catheter [52]. Around 5% of infections are due to contamination at the point of catheter insertion [82]. A further $\sim 5\%$ seem to be due to bacteria already present in the bladder, prior to catheterisation (there is a subpopulation of people whose urine cultures are *not* generally aseptic – this is frequently asymptomatic [114]). Most of the remaining infections ($\lesssim 25\%$) are attributed to bacteria infecting the drainage bag or port and then ascending the internal (intraluminal) surface of the catheter.

Moreover, in their estimation of the upstream velocity, Kaya and Koser [55]

assumed an internal luminal diameter of 4.4 mm, which seems questionably large, given that typical catheters in use have size 12 – 16 Fr, corresponding to an *external* diameter of ~ 4 mm [31]. We can calculate the shear rate for parameters as we assumed in §1.1 instead, where the urine flow rate $\lambda = 1$ mL min^{-1}, and the catheter internal radius $R = 1$ mm. Recall Eq. 1.4, describing the urine velocity within the catheter:

$$u(r) = \frac{2\lambda}{\pi R^4}\left(R^2 - r^2\right).$$

The shear rate of this flow at the catheter surface is

$$\left.\frac{\partial u}{\partial r}\right|_{r=R} = -\frac{4\lambda}{\pi R^3} \sim 21 \text{ s}^{-1}. \tag{1.5}$$

This is very different to the shear rate estimated by Kaya and Koser [55] of 2.9 s^{-1}, and indeed is well above the critical threshold identified by Hill et al. [47] for upstream swimming (~ 10 s^{-1}). It seems likely therefore that not only is the phenomenon of upstream swimming insignificant in considering urinary catheters (as we discussed above), but in fact, it may not occur at all.

1.4 Clinical interventions

The addition of a closed drainage system to indwelling catheters in the 1960s was the last successful major change to catheterisation practices [64, 111]. To date, although there have been many proposed changes to catheter design and best practice, there is still limited understanding of the importance of different factors in the development of CAUTI [44, 48, 71, 78, 82].

In recent years, the use of novel materials for catheters has attracted much attention [4, 32, 85]. Historically Foley catheters were manufactured from latex, while many modern catheters are made of silicone [31]. Newer materials that have been explored include silver coatings, hydrogel[14] coatings and catheters which release antimicrobials into the bladder [68]. Some research has also been done on antibiotic coatings/impregnation with minocycline-rifampim, but this is less promising for urinary catheters, as this is known to be much less effective against Gram-negative bacteria (which constitute the majority of infections) [85]. None of these design changes have been found to be effective [85]. Silver coated

[14] *hydrogel* – materials with hydrophilic structure, "capable of holding large amounts of water in their three-dimensional networks" [2]

catheters were promising in laboratory experiments, but so far proved ineffective in patient studies [4]. Hydrogel catheters reduce binding of fibrinogen, and reduce irritation to host membranes, but have been found to allow swifter microorganism migration [85] and aggregation [56]. Antimicrobial catheters are often found to have only limited effect strength [90], often outweighed by the risk of promoting the growth of antimicrobial resistant strains [4].

Some work also exists on novel catheter design, including a catheter that can debond biofilms (and so remove blockages) through the application of mechanical strain [68], and a catheter with spiralling tubing to improve drainage [40]. Much of the literature is however focused on interventions in nursing/clinical practice [44, 48, 71, 77, 78]. One example of such an intervention is the introduction of stop orders – "prewritten orders for the removal of urinary catheters if specified criteria were not met" (Hooton et al, 2010, p. 640 [48]) – to reduce unnecessary catheterisation. However, many of these types of interventions have also proven ineffectual, or even harmful. For example, one attempt at reducing infection, by applying the antiseptic chlorhexidine to block all routes of infection, resulted in a major outbreak of chlorhexidine resistant, multidrug resistant *P. mirabilis* [30].

1.5 Relevance of biophysical modelling

Physics has a lot to offer for modelling these phenomena [9, 108]. A previous model for the bladder hydrodynamics of a urinary tract infection has highlighted how the relationship between bacterial growth rate and rate of urine production determines infection success [43]. Gordon and Riley [43] modelled a bladder that periodically filled and emptied, with a minimum volume $V_{\min}$, a maximum volume $V_{\max}$, and a filling rate λ. The volume of urine in the bladder is given by

$$V(t) = V_{\min} + \lambda t, \qquad t \in \left[0, \tau = \frac{V_{\max} - V_{\min}}{\lambda}\right), \tag{1.6}$$

where τ is the interval between micturitions[15]. Assuming exponential bacterial growth, in the time between micturitions, the number of bacteria in the bladder is

$$N(t) = N_0 \exp\left(r_B t\right), \tag{1.7}$$

[15] *micturition* – urination [88]

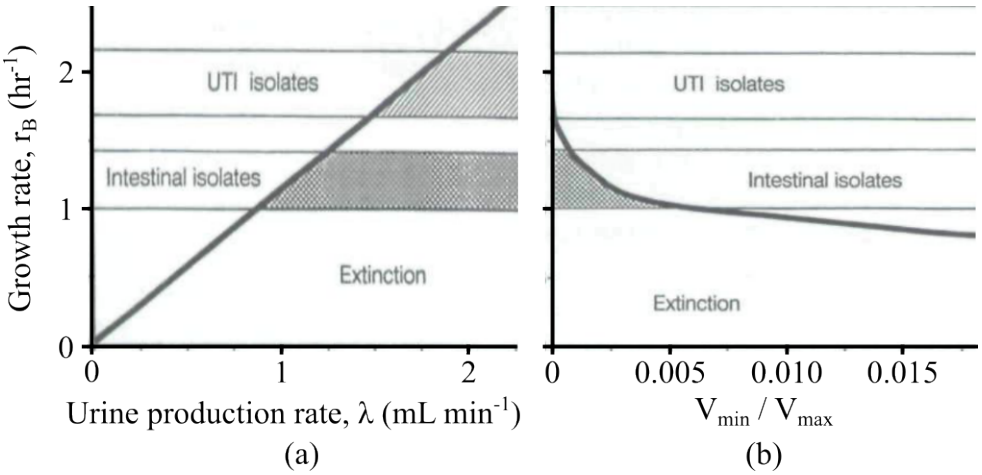

Figure 1.6 *An establishment-extinction condition on the bacterial growth rate for urinary tract infections. Marked are the mean growth rates (±1 standard deviation) of clinical E. coli isolates. Shaded regions indicate where Eq. 1.9 predicts the bacteria would fail to establish a population in the bladder. (a) Effect of urine production rate on the establishment condition. (b) Effect of bladder volumes on the establishment condition. Figure modified from Gordon and Riley (1992; [43]).*

where r_B is the bacterial growth rate within the bladder, and N_0 is the number of bacteria present in the residual urine at the start of the time interval. Then, with N_k being the bacterial population in the bladder after k micturition events, the bacterial population after the k+1th micturition event is given by

$$N_{k+1} = \frac{V_{\min}}{V_{\max}} N_k \exp\left(r_B \tau\right). \tag{1.8}$$

By requiring an 'establishment criterion' of $N_{k+1} > N_k$ – i.e., that the population should grow in successive cycles – Gordon and Riley found a condition on the growth rate:

$$r_B > \log\left(\frac{V_{\max}}{V_{\min}}\right) \frac{\lambda}{V_{\max} - V_{\min}}. \tag{1.9}$$

Gordon and Riley applied Eq. 1.9 to make predictions for the conditions under which *E. coli* might colonise the urine within the bladder: low urine production rate (dehydration; Figure 1.6a), or incomplete voiding of the bladder (Figure 1.6b).

For our model, the angle of interest is primarily the population dynamics of an infecting bacterial population. There are many interesting avenues of research here. From the growth of biofilms on complex surfaces [9, 37, 58], in particular the spatial development of biofilms colonising the surfaces of a catheter [124], to

the effects of antibiotic treatment on bladder infections [22]. Simple models of the dynamics of bacterial growth in the bladder exist [43] (as discussed above), but do not consider the effect of catheterisation, while models for catheter encrustation focus on crystalline aggregation [5], rather than bacterial growth (§Catheter blockage). We must also consider hydrodynamics: urine flow within a catheter is an example of laminar flow – due to its low Reynolds number [118] (§1.1), while the problem of how bacteria behave near a surface in a flow is a topic of recent research [27, 65, 109] (as discussed briefly in §1.3), and much is still unknown for the growth of a biofilm subject to continuous flow [58].

1.6 Biophysical modelling of bacterial colonisation of urinary catheters

In this thesis we present a quantitative model for the dynamics of bacterial colonisation of a urinary catheter, which identifies parameters that are critical for clinical outcome. Our study focuses on the indwelling Foley catheter, in which the catheter tip sits inside the bladder, held in place by a balloon, while the catheter tubing passes through the urethra, terminating at an external drainage bag (Figure 1.2). We model the population dynamics of infecting bacteria as they migrate up the catheter, proliferate in the residual sump of urine that remains in the bladder during the period of catheterisation [30, 31, 40, 43], and travel out of the bladder in the urine flow through the catheter lumen, where they can attach to the inner lumen surface [48] and trigger biofilm formation that can block the catheter [82].

Combining these processes into a unified model allows us to predict the time course of bacterial colonisation and to identify the key parameters controlling clinical observables such as bacterial density in the bladder and the time before bacteriuria (bacteria in the urine) is detected, as well as the time to formation of a luminal biofilm. These parameters include the rate of urine production by the kidneys, the volume of residual urine in the bladder, and the length of the urethra. We find that the rate of urine production governs a transition between a high-density bladder state (bacteriuria) and a diluted, 'washed out' state with low bacterial density. We also show how different spatial patterns of bacterial biofilm growth are expected on the catheter depending on the initial conditions, suggesting that it might be possible to infer the source of the colonising bacteria

from these patterns.

Considering the model as a mapping from 'parameter space' to 'outcome space', we identify parameters that are particularly critical in determining the outcomes over different timescales (short-term catheterisation is typically $\lesssim$ 14 days, while long-term catheterisation can be multiple months). By considering the timescales and stationary states of the system, we find that clinical interventions with the goal of preventing bacterial colonisation long-term must act on the stationary states of the system, but that interventions that alter the dynamics may have significant effect over shorter timescales. This leads us to classify clinical interventions according to their actions on the model parameters, stationary state(s), and dynamics: postponement, mitigation, or prevention. We apply the model to find new perspectives on both *in vitro* and *in vivo* studies, and demonstrate how the model can predict the outcomes of a clinical trial of catheter interventions (the CATHETER trial [90]). We show that our model provides quantitatively better fits to clinical data than models previously applied within the literature, and identifies an outcome (reduced incidence of bacteriuria associated with the use of silver-alloy catheters in males) that was present in the study dataset, but not discussed in the original study.

Part I

A mathematical model

Chapter 2

Construction of a modelling framework

2.1 Introduction

When building a model for bacterial colonisation of the bladder (bacterial colonisation being a necessary but not sufficient step for the occurrence of CAUTI), we can identify three distinct relevant spaces: the bladder, the urethra, and the catheter itself. The bladder is an elastic volume, which under normal circumstances steadily fills with urine (flowing in from the kidneys via the ureters) and periodically empties (via the urethra). When catheterised the bladder does not empty periodically, but instead contains a constant volume of urine, which is diluted by fresh urine from the kidneys.

These three spaces do not exist in isolation, but rather are connected as one system. The catheter is located inside the urethra, with the extraluminal surface of the catheter in contact with the urethral lining (Figure 1.2). The tip of the catheter is within the bladder, such that the extraluminal surface of the catheter provides an uninterrupted connection from the bladder all the way out of the body to the skin. Within the catheter is the lumen, through which urine flows from the bladder into a drainage bag external to the body (recall Figure 1.1). This forms a closed system; however, the bag must be regularly emptied, which provides a periodic possibility for contamination of the drainage bag.

We must also consider how bacteria are introduced in our mathematical model,

i.e., how the system becomes contaminated. As discussed in §1.3, bacterial contamination is known to occur at several different locations within the system. The most common origin of bacterial contamination is the interface between the extraluminal catheter surface and skin; however, contamination of the drainage bag, contamination of the catheter during insertion, or a pre-existing bacterial population within the bladder are all also possible.

2.2 The model system

Figure 2.1 depicts a minimal model for bacterial colonisation of a catheter. The model consists of four parts: the extraluminal surface of the catheter, the bladder, the urine flow within the catheter, and the intraluminal surface of the catheter. These are coupled such that bacterial contamination can cross between the different parts of the system. Colonising bacteria may therefore originate anywhere within the system, allowing for all the major infection pathways (extraluminal, intraluminal, contamination on insertion), as well as for an infection originating in the bladder (e.g., after a catheter is replaced).

The catheter is treated as a rigid open cylindrical tube, with rotational symmetry. The bladder is assumed to be well-mixed with the rate of urine production and the volume of residual urine assumed to be constant during each period of catheterisation. All external forces on the bacterial cells are neglected, and we assume there is no backflow from the drainage bag. We assume the catheter is colonised by a single bacterial species and base the parameters on *E. coli*, which is present in 40–70% of CAUTI [82]. This model does not account for the response of the human host and therefore does not distinguish between asymptomatic and symptomatic (CAUTI) infection [18] (since the key distinction is via symptoms such as fever that arise from the host response to the infection).

2.3 Notation

Within this model we consider the bacterial population as a continuous density, rather than as discrete countable individuals. Thus, we model the bacterial population via surface densities and volume densities in the various parts of the model, rather than absolute bacterial numbers (Table 2.1). It is of course always

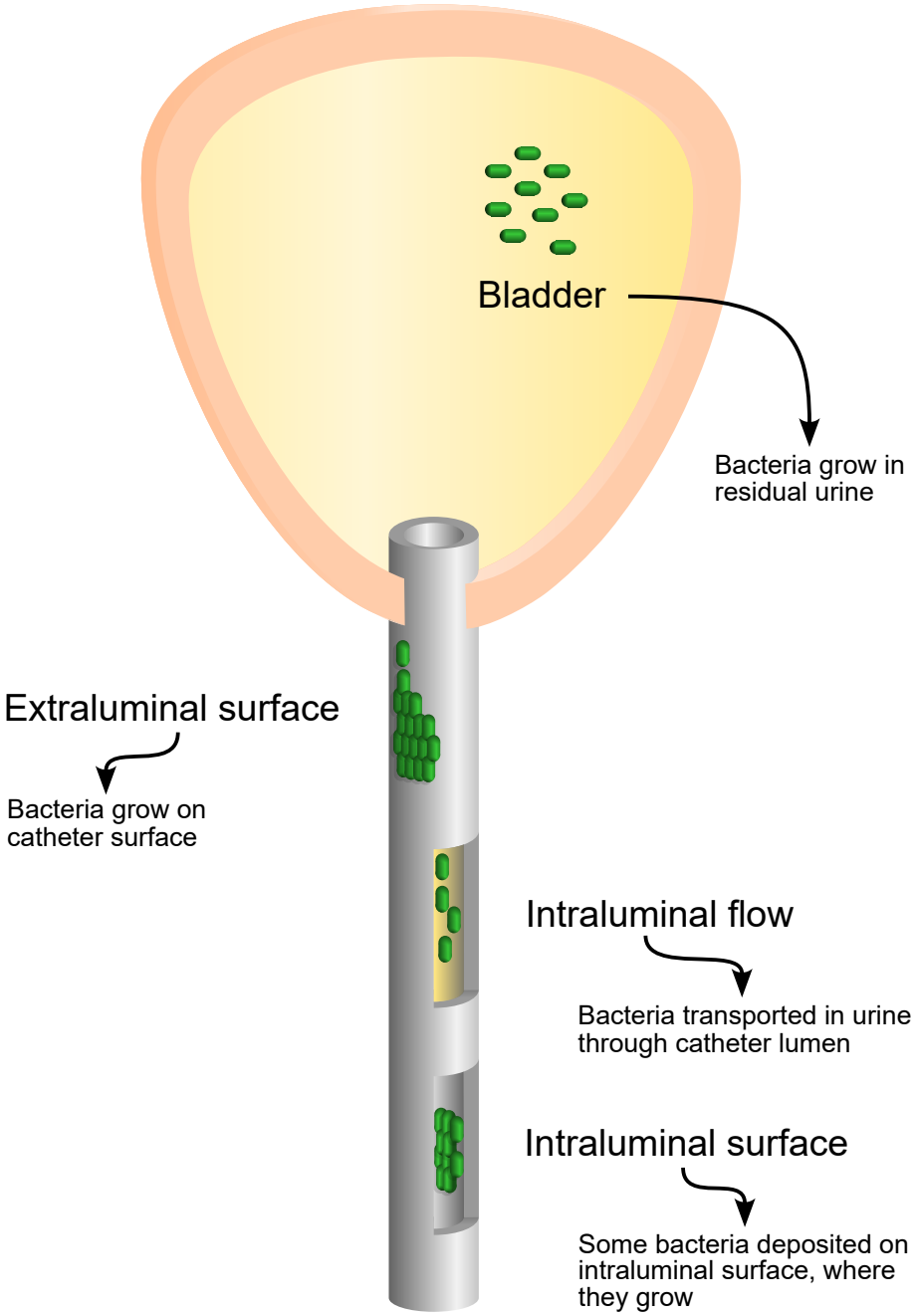

Figure 2.1 *Sketch of the system being modelled. Bacteria can grow and spread as a wavefront on the external (extraluminal) surface of the catheter. They can grow in the residual urine within the bladder, before being transported downwards by the flow within the catheter. Some bacteria attach to the intraluminal surface of the catheter, where they grow and spread just as on the extraluminal surface.*

Subsystem	System spatial dimensions	Density type	Notation
Extraluminal surface	1	surface	$n(x,t)$
Bladder	0	volume	$\rho(t)$
Intraluminal flow	2	volume	$\sigma(x,r,t)$
Intraluminal surface	1	surface	$m(x,t)$

Table 2.1 *We model the bacterial populations in each subsystem as a density. However, for some parts of the model we consider a surface density of bacteria, while for other sections it is a volume density. Moreover, the spatial dimensions differ in different parts of the model. The various forms of bacterial density in the model are summarised here, alongside the notation they are represented by.*

possible to retrieve the absolute bacterial numbers by integrating the population density over the relevant geometry.

Each subsystem of the model has a distinct local geometry. For example, we can write $n(x,t)$ as the bacterial surface density (i.e., per unit area) on the extraluminal catheter surface, at a longitudinal distance x along the catheter, and a time t. Here $x = 0$ is defined at the bladder, and $t = 0$ at the time of initial contamination. Note that here we have neglected the rotational dimension, since we have assumed the catheter to have rotational symmetry.

On the intraluminal surface, we can define a quantity $m(x,t)$ similarly, as the bacterial surface density on the intraluminal catheter surface. Again, $x = 0$ is located at the bladder, and we neglect the rotational dimension.

For the bacterial populations within the urine, we need to consider volume densities rather than surface densities. Therefore, we denote $\rho(t)$ as the bacterial volume density within the bladder, and $\sigma(x,r,t)$ as the bacterial volume density in the urine flow within the catheter lumen, where x is as defined for the intraluminal surface, and r is the radial distance in the lumen (with $r = 0$ as the centre of the lumen). This notation is summarised in Table 2.1.

2.4 Parameterisation

Since the objective of this work is to model a real clinical problem, the model should ideally be parameterised based on literature reports of measured values

in a clinical setting. Where this is not possible, measurements that have been taken in a laboratory setting are used, trying where possible to match the clinical environment. Table 2.2 lists the parameters required for this model, their expected range in a clinical setting (based on literature), and the 'default' values for them that will be assumed within the following chapters (Chapters 3 to 6).

Parameter		Default value in simulations	Justification and expected range
Urethral length	L	40 mm	Women: 40 mm. Men: 160 mm [31]. Choosing the shorter length leads to shorter runtimes for numerical simulations.
Residual urine volume	V	50 ml = $5{\times}10^4$ mm^3	$10-100$ ml [31] but may be up to 500 ml in immobile patients [40].
Urine production rate	λ	1 ml min^{-1} = 16.7 mm^{3}s^{-1}	Average of 1 ml min^{-1} [31].
Dilution rate	k_D	1.2 hr^{-1} = $3.33{\times}10^{-4}$ s^{-1}	Defined by $k_D := \lambda/V$.
Catheter internal radius	R	1 mm	Outer diameter: 4-5 mm [31], wall thickness is manufacturer dependent, so the internal radius is likely 1-2 mm.
Bacterial surface diffusivity	D_S	10^{-2} μm^{2}s^{-1} = 10^{-8} mm^{2}s^{-1}	This depends heavily on factors such as surface 'wetness' (see §3), so there is a high degree of uncertainty for this parameter. There are very few experimental measurements in the literature, but the 'dry' surface diffusivity of *P. aeruginosa* has been measured as 10^{-2} μm^2 s^{-1} [41].
Bacterial bulk diffusivity	D_B	10^2 μm^{2}s^{-1} = 10^{-4} mm^{2}s^{-1}	Parameterising a cell swimming in a liquid medium as a random walker: 100 μm^2 s^{-1} for *E. coli* [100]. This provides an upper bound on estimates for the bacterial surface diffusivity, D_S, on a 'wet' surface.

Table 2.2 *Model parameters and values. Table continues on next page.*

Parameter		Default value in simulations	Justification and expected range
Catheter surface bacterial growth rate	r_S	0.69 hr^{-1} = 1.93×10^{-4} s^{-1}	This is difficult to experimentally determine, as *in vitro* catheter surface properties differ significantly from *in vivo*. However, the doubling time of *E. coli* on poor growth media[1] is $\sim$ 1 hr [10].
Bacterial growth rate in bladder	r_B	1.39 hr^{-1} = 3.85×10^{-4} s^{-1}	Doubling time of *E. coli* in UTIs is 30-35 mins [35].
Catheter surface carrying capacity	κ_S	10^9 cm^{-2} = 10^7 mm^{-2}	Biofilms with densities of 5×10^9 cm^{-2} have been found on catheters [111].
Bladder carrying capacity	κ_B	10^9 ml^{-1} = 10^6 mm^{-3}	Bacterial densities of 10^8 CFU g^{-1} have been observed for *E. coli* growth in urine in the bladders of mice [35]. And in rich LB medium[2] [103], with a similar doubling time to urine, the density of *E. coli* has been measured as 10^9 cells mL^{-1}.
Bacterial detachment rate	k_d	1.93×10^{-4} s^{-1}	Assume that all new growth detaches: $k_d = r_S$.
Bacterial attachment rate	k_a	1.26×10^{-6} s^{-1}	Smoluchowski diffusion rate limited constant [119]: $4\pi D_B \cdot 1$ μm.

Table 2.2 *Model parameters. The values used in the model are listed together with the expected range of values for each parameter. Within the model standard units are taken to be mm and s, however parameters are also given here in more physically intuitive units where applicable.*

We discuss the model in depth in the following chapters. In Chapters 3 to 5 we construct mathematical descriptions for each of the subsystems and explore their implications for the bacterial population dynamics. Then, in Chapter 6, we couple all the parts together, to form one unified model for the bacterial colonisation of a urinary catheter. In Chapter 7, we perform a parameter space exploration of the model, and interpret these results through the lens of the clinical literature.

[1] *poor growth medium* – a growth medium lacking some or all amino acids requisite for bacterial growth, such that bacterial cells must synthesize these nutrients for growth.

[2] *LB medium* – a common (complex) growth medium used in microbiology cell culture, containing amino acids from yeast extract.

Finally, in Chapter 8, we apply the model to find new perspectives on both *in vivo* and *in vitro* studies, and discuss the implications of the model for understanding the efficacy of clinical interventions.

Chapter 3

Modelling the extraluminal surface

3.1 Introduction

In CAUTI, the interaction between bacteria and the catheter surface is thought to play an important role [82, 111]. It is thought that the surface provided by the catheter assists in the transport of bacteria up the urethra into the bladder, contributing to the much higher rate of infections in catheterised patients compared to uncatheterised patients [52]. Different bacterial species have different ways of ascending the catheter [54], which also depend on the surface material [25, 32]. *E. coli* is able to adhere to a thin film of proteins, particularly fibrinogen, that inevitably coats the catheter after insertion [85] (§1.2). The cells then produce an extra-cellular matrix, within which they can reproduce in relative safety from the host's immune system [9].

In Figure 3.1, an example microscopy image that I obtained of bacteria colonising the extraluminal surface of a catheter is shown. These images were taken with epifluorescence microscopy[1], and show *E. coli* biofilms that were allowed to colonise a catheter for 72 hours *in vitro*. For full details of how this sample was prepared and images obtained, see §A.1.3. Within this chapter, we establish a model for bacterial colonisation of the extraluminal catheter surface and discuss the implications of the model for predictions of both the bacterial density distributions over the catheter surface, and the timescale of bacterial ascension of

[1] *epifluorescence microscopy* – a form of optical microscopy, whereby light at a specific wavelength from the microscope excites fluorophores in the sample, which then emit light at a different wavelength [88]

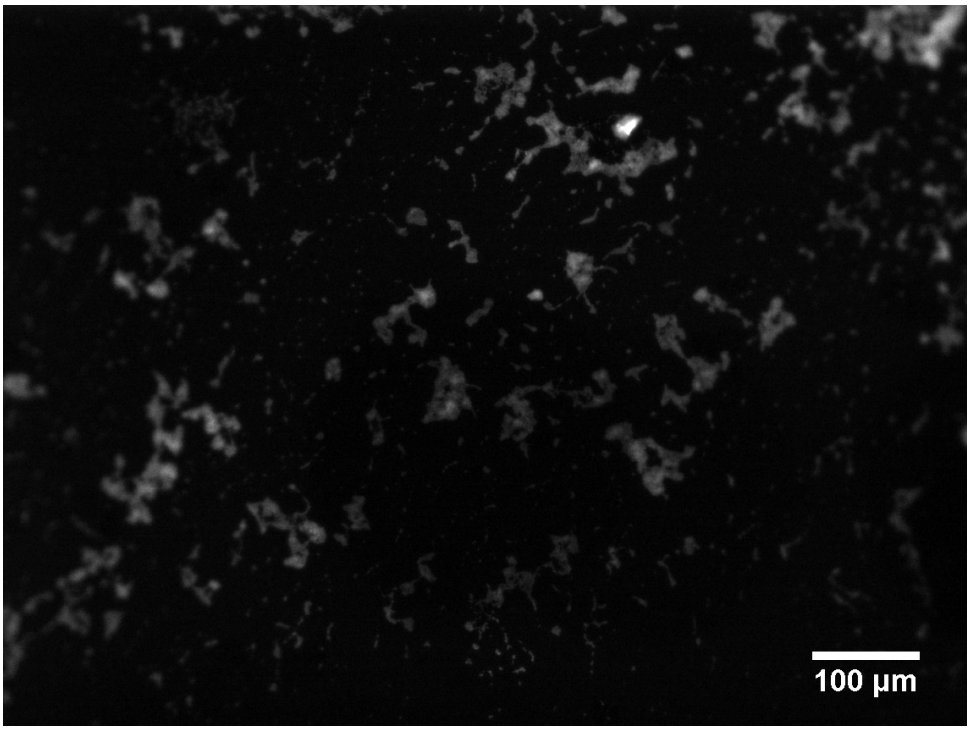

(a)

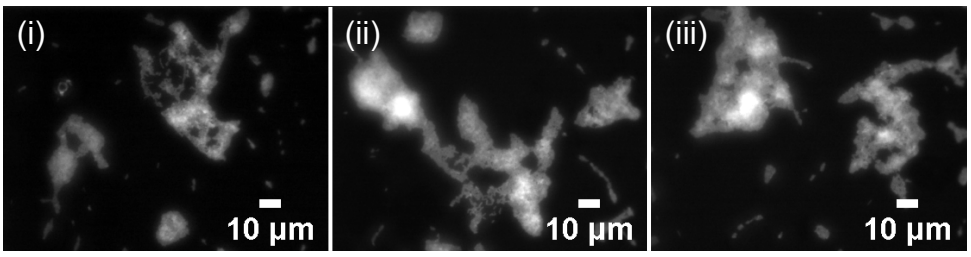

(b)

Figure 3.1 *Fluorescence images of E. coli biofilms grown on the extraluminal surface of urinary catheters. (a) A* 0.90×0.67 *mm section of catheter surface, imaged with a* $10\times$ *objective. (b) A zoomed view of the same section of catheter surface, imaged with a* $60\times$ *objective.*

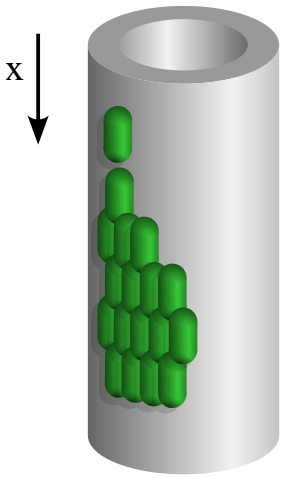

Figure 3.2 *Bacteria grow and diffuse as a wavefront on the extraluminal surface.*

the extraluminal catheter length (from the skin-urethra interface to the bladder).

3.2 A mathematical model

On the extraluminal surface of the catheter, bacteria grow and diffuse over the surface, as illustrated in Figure 3.2. The rotational symmetry of the catheter means this can be reduced to a 1-dimensional problem, parameterised only by the longitudinal distance along the catheter, x. A simple model for this is an FKPP equation [33, 61, 79]:

$$\frac{\partial n}{\partial t} = \underbrace{D_S \frac{\partial^2 n}{\partial x^2}}_{\text{motility}} + \underbrace{r_S n \left(1 - \frac{n}{\kappa_S}\right)}_{\text{growth}}. \tag{3.1}$$

Here $n(x,t)$ is the bacterial surface density, D_S the diffusivity of the bacteria on the catheter surface, r_S the bacterial growth rate on the catheter surface, and κ_S the bacterial carrying capacity of the catheter surface (as defined in Table 2.1 and Table 2.2). We shall discuss the specific boundary conditions for Eq. 3.1 and the numerical implementation of this equation later, in Chapter 6.

The bacterial surface density, $n(x,t)$ has dimensions of $[n] = \mathrm{L}^{-2}$ (recall Table 2.1). Hence, the total number of bacteria on the outside of the catheter at a given time is given by

$$N_{\text{extraluminal}}(t) = \int n \, \mathrm{d}S = \int_0^L 2\pi R_e \, n(x,t) \, \mathrm{d}x,$$

where $\mathrm{d}S$ is a surface element, L is the length of the catheter, and R_e is the external radius of the catheter.

The right-hand side of Eq. 3.1 is composed of two terms: a diffusive term describing the motility of the bacteria, and a reaction term describing the growth of the population. The form of the growth term is logistic; describing a population which initially grows exponentially with growth rate r_S but is subsequently constrained by the environment to a maximum density of κ_S. Choosing to describe the bacterial motility by a diffusive term enables the parameterisation of the motility by a single experimentally determinable parameter: an effective diffusion coefficient D_S (since as we discussed in §1.2 we can consider a bacterial cell as a random walker). However, it carries a significant limitation, reducing the complexity of bacterial motility on the surface to just diffusion and hence overlooking any more complicated behaviours, e.g. swarming – the "rapid multicellular movement of bacteria across a surface, powered by rotating flagella" (Henrichsen, 1972, as quoted in Kearns, 2010; [46, 57]).

We already discussed the estimated ranges for these parameters in Chapter 2. Here it is important to highlight the large range in estimates for the bacterial surface diffusivity. This arises in part from difficulties in experimentally assessing bacterial motility on catheter surfaces: bacterial surface motility depends significantly on surface 'wetness' [57] (that is, bacteria are typically constrained to slow 'twitching' styles of motility on dry surfaces, whereas cells can often more effectively utilise their flagella – and hence move faster – when there is a fluid layer covering the surface), and the surface properties of the catheter differ significantly *in vitro* versus *in vivo* [97], due at least in part to host-catheter interactions that result in the formation of a conditioning film on the catheter surface [34]. However, the large range is also an inevitable consequence of the limitation discussed above, that we are describing the bacterial motility as simple diffusion. In reality, there are enormous differences in motility from species to species [46], but even within a single bacterial strain there can be multiple modes of motility. For example, a population of cells growing within a biofilm often have very limited motility, resulting in a population that spreads primarily by growth [9] ($D_S \sim 10^{-9}$ mm^{2}s^{-1}), while bacterial cells actively crawling or swimming over a surface show motility that is heavily influenced by surface 'wetness' [41, 57, 100] (from $D_S \sim 10^{-8}$ mm^{2}s^{-1} to $D_S \sim 10^{-4}$ mm^{2}s^{-1}), and bacteria exhibiting swarming behaviour are highly motile [57] (swarming cells perform super-diffusion [6], with swarming colonies expanding rapidly, with

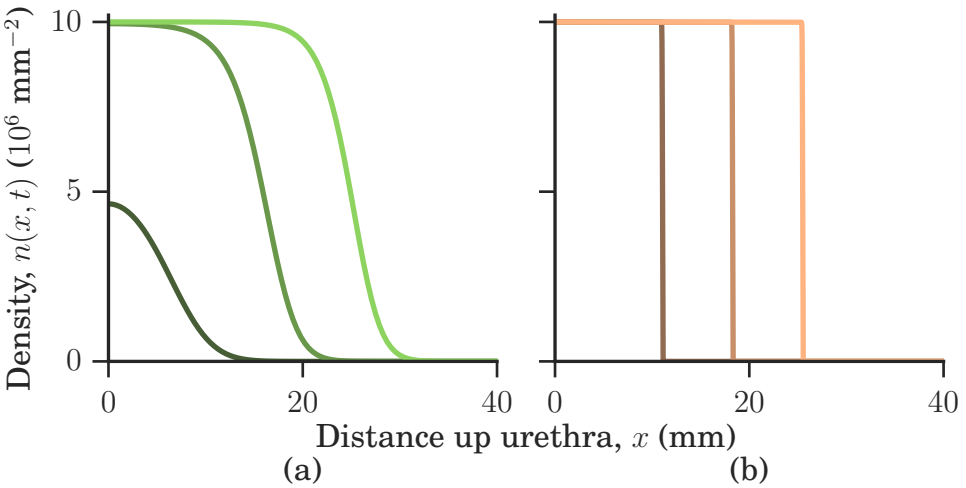

Figure 3.3 *Numerical solutions to Eq. 3.1, with an initial inoculation of* 100 mm^{-2} *at* $x = 0$*, and all parameters except* D_S *as given in Table 2.2. Reflecting boundary conditions* ($\partial n/\partial x = 0$) *were applied at* $x = -100$ *mm and* $x = 140$ *mm, such that the region of interest* ($x \in [0, 40$ *mm*]) *is far from the boundaries. Details of the numerical scheme are given in §6.3.1. (a)* $D_S = 10^{-4}$ $mm^2 s^{-1}$*. Each curve is a snapshot of the density profile at 20 (▬), 28 (▬) and 36 (▬) hours respectively. (b)* $D_S = 10^{-8}$ $mm^2 s^{-1}$*. Each curve is a snapshot of the density profile at 30 (▬), 60 (▬) and 90 (▬) days respectively.*

expansion speeds[2] $\sim 10^{-3}$ mms^{-1} [21, 46]). This vast range of potential values for the bacterial surface diffusivity results in variability in predictions of the infection timescale (compare Figure 3.3a and 3.3b), as well as having consequences for the stability of a numerical implementation of Eq. 3.1 (see §A.1.2).

3.3 Existence & implications of travelling wave solutions

Eq. 3.1 is used in our model to describe bacteria spreading up the length of the catheter. If there is an initial inoculation at the base of the catheter (at the skin), then the infection will spread in a wave-like manner up the catheter (Figure 3.3). This travelling wavefront behaviour is interesting because it suggests that the shape of the bacterial distribution on the outside of the catheter could provide insight into the start of the infection. In particular, we would expect to see (at

[2]As we shall see later, a swimming bacteria as described by diffusion would have a velocity $2\sqrt{r_S D_S} \sim 10^{-6}$ mms^{-1} (for parameter values as in Table 2.2). We might compare this with the value $\sim 10^{-6}$ mms^{-1}, which is the literature recorded rate of increase in colony radius of *E. coli* [46].

early times) a higher density of bacteria near the point of infection than in regions that the infection has not yet spread to. In fact, depending on initial conditions, there is often much more we can say about these travelling wavefronts. For example, we can calculate the wavefront speed, and hence estimate the timescale of bacterial ascension of the catheter.

3.3.1 Wavefront solutions to the dimensionless FKPP equation

While Eq. 3.1 is not generally solvable, for certain initial conditions the properties of the travelling wave solutions are known. Taking the following transform,

$$\begin{aligned} n &\to \frac{n}{\kappa_S} \\ x &\to x\sqrt{\frac{r_S}{D_S}} \\ t &\to r_S t, \end{aligned} \tag{3.2}$$

we non-dimensionalise Eq. 3.1, giving rise to the nondimensionalised FKPP equation:

$$\frac{\partial n}{\partial t} = \frac{\partial^2 n}{\partial x^2} + n\left(1-n\right). \tag{3.3}$$

This equation has been studied extensively, particularly as regards its asymptotic properties [79, 117]. Since this equation describes a stable state ($n(x,t) = 1$) propagating into an unstable state ($n(x,t) = 0$), there is an associated linear spreading velocity: the velocity at which perturbations to the (unstable) zero state spread, obtained by linearisation of the equation about that unstable state [117]. For Eq. 3.3, this linear spreading velocity can be shown to be $v^* = 2$, see §A.1.1.

The linear spreading velocity places a constraint on the wave speeds of asymptotic solutions of Eq. 3.3: $v_{\text{asym}} \geq v^*$ for all initial conditions. In fact, all travelling wave solutions to Eq. 3.3 can be split into two classes. Wavefronts travelling with speed $v_{\text{asym}} = v^*$ are *pulled* solutions, with the spreading perturbation 'pulling' the nonlinear behaviour behind it. Wavefronts travelling with speed $v_{\text{asym}} > v^*$ are *pushed* solutions, with the nonlinear behaviour 'pushing' forward the perturbation into the zero state [117].

Which of these possible solutions actually occurs is determined by the initial

conditions. It has been shown that the asymptotics of the travelling wave solution is determined by the asymptotics of the initial conditions [79]. Any initial conditions with *compact support* (that is, that are non-zero only on some finite domain) will have the same asymptotic behaviour. In other words, for initial conditions of the form

$$n(x,0) = \begin{cases} f(x) > 0 \text{ if } x < a \\ 0 \text{ if } x \geq a \end{cases} \tag{3.4}$$

for some finite a, this equation has travelling wave solutions [79] with speed $v^* = 2$ and width[3] $w = 4v^*$, and these travelling wave solutions have the approximate form

$$n(x,t) \sim \frac{1}{1 + \mathrm{e}^{(x - v^* t)/v^*}}. \tag{3.5}$$

In fact, many other initial conditions also lead to asymptotic wavespeed $v_{\text{asym}} = v^*$, even if the initial density is non-zero everywhere. Since the asymptotic solution is determined by the asymptotics of the initial condition, it is sufficient to require that the initial condition be sufficiently *steep*. If we can write the initial condition in the asymptotic form $n(x, t{=}0) \sim Ae^{-\lambda x}$ for $\lambda > 0$ and arbitrary $A > 0$, then *steep* initial conditions must decay exponentially with rate $\lambda > \lambda^*$, where $\lambda^* = 1$ is the asymptotic spatial decay rate (as found in § A.1.1). All initial conditions which satisfy this criterion will have asymptotic wavespeed $v_{\text{asym}} = v^*$, and approximate form as in Eq. 3.5 [79].

The condition for pushed fronts, $v_{\text{asym}} > v^*$, is that the initial condition must decay 'more slowly' than the asymptotic spatial decay rate. In this case, $\lambda < \lambda^*$, the travelling waves travel with asymptotic wave speed $v_{\text{asym}} = \lambda + \frac{1}{\lambda}$. These solutions with $v_{\text{asym}} > v^*$ have the approximate asymptotic form [79]

$$n(x,t) \sim \frac{1}{1 + \mathrm{e}^{\zeta}} + \frac{\mathrm{e}^{\zeta}}{v_{\text{asym}}^2 (1 + \mathrm{e}^{\zeta})^2} \ln\left[\frac{4\mathrm{e}^{\zeta}}{(1 + \mathrm{e}^{\zeta})^2}\right], \tag{3.6}$$

where $\zeta = x/v_{\text{asym}} - t$.

[3] width being defined as the inverse steepness of the wavefront

3.3.2 Infection pathways: specifying initial and boundary conditions

Returning to Eq. 3.1, by redimensionalising the results of §3.3.1 (see §A.1.1) we see that the linear spreading velocity is $v^* = 2\sqrt{r_S D_S}$. Thus, for initial conditions with compact support, the solutions are travelling waves, with velocity $v = 2\sqrt{r_S D_S}$, width $w = 8\sqrt{D_S/r_S}$, and approximate form

$$n(x,t) \sim \frac{\kappa_S}{1 + \mathrm{e}^{(\sqrt{r_S/4D_S}x - r_S t)}}. \tag{3.7}$$

Many of the infection pathways discussed in Chapter 2 satisfy this condition of compact support (that is, they satisfy Eq. 3.4). In fact, infections that originate at the skin (a bacterial reservoir at the 'bottom' of the extraluminal surface), drainage bag (a bacterial reservoir at the 'bottom' of the intraluminal surface) or bladder (i.e., a dynamic, growing, bacterial reservoir at the top of the catheter), as well as the delta condition at the bottom of the catheter as considered in Figure 3.3, all satisfy compact support. This may be surprising, given that several of these scenarios are formulated as boundary conditions for the bacterial density rather than as initial conditions (i.e., are not only a condition at $t = 0$ – an initial condition, as required by Eq. 3.4 – but rather must be true at all times), but we can see that compact support holds for these three boundary conditions by the following graphical argument.

The boundary condition may be static (as in the case of the skin acting as a reservoir), or dynamic (as in the case of bacterial growth within the bladder). Regardless, we can without loss of generality, write this boundary condition as $n(x{=}0,t) = b(t)$. In all the scenarios discussed in the previous paragraph, the catheter is assumed to be clean at time $t = 0$, such that the initial condition is $n(x,t{=}0) = b(0)\delta(x)$. This is a perturbation to the unstable zero state, which will spread at a speed no less than v^*. As this perturbation spreads it will grow, according to the nonlinear behaviour of Eq. 3.1. If this initial perturbation corresponds to a single bacterium (since there is no physical meaning to a perturbation that is smaller than a single bacterium), then there is some finite distance[4] $x_1 = \mathcal{B}$ and finite time t_1, such that $n(x_1,t_1) \approx \kappa_S$. Since

[4]If we consider Eq. 3.1, the nature of the nonlinear logistic term is such that although $n(x,t) \to \kappa_S$, it does not converge in finite time or distance. However, since bacteria are discrete and finite, in practice n has finitely many possible values, and hence converges in finite time/distance. Within our simulations we define $\mathcal{B}$ as the distance x at which $n(x{=}\mathcal{B}, t{\to}\infty) = 0.999\kappa_S$, when there is a fixed boundary condition of $n(x{=}0,t) = 1$ mm^{-2}. This scales with

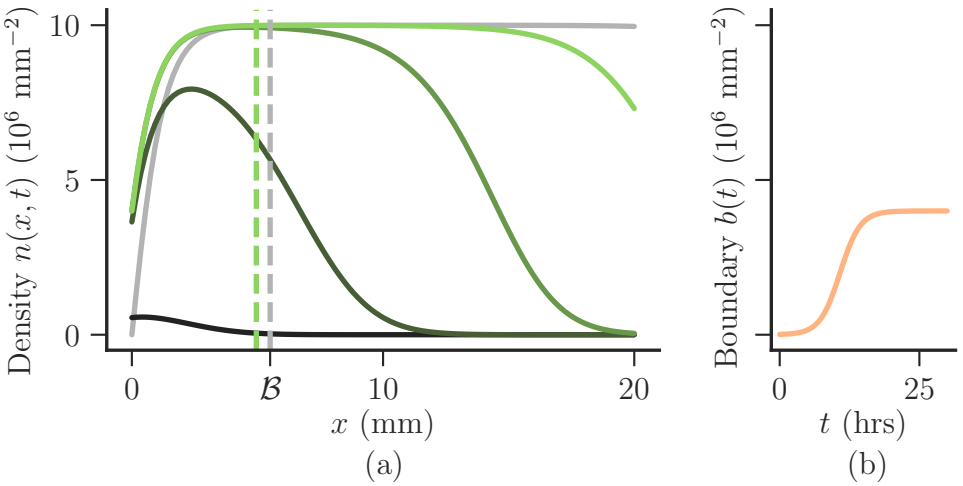

Figure 3.4 *The maximal boundary effect distance for bacterial density wavefronts on a catheter. (a) Eq. 3.1 simulated with a time dependent boundary, $b(t)$ (Eq. 3.8 – shown in (b)) at the origin, and a reflecting boundary $\partial n/\partial x = 0$ at $x = 140$ mm. Parameters are as in Table 2.2, with the exception of D_s, which here is 10^{-4} mm^{2}s^{-1}. In green is the bacterial density profile on the catheter after 7.5(▬), 15(▬), 22.5(▬) and 30(▬) hrs. In grey (▬) is the long-time behaviour of Eq. 3.1 with the same parameters, but with instead a fixed boundary of $n(0,t) = 1$ mm^{-2}. The grey vertical line (- -) shows the maximal boundary effect distance $\mathcal{B}$. Next to it, the green vertical line (- -) is the position at which $n(x, 30)$ has attained $0.999\kappa_S$ – illustrating how x_1 may shift leftwards. (b) The dynamic boundary condition applied in (a): Eq. 3.8.*

$n(x,t) = \kappa_S$ is the stable state for Eq. 3.1, we have for all $x > x_1$ and $t > t_1$ that $n(x,t)$ is independent of anything left of x_1, i.e. independent of the boundary conditions. Since a single bacterium was the smallest possible perturbation, the only possible effects of changing the boundary condition (i.e., increasing the size of the perturbation) is to drive x_1 leftwards, closer to the origin. The distance $\mathcal{B}$, set by the limit of a single discrete bacterium perturbation, is the maximal boundary effect distance, just as v^* is the minimal asymptotic speed.

In Figure 3.4 we illustrate this argument with an example. We simulate Eq. 3.1 (Figure 3.4a) for a boundary condition that has logistic form (Figure 3.4b),

$$b(t) = \frac{0.4\kappa_S \mathrm{e}^{0.8 r_S t}}{4 \cdot 10^{-4} \kappa_S + \mathrm{e}^{0.8 r_S t}}, \tag{3.8}$$

chosen to approximate the behaviour of the bacterial density in the bladder (Chapter 4). We see that after some time t_1, the density attains a value $n(x_1, t_1) \approx \kappa_S$ at some position x_1. To the right of this point, the density wave solution propagates as if from an initial condition $n(x{-}x_1{=}0, t{-}t_1{=}0) = \kappa_S$, i.e. independently of the values of the density profile $n(x{<}x_1, t)$. This position x_1 can be seen to lie closer to the origin than $\mathcal{B}$ (superimposed in grey in Figure 3.4a).

The only infection pathway that does not have compact support over the extraluminal surface is the scenario in which the catheter is contaminated at time of insertion, so that there is non-zero bacterial density over the entire extraluminal catheter surface. If the initial contamination is sufficiently uniform, then there will be no travelling wave solutions. Assuming non-uniform initial contamination, then the behaviour of the travelling wave solutions is determined by the asymptotic behaviour of the initial conditions, as discussed earlier in §3.3.1.

3.3.3 Relaxation behaviour and timescales

All the wavespeeds we have discussed so far in this chapter are asymptotic wavespeeds. The true solutions converge towards these asymptotic wavespeeds rapidly following some establishment time, $\mathcal{T}$. These establishment times scale logarithmically with the initial condition (Figure 3.5), $\mathcal{T} \sim \log(\kappa_S/n_0)$, which

the 'width' of the pulled solutions we have discussed earlier: $8\sqrt{D_S/r_S}$. We might worry about whether this boundary effect distance is actually small relative to the system size: the catheter length L. For $D_S = 10^{-4}$, $\mathcal{B} \approx 5$ mm. And for $D_S = 10^{-8}$, $\mathcal{B} \approx 0.05$ mm. Comparing these to the lengths of a catheter, 40 - 200 mm, we see that $\mathcal{B}$ is indeed small.

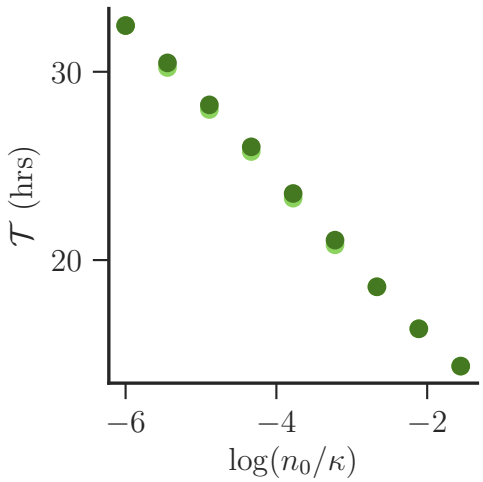

Figure 3.5 *The solutions to Eq. 3.1 relax to the asymptotic form of Eq. 3.7 following an establishment time $\mathcal{T}$. Plotted is $\mathcal{T}$ for varying initial condition, $n(x,0) = n_0\delta(x)$, for D_S equal to 10^{-8} (●) and 10^{-4} (●) mm^2s^{-1}. All other parameters are as in Table 2.2.*

emerges from the scaling behaviour of the linearised form of Eq. 3.1. In fact, the wavespeeds relax exponentially to the asymptotic wavespeed from above [117]. We can think of this as the wavefront being initially pushed by the nonlinear behaviour close to the front, due to the steepness of the initial conditions. This nonlinear front is then overtaken by the linear spreading front, so the relaxation time is the speed at which the linear front overtakes the nonlinear front. The timescale that this occurs over, $\mathcal{T} \sim 30$ hrs, is small compared to the overall timescale of the wave travelling over the catheter (e.g. $L/v^* \sim 4000$ hrs for parameter values as in Table 2.2) for most parameter values (this is not true for $L/v^* \sim 40$ hrs when $D_s = 10^{-4}$ mm^{3}s^{-1} and $L = 40$ mm), so we can generally consider the timescale of bacterial ascension of the catheter to simply be the time associated with the FKPP wavespeed, L/v^*.

3.4 Summary

The spread of bacteria over the extraluminal surface of the catheter is modelled by the one-dimensional FKPP equation (Eq. 3.1):

$$\frac{\partial n}{\partial t} = D_S \frac{\partial^2 n}{\partial x^2} + r_S n \left(1 - \frac{n}{\kappa_S}\right),$$

where $n(x,t)$ is the bacterial surface density, D_S is the diffusivity of the bacteria on the catheter surface, r_S is the bacterial growth rate on the catheter surface, and κ_S is the bacterial carrying capacity of the catheter surface.

This equation supports travelling wave solutions for many initial conditions, with the propagation direction of the wave carrying information on the location of the initial contamination. Where the initial condition is mostly zero, with contamination limited to a small region, an approximate form of the wave profile can be written, and these solutions have wave speed $2\sqrt{r_S D_S}$.

The dimensionless number $\rho = r_S L^2/D_S$ is the ratio of the growth timescale to the motility timescale, and scales with the ratio of wavewidth to catheter length – parameterising the shock-like behaviour of the system. The motility of the bacteria is captured by an effective diffusion term, with the different possibilities for both catheter surface properties and bacterial motility resulting in an extremely large parameter space for D_S, spanning 5+ orders of magnitude. Since the ratio of the growth timescale to the motility timescale, $\rho \sim 1/D_S$, this also implies a large physical range for ρ in this system. This has implications for the numerical stability of the system, as well as for any estimates of the timescales of infections.

For most parameterisations (excluding the case of short urethral length and high bacterial motility), the timescale of bacterial ascension of the catheter is approximately the time taken for the asymptotic FKPP wave to travel the length of the catheter: $L/v^* = L/2\sqrt{r_S D_S}$. The distance over which the waveform approaches its asymptotic form, $\mathcal{B}$, is small relative to L for all physically relevant parameters, so we can more accurately consider the timescale of bacterial ascension to be the timescale of the asymptotic wave plus the establishment time over which the wave relaxes to the asymptotic form: $\mathcal{T} + L/v^*$.

Chapter 4

Modelling the bladder

4.1 Introduction

The bladder is an elastic balloon-like volume which, under normal circumstances, periodically fills and empties. At any moment the volume of the bladder is equal to the volume of urine contained within it, i.e., there is no air or 'empty space' within the bladder. The filling of the bladder is controlled by the rate of urine production by the kidneys, which is continuous but variable. In the absence of excess fluid intake, the kidneys produce urine at a rate of 1 mL min^{-1} [31], however the rate may be much higher after the intake of fluids.

When a continuously draining (Foley) catheter is introduced to this system the normal cycle of filling and emptying is disrupted [64]. The balloon of a Foley catheter causes some urine to be retained [30], as the eyelets of the catheter sit some distance above the base of the bladder (Figure 1.2). Additionally, pressure differentials, often caused by kinks in the tubing, mean that the catheter frequently fails to drain the bladder [40]. As a result, there is a roughly constant sump of residual urine within the bladder. There is no consensus on typical values for this volume, only a claim by Feneley et al. [31] of a range of 10–100 mL. In immobile patients with indwelling catheters, residual volumes as high as 500 mL have been recorded [40], with the mean volume closer to 100 mL. Even in the absence of a catheter, the bladder is known to retain a small volume of urine [43], and studies on intermittent catheterisation[1] have found mean residual volumes

[1] *intermittent catheterisation* – a catheter is inserted and left in place only long enough for full drainage of the bladder ($\sim$ 1 min)

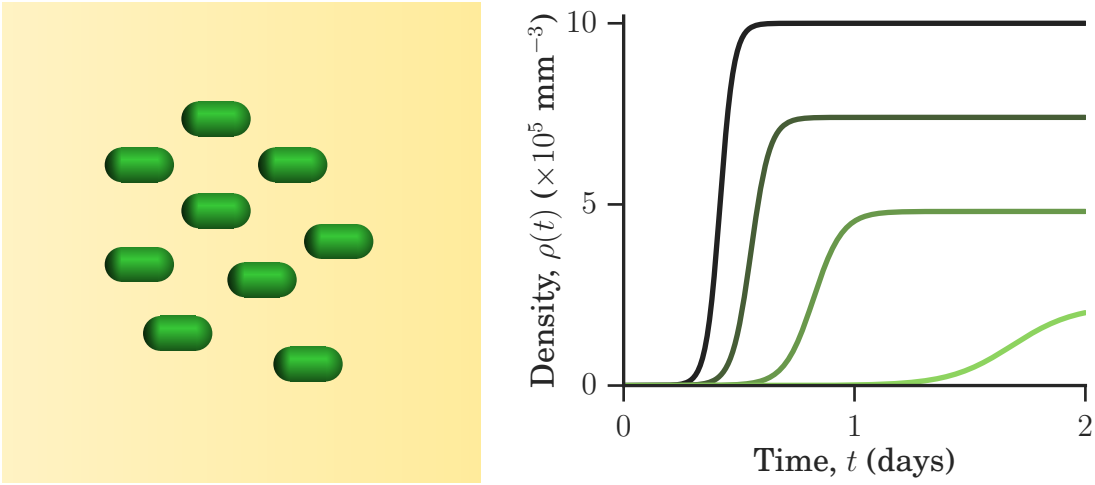

(a) **(b)**

Figure 4.1 *(a) Bacteria grow in residual urine within the bladder. (b) Behaviour of Eq. 4.3, with an initial inoculation of* 1 mm^{-3}*, subject to different dilution rates* k_D*. Each curve is a numerical solution for the bacterial density, with dilution rates of 0 (▬), 1 (▬), 2 (▬), and 3 (▬)* $\times 10^{-4} s^{-1}$ *respectively. Other parameters are as given in Table 2.2.*

in the range of $5 - 25$ mL [8, 63]. Within this chapter, we assume the volume of the residual urine sump to be 50 mL (as in Table 2.2).

Under normal conditions the periodic cycle of the bladder results in the urethra being regularly flushed, helping to prevent the adhesion of bacteria. In the presence of a catheter this is no longer the case. To make matters worse still, the catheter erodes the mucosal surface of both the bladder and urethra: surfaces that would otherwise have provided some protection against bacterial adhesion [30].

4.2 A mathematical model

Previous work by Gordon and Riley [43] assumed exponential bacterial growth in a model for micturition (urination) dynamics and urinary tract infection. Since bacteria replicate by division, exponential growth is the simplest possible model for bacterial population growth,

$$\frac{dN}{dt} = rN, \tag{4.1}$$

where N is the population size, and r the growth rate. However, an exponential growth model is unbounded, rapidly tending toward infinite bacterial densities, rendering it appropriate only for short timescales. Logistic growth represents the simplest modification that can be made to an exponential growth model to enforce an upper bound on the population density [79]:

$$\frac{dN}{dt} = rN\left(1 - \frac{N}{\kappa}\right), \tag{4.2}$$

where κ is the carrying capacity – the maximum population size supported by the environment. For the logistic growth model, in the limit of late time, the population size achieves a steady state $N = \kappa$.

While the logistic growth model is simple, it has no mechanistic justification. An alternative model would be that of a chemostat: a device in which bacteria grow under conditions of continuous dilution [92], which closely resembles the situation of bacterial growth in a catheterised bladder. Chemostat theory predicts the dynamics of the bacterial population and the nutrient concentration in such a device. However, chemostat theory describes bacterial growth only on a single, simple limiting substrate, e.g., glucose as the sole carbon source. Urine is not a simple substrate, and no chemostat model has yet been developed to describe quantitatively bacterial growth on media with multiple nutrient sources, such as urine. As a minimal model, therefore, assuming logistic growth dynamics may be a reasonable approximation.

Bacteria proliferate in the residual sump of urine that remains in the bladder during catheterisation [30, 31, 40] (Figure 4.1a; §Bacteriuria), and then are removed from the bladder by urine flow. Assuming the residual urine in the catheterised bladder to be well-mixed and of constant volume, we model bacterial dynamics with a logistic growth equation, supplemented by a dilution term [79]:

$$\frac{d\rho}{dt} = \underbrace{r_B\rho\left(1 - \frac{\rho}{\kappa_B}\right)}_{\text{growth}} - \underbrace{k_D\rho}_{\text{dilution}}. \tag{4.3}$$

Here, $\rho(t)$ is the bacterial volume density at time t, r_B is the (maximum) growth rate of the bacteria in urine, and κ_B is the carrying capacity of urine. The dilution rate is given by $k_D = \frac{\lambda}{V}$, where λ is the rate of urine production by the kidneys, and V is the volume of residual urine in the bladder (see Table 2.2). The behaviour of Eq. 4.3 is illustrated in Figure 4.1b for numerical simulations

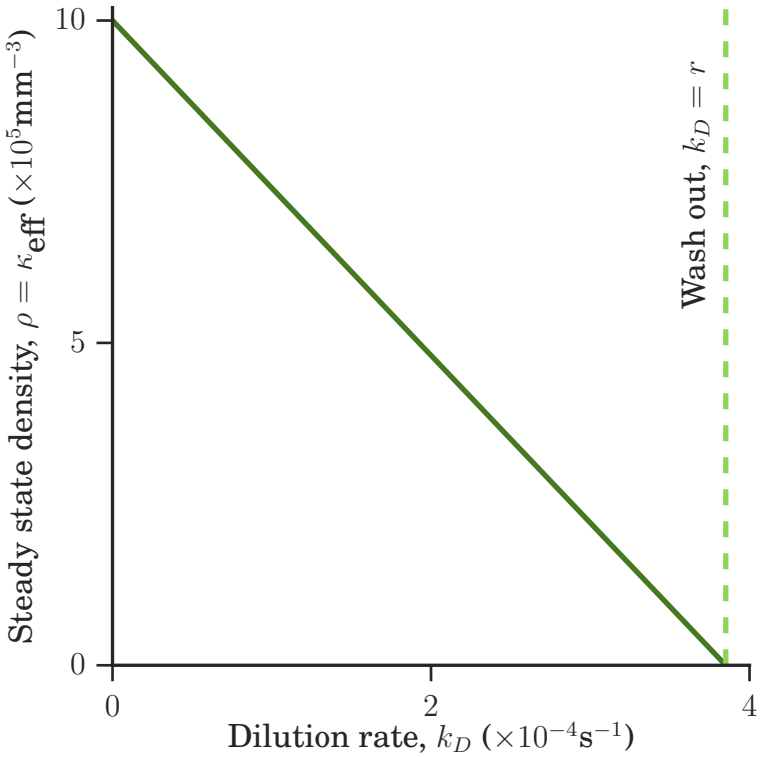

Figure 4.2 *The dependence of the steady state solution of Eq. 4.3, $\rho = \kappa_{eff}$, on the dilution rate, k_D. The steady state bacterial density decreases linearly as the dilution rate increases. A washout transition occurs at $k_D = r_B$, marked here by a vertical line (--).*

(§6.3.2, §A.2.2) of several different values of the dilution rate, where the initial condition of $\rho(0) = 1$ mm^{-3} is equivalent to the presence of 10^3 CFU/mL bacteria within the urine (recall from §1.3 that CFU = colony forming units).

The bacterial volume density $\rho(t)$ within the bladder has dimensions $[\rho] = \text{L}^{-3}$ (recall Table 2.1). The total number of bacteria within the bladder at a given time is then

$$N_b(t) = \int \rho \, \text{d}V_b = V \, \rho(t). \tag{4.4}$$

4.3 Establishment criterion for bacterial growth: criticality of the dilution rate

As we show in Figure 4.1b, modifying the dilution rate alters both the stationary state bacterial density within the bladder and the time taken to attain that steady state. In fact, from the form of Eq. 4.3 one can infer the existence of a washout

transition; occurring at $k_D = r_B$ – we discuss this transition in detail in §4.3.1. Washout is a phenomenon observed in continuous culture: when bacteria grow in continuously diluted medium it is well known that a bacterial population can only be sustained for dilution rates less than the bacterial growth rate [3, 92]. This transition is illustrated in Figure 4.2, where the stationary state of the bacterial density (i.e., the sustained bacterial population within the bladder) falls to zero for dilution rates greater than the bacterial growth rate.

4.3.1 Rescaled logistic growth

To see how this washout phenomenon arises from Eq. 4.3, we rearrange the equation to obtain a rescaled logistic growth equation:

$$\begin{aligned} \frac{d\rho}{dt} &= (r_B - k_D)\rho\left(1 - \frac{r_B\rho}{(r_B - k_D)\kappa_B}\right) \\ &= r_{\text{eff}}\rho\left(1 - \frac{\rho}{\kappa_{\text{eff}}}\right). \end{aligned} \tag{4.5}$$

Here we have identified an effective growth rate

$$r_{\text{eff}} = r_B - k_D, \tag{4.6}$$

and an effective carrying capacity

$$\kappa_{\text{eff}} = \frac{(r_B - k_D)\kappa_B}{r_B}. \tag{4.7}$$

Therefore, by analogy with logistic growth [79], we must have a stationary state bacterial density equal to κ_{eff}, i.e., $\kappa_B(1 - \frac{k_D}{r_B})$. Hence as $k_D \to r_B$, $\kappa_{\text{eff}} \to 0$, and the stationary state bacterial density goes to zero. At the same time, the time taken to achieve the stationary state increases, because $r_{\text{eff}} = r_B - k_D$. That is, the bacteria grow slower, and reach a lower population density, as the dilution rate increases.

Since the solution to the logistic equation is known (see §A.2.1), through this rescaling argument we can also obtain the dynamics of the bacterial density within

the bladder:

$$\begin{aligned}\rho(t) &= \frac{\kappa_{\text{eff}}\rho_0 \mathrm{e}^{r_{\text{eff}}t}}{\kappa_{\text{eff}} + \rho_0(\mathrm{e}^{r_{\text{eff}}t} - 1)} \\ &= \frac{(r_B - k_D)\kappa_B\rho_0 \mathrm{e}^{(r_B - k_D)t}}{(r_B - k_D)\kappa_B + r_B\rho_0\left(\mathrm{e}^{(r_B - k_D)t} - 1\right)},\end{aligned} \tag{4.8}$$

where ρ_0 is the bacterial density at time $t = 0$.

We can now see that the value of the dilution rate is critical to the behaviour of this model: governing both the bacterial steady state density in the bladder, and the timescale over which the steady state is attained. This dependence of the model on the dilution rate is very similar to the behaviour of other (uncatheterised) micturition models, where there is a critical relationship between the urine dilution rate and the bacterial growth rate [43].

4.3.2 A simple model for micturition dynamics leading to an establishment criterion for bacterial growth

In 1992, Gordon and Riley [43] presented a mathematical model of human micturition dynamics and bacterial growth, which they used to predict an establishment criterion for infection in the absence of adhesin-mediated surface growth. As we discussed in §1.5, in the model of Gordon and Riley the bladder is assumed to periodically fill and empty, with a minimum volume V_n, a maximum volume V_x, and a filling rate λ. Thus the volume of urine in the bladder is given by

$$V(t) = V_n + \lambda t, \qquad t \in \left[0, \tau = \frac{V_x - V_n}{\lambda}\right). \tag{4.9}$$

Assuming exponential bacterial growth, in the time between micturition events, the number of bacteria in the bladder is given by

$$N(t) = N_0 \exp\left(r_B t\right), \tag{4.10}$$

where r_B is the bacterial growth rate within the bladder and N_0 is the number of bacteria present in the residual urine at the start of the time interval. Then, with N_k being the population after k micturition events, the bacterial population

after the $k+1$th micturition event is given by

$$N_{k+1} = \frac{V_n}{V_x} N_k \exp\left(\frac{r_B(V_x - V_n)}{\lambda}\right). \tag{4.11}$$

The 'establishment criterion' is that $N_{k+1} > N_k$, i.e., that the population should grow in successive cycles. This establishment criterion implies a condition on the growth rate:

$$r_B > \log\left(\frac{V_x}{V_n}\right) \frac{\lambda}{V_x - V_n}. \tag{4.12}$$

This work by Gordon and Riley is relevant to, but differs substantially from, my own work. First, Gordon and Riley's model does not consider the case of a urinary catheter. Additionally, their model applies only at early times when the infection is still establishing. Their assumption of exponential growth results in an unbounded bacterial population that rapidly diverges in an unphysical manner. However, I have applied their methodology to explore my own model for the bacterial dynamics of the bladder in the presence of a urinary catheter (§4.3.3).

4.3.3 Establishment criterion for bacterial growth in the presence of a catheter

In establishing Eq. 4.3 we took a continuum description of the bacterial and urine dynamics in the bladder. Here we shall show that our model (Eq. 4.3) is equivalent to applying the modelling methodology of Gordon and Riley to the case of a catheterised bladder (where the time interval between micturition events goes to zero).

Catheterised exponential bacterial growth

Gordon and Riley presented a model for the bladder in which the volume of urine varies periodically between defined minimal and maximal values. When a catheter is added to the system this is no longer the case. Simplistically applying the approach of Gordon and Riley, we might assume that the bladder now empties at the same rate as it fills (a rate we denote by λ), and hence that $V_x = V_n$. Following through with this assumption we see that $N_{k+1} \equiv N_k$, i.e., that the bacterial population is in equilibrium.

Instead let us consider the limit of $V_x \to V_n$. Now we can write

$$t \in [0, \varepsilon)\,, \qquad \varepsilon \to 0, \tag{4.13}$$

where ε is a small variable. Then using that $V_x = V_n + \lambda\varepsilon$ (from Eq. 4.9), we can apply Eq. 4.11 to write

$$N_{k+1} = \left(1 - \frac{\lambda\varepsilon}{V_n + \lambda\varepsilon}\right) N_k \exp(r_B\varepsilon). \tag{4.14}$$

Therefore, the establishment criterion for bacterial growth becomes

$$r_B > \log\left(1 + \frac{\lambda\varepsilon}{V_n}\right)\frac{1}{\varepsilon}. \tag{4.15}$$

By Taylor expanding $\log(1+x) = x - \frac{1}{2}x^2 + \ldots$, we find

$$r_B > \frac{\lambda}{V_n} - \frac{\lambda^2}{2V_n^2}\varepsilon + \ldots. \tag{4.16}$$

And hence as $\varepsilon \to 0$, our criterion is simply

$$r_B > \frac{\lambda}{V_n}. \tag{4.17}$$

In other words, to remain in the bladder, bacteria must grow faster than they are diluted out. This is exactly the washout phenomenon that we discussed in § 4.3.1.

Logistic bacterial growth

In deriving Eq. 4.17, we assumed exponential bacterial growth. However, as we discussed in §4.2, exponential growth is not a physical model for growth within the bladder, while logistic growth is more suitable (Eq. 4.2). As discussed above (§4.3.1), in the limit of late time, the logistic growth model (Eq. 4.2) achieves a steady state $N = \kappa_B$, and with the initial condition $N(0) = N_0$ it has the solution (see §A.2.1)

$$N(t) = \frac{N_0\kappa_B \exp(r_B t)}{\kappa_B + N_0\left(\exp(r_B t) - 1\right)}. \tag{4.18}$$

We can follow through the argument of Gordon and Riley for the uncatheterised bladder with periodic micturition dynamics, this time applying it to the case of

logistic growth:

$$N_{k+1} = \frac{V_n N_k}{V_x} \cdot \frac{\kappa_B \exp(r_B \tau)}{\kappa_B + \frac{V_n N_k}{V_x}(\exp(r_B \tau) - 1)}, \tag{4.19}$$

where τ is as defined in Eq. 4.9, $\tau = (V_x - V_n)/\lambda$. The growth condition is $N_{k+1} > N_k$, so we have

$$\frac{V_n}{V_x} \cdot \frac{\kappa_B \exp(r_B \tau)}{\kappa_B + \frac{V_n N_k}{V_x}(\exp(r_B \tau) - 1)} > 1, \tag{4.20}$$

which can be rearranged to find

$$r_B > \log\left(\frac{V_x \kappa_B - V_n N_k}{V_n(\kappa_B - N_k)}\right)\frac{1}{\tau}. \tag{4.21}$$

Unlike in the exponential case, here we see that the condition for sustained growth in the bladder depends on the current bacterial population size, and that there is no growth rate r for which the population will always increase. This isn't a surprise, given that logistic growth is by nature self-limiting.

Catheterised logistic bacterial growth

Now once again we can introduce a catheter to the system and consider the limit in which the time interval for micturition goes to zero: $t \in [0, \varepsilon)\,,\ \varepsilon \to 0$. Again, using the fact that $V_x = V_n + \lambda\varepsilon$, and rearranging some terms, we obtain

$$\begin{aligned} r_B &> \log\left(\frac{\kappa_B(V_n + \lambda\varepsilon) - N_k V_n}{V_n(\kappa_B - N_k)}\right)\frac{1}{\varepsilon} \\ &= \log\left(1 + \frac{\kappa_B \lambda \varepsilon}{V_n(\kappa_B - N_k)}\right)\frac{1}{\varepsilon} \\ &= \frac{\kappa_B \lambda}{V_n(\kappa_B - N_k)} - \frac{1}{2}\left(\frac{\kappa_B \lambda}{V_n(\kappa_B - N_k)}\right)^2 \varepsilon + \dots \end{aligned} \tag{4.22}$$

Note that the above Taylor expansion is valid for $0 < \varepsilon < \frac{V_n(\kappa_B - N_k)}{\kappa_B \lambda}$, and so it does not hold for $N_k \geq \kappa_B$. In fact, for $N_k \geq \kappa_B$ it is obvious that there can be no value of the growth rate for which the population increases. This is because logistic growth enforces the population maximal bound of κ_B through the nonlinear term $r_B N_k(1 - N_k/\kappa_B)$, so when the population size N_k exceeds κ_B, any non-zero value of the growth rate r_B results in a negative rate of change of population size.

Now, taking the limit $\varepsilon \to 0$ (our 'catheterisation limit'), we obtain a condition on the growth rate for sustained bacterial growth of

$$r_B > \frac{\kappa_B \lambda}{V_n(\kappa_B - N_k)}. \tag{4.23}$$

In the limit $N_k \ll \kappa_B$ (a small population that is not close to the carrying capacity) the logistic growth model tends to exponential growth, and the condition is once again more simply

$$r_B > \frac{\lambda}{V_n}. \tag{4.24}$$

In the context of a catheterised bladder, this inequality is a property of the washout transition mentioned in §4.3: that the bacterial population size will increase only if the bacteria grow faster than they are diluted out of the bladder.

Stationary state

From Eq. 4.23 we see that for the scenario of logistic growth in a catheterised bladder, the stationary state solution is no longer $N = \kappa_B$, as it was in the case of simple logistic growth[2]. The maximum value of the population size N occurs at the limit of Eq. 4.23, i.e., when

$$r_B = \frac{\kappa_B \lambda}{V_n(\kappa_B - N)}. \tag{4.25}$$

Hence, in this model the stationary state is now

$$N = \kappa_B \left(1 - \frac{\lambda}{V_n r_B}\right). \tag{4.26}$$

We can compare this to the stationary state we found in §4.3.1, which also corresponded to logistic growth with dilution (Eq. 4.7):

$$\kappa_{\text{eff}} = \frac{(r_B - k_D)\kappa_B}{r_B}.$$

[2]We can also find the maximum population in the non-catheterised logistic growth case, by assuming that the growth criterion in Eq. 4.21 fails exactly:

$$N = \kappa_B \left(\frac{\exp(r_B\tau) - \frac{V_x}{V_n}}{\exp(r_B\tau) - 1}\right); \qquad \tau = \frac{V_x - V_n}{\lambda}.$$

Since $k_D := \lambda/V$, we see that the two steady state solutions, Eq. 4.7 and Eq. 4.26 are in fact the same state (for $V = V_n$).

Washout condition emerges from the 'population growth rate'

The above discussion was framed around the concept of a bacterial growth rate r_B, which characterises exponential growth of a bacterial strain on a given medium; we then used the logistic term to describe saturation of growth at large population sizes. An alternate framing of the same logistic model is to define a 'population growth rate' $r_{\text{pop}} := r_B\left(1 - \frac{N}{\kappa_B}\right)$, giving

$$\frac{dN}{dt} = r_{\text{pop}}(N)N. \tag{4.27}$$

Now we find in the steady state that the population growth rate is given by

$$\begin{aligned} r_{\text{pop}} &= r_B\left(1 - \frac{N}{\kappa_B}\right) \\ &= r_B\left(1 - \left(1 - \frac{\lambda}{V_n r_B}\right)\right) \\ &= \frac{\lambda}{V_n}. \end{aligned} \tag{4.28}$$

This is of course exactly what we expect for the steady state of a bacterial population in a diluting medium: that the growth of the population equals the 'wash-out' rate.

4.4 Summary

Assuming the residual urine in the catheterised bladder [30, 31, 40] to be well-mixed and of constant volume, we model bacterial dynamics in the bladder with a logistic growth equation, supplemented by a dilution term [79], Eq. 4.3:

$$\frac{d\rho}{dt} = r_B\rho\left(1 - \frac{\rho}{\kappa_B}\right) - k_D\rho.$$

Here, $\rho(t)$ is the bacterial volume density at time t, r_B is the (maximum) growth rate of the bacteria in urine, and κ_B is the carrying capacity of urine. The dilution rate is given by $k_D = \frac{\lambda}{V}$, where λ is the rate of urine production by the kidneys,

and V is the volume of residual urine in the bladder (see Table 2.2) .

The value of the dilution rate is critical to the behaviour of this model, governing a transition (at $k_D = r_B$) between an 'infected' (bacteriuric) non-zero state and a 'washed-out' zero state. As we showed in §4.3.3, this model (Eq. 4.3) is equivalent to a logistic modification to the model for micturition dynamics and bacterial growth proposed by Gordon and Riley [43], in the limit of the micturition interval τ tending to zero, where the maximal volume tends to the minimal volume, $V_x \to V_n$.

Chapter 5

Modelling the intraluminal flow & surface

5.1 Introduction

Urine leaving the bladder flows through the catheter lumen, transporting bacteria downwards. Some bacteria become stuck to the catheter surface, where they form a biofilm. These biofilms on the inside of the catheter are particularly troublesome, as they may result in the blockage of the catheter. The most problematic of these blockages are crystalline (formed by precipitates arising from the alkalisation of the urine by *P. mirabilis*, recall §1.2), however even the more viscous biofilms formed by *E. coli* can disrupt flow and alter the performance of the catheter [30, 111]. Any biofilm can also act as a reservoir for bacteria, resulting in frequent reinfections of the bladder, and are often resistant to antibiotic treatment [9]. In our model, the biofilm is assumed to be thin, such that it does not alter the flow profile of urine within the catheter. The bacterial density becoming too high for this to be a reasonable assumption is taken as an end state for the model.

Figure 5.1 shows some examples of bacteria colonising the intraluminal surface of a catheter. These images were taken with Mesolens [76], in collaboration with the group of Gail McConnell (Strathclyde University), and show *E. coli* biofilms that were allowed to colonise a catheter for 24 hours *in vitro*. For full details of how these samples were prepared and images obtained, see §A.3.6.

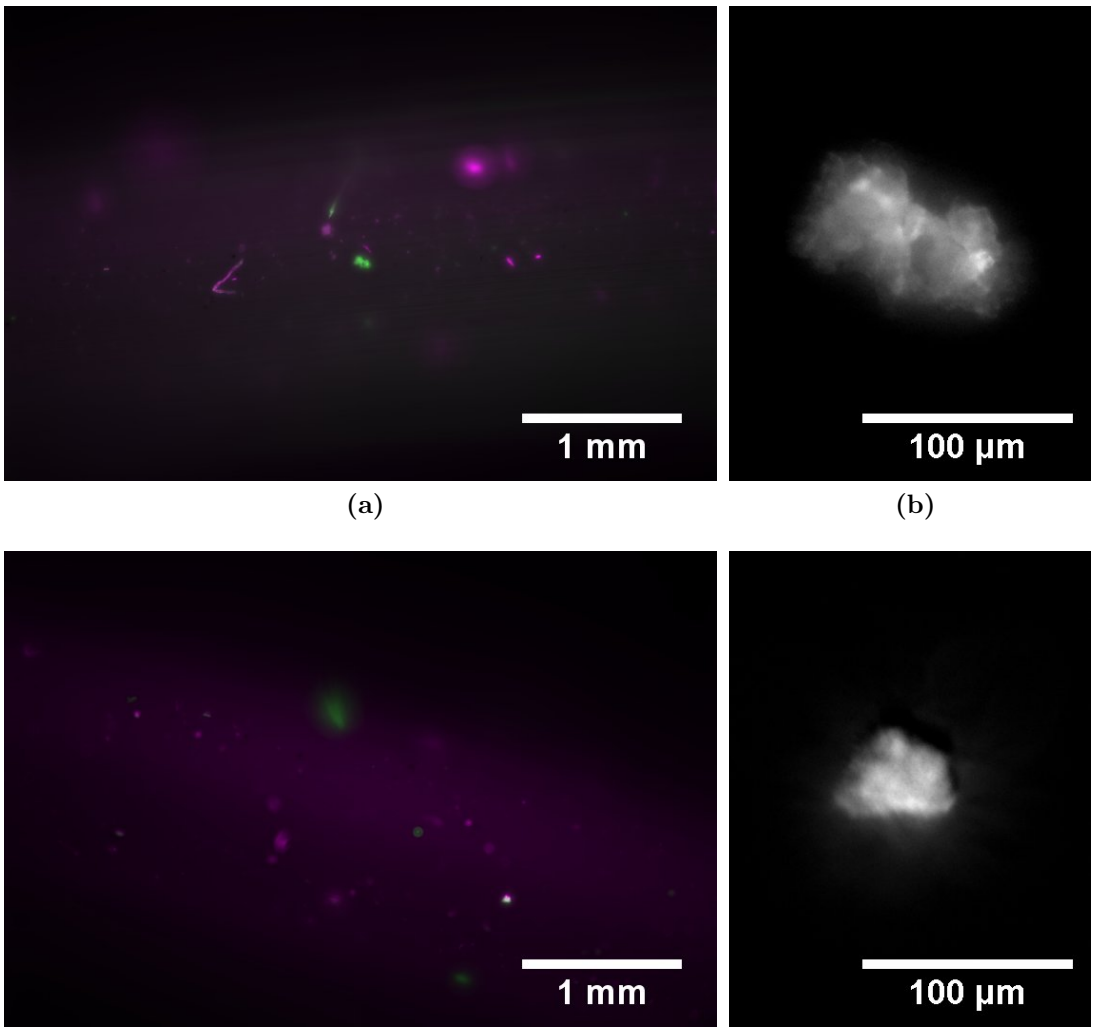

Figure 5.1 *Fluorescence images of E. coli biofilms grown on the intraluminal surface of urinary catheters. (a) A 6 mm catheter segment. In green are biofilms formed by E.coli strain AD51, in magenta is the background fluorescence of the catheter. (b) Enlarged AD51 biofilm image, cropped from (a). (c) A 6 mm catheter segment. In green are biofilms formed by E.coli strain RJA002, in magenta is the background fluorescence of the catheter. (d) Enlarged RJA002 biofilm image, cropped from (c).*

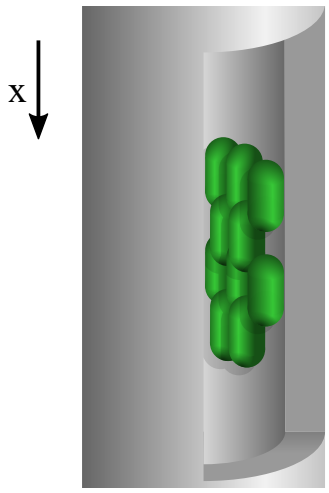

Figure 5.2 *Bacteria are deposited by the urine flow. They then grow and spread as a wave over the surface.*

5.2 A mathematical model

5.2.1 Bacterial growth on the intraluminal surface

We model the growth of bacteria on the intraluminal surface very similarly to our model for growth on the extraluminal surface (Chapter 3). Again, bacteria are growing and diffusing over the surface, as illustrated in Figure 5.2. However there is now an additional source term arising from the deposition of bacteria from the urine flow:

$$\frac{\partial m}{\partial t} = \underbrace{D_S \frac{\partial^2 m}{\partial x^2}}_{\text{motility}} + \underbrace{r_S m \left(1 - \frac{m}{\kappa_S}\right)}_{\text{growth}} + \underbrace{j(x)}_{\text{deposition}} . \tag{5.1}$$

Similarly to the extraluminal surface, $m(x,t)$ is the bacterial surface density (but note that x is now measured from top to bottom of the catheter – in the direction of urine flow); D_S, r_S, and κ_S are, as defined previously, the bacterial diffusivity, growth rate, and carrying capacity (Table 2.2). The additional term $j(x)$ is the source term representing the bacterial deposition flux, which couples the intraluminal surface to the urine flow. We will discuss the boundary conditions of Eq. 5.1 later in §6.3.3.

5.2.2 Dynamics of urine flow through a catheter

To find the form of the bacterial deposition flux, $j(x)$ in Eq. 5.1, we need to describe the bacteria within the intraluminal urine flow. First we must consider the behaviour of the urine flow itself. As discussed in §1.1, within the catheter, urine flows downwards at a rate equal to the production rate of the kidneys. This is typically around 1 mL min^{-1}, or 16.7 mm^3s^{-1} (see Table 2.2). The hydrodynamics of flow through a pipe is well-established, with its properties determined by its Reynolds number [118]. In §1.1, we calculated the Reynolds number for a 'typical' catheter of radius $R = 1$ mm, and urine flow rate of $\lambda = 1$ mL min^{-1}, to be $Re = 6$ (Eq. 1.2). Thus, the flow of urine through a catheter is laminar, and can be described by Eq. 1.4:

$$u(r) = \frac{2\lambda}{\pi R^4}\left(R^2 - r^2\right),$$

where λ is the rate of urine production by the kidneys, R is the internal radius of the catheter, and r is our radial coordinate. This results in the flow profile shown in Figure 1.3b.

We note that this laminar flow regime is the steady state for the established flow within a pipe; it does not describe the initial hydrodynamic inlet region (right at the top of the pipe). The distance downstream at which the flow has achieved 99% of its final axial velocity (and so can be said to be essentially laminar) is given by [69] $h \sim 0.1R \cdot Re$, which for the values discussed above in Eq. 1.2 is $h \sim 0.6$ mm. Compared to the typical lengths of catheters of $40 - 200$ mm, this length is negligible. Further, this initial region is also in the reality of complex geometry (i.e., catheter eyelets), which we are neglecting within this model.

5.2.3 Transport of bacteria within the intraluminal urine flow

When there is a (catheter-associated) urinary tract infection, the urine flow will transport bacteria downwards, as illustrated in Figure 5.3a, depositing some on the intraluminal surface of the catheter. The bacteria diffuse within the urine flow, with the bacterial flux onto the surface then being the depositional source term, $j(x)$, mentioned in Eq. 5.1.

When considering the bacterial dynamics within the intraluminal flow, we can neglect the growth of bacteria, as it occurs on timescales very much slower than

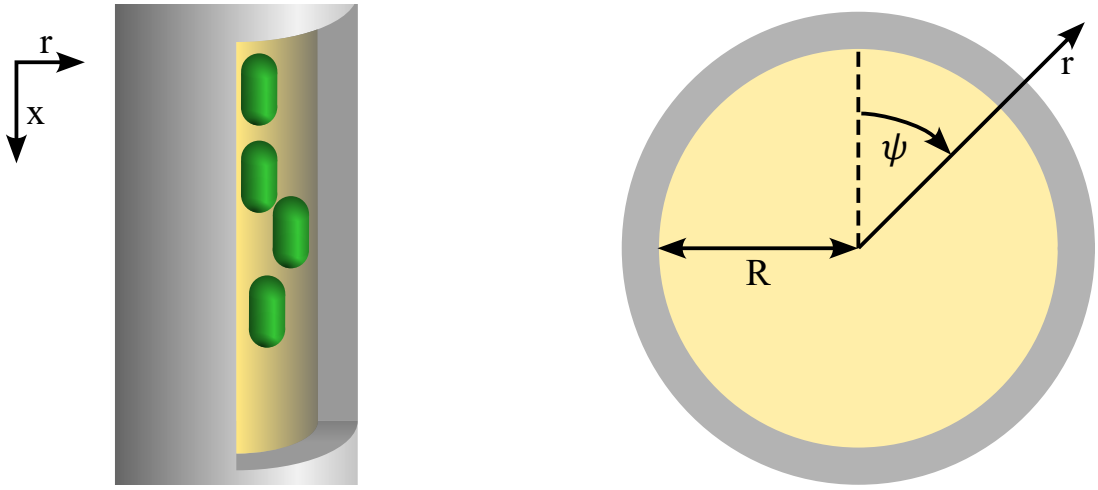

Figure 5.3 *(a) Urine transports bacteria downwards through the catheter. (b) The geometry of a cross section across the catheter. The catheter can be seen to have rotational symmetry, allowing us to neglect ψ.*

those of the fluid flow. The characteristic timescale of bacterial growth is the doubling time, $\tau_b = \frac{\log 2}{r} \sim 1800$ s. The timescale of the flow is the average time taken for urine to pass through the catheter, $\tau_c = \frac{\pi R^2 L}{\lambda} \sim 7$ s, so $\tau_c \ll \tau_b$. The characteristic timescales for the radial and longitudinal diffusive processes are $R^2/D_B = 1 \times 10^4$ s and $L^2/D_B = 1.6 \times 10^7$ s. Both of these processes are clearly much slower than the convective flow timescale (7 s). For this reason, we neglect longitudinal diffusion within the model, although radial diffusion cannot be neglected, as it has significant effects over small radial distances – such as close to the catheter wall.

The rotational symmetry of the catheter, as illustrated in Figure 5.3b, allows us to reduce the dimensionality of the problem, resulting in a 2-dimensional convection-diffusion equation [70, 112]:

$$\frac{\partial \sigma}{\partial t} = \underbrace{D_B \left(\frac{\partial^2 \sigma}{\partial r^2} + \frac{1}{r} \frac{\partial \sigma}{\partial r} \right)}_{\text{motility}} - \underbrace{u(r) \frac{\partial \sigma}{\partial x}}_{\text{flow}}. \tag{5.2}$$

Here $\sigma(r, x, t)$ is the bacterial volume density within the urine, D_B is the diffusivity of bacteria within urine, and $u(r)$ is the (Poiseuille) flow profile given by Eq. 1.4.

5.2.4 Full bacterial dynamics in the catheter lumen

Finally, we can obtain the bacterial deposition flux, $j(x)$, that appears within the description of the intraluminal surface growth in Eq. 5.1:

$$j(x) = -D_B \frac{\partial \sigma}{\partial r}\bigg|_{r=R}. \tag{5.3}$$

Gathering everything so far together, we have a system of equations describing the evolution of the bacterial density within the catheter lumen:

$$\begin{aligned}
\frac{\partial m}{\partial t} &= D_S \frac{\partial^2 m}{\partial x^2} + r_S m \left(1 - \frac{m}{\kappa_S}\right) + j(x) \\
j(x) &= -D_B \left.\frac{\partial \sigma}{\partial r}\right|_{r=R} \\
\frac{\partial \sigma}{\partial t} &= D_B \left(\frac{\partial^2 \sigma}{\partial r^2} + \frac{1}{r}\frac{\partial \sigma}{\partial r}\right) - u(r)\frac{\partial \sigma}{\partial x} \\
u(r) &= \frac{2\lambda}{\pi R^4}\left(R^2 - r^2\right)
\end{aligned} \tag{5.4}$$

Dimensions, densities and absolute bacterial numbers

In our model we consider the dynamics of bacterial densities, rather than absolute numbers of bacteria. This makes for generally simpler equations and is consistent with the continuum approach that we adopt here. However, it is important to clarify when we are discussing surface densities and when instead we have volume densities. For the inside surface, Eq. 5.1, $m(x,t)$ is a bacterial surface density, with dimension $[m] = \mathrm{L}^{-2}$. The absolute number of bacteria this bacterial surface density corresponds to is given by the surface integral

$$N_{\text{intraluminal surface}}(t) = \int m \, \mathrm{d}S = \int_0^L 2\pi R \, m(x,t) \, \mathrm{d}x, \tag{5.5}$$

where $\mathrm{d}S$ is a surface area element.

For the inside flow of Eq. 5.2, $\sigma(x,r,t)$ is instead a bacterial volume density, with dimension $[\sigma] = \mathrm{L}^{-3}$. This corresponds to an absolute number of bacteria within the urine in the catheter lumen of

$$N_{\text{intraluminal flow}}(t) = \int \sigma \, \mathrm{d}V = 2\pi \int_0^L \int_0^R \sigma(r,x,t) \, r \mathrm{d}r \, \mathrm{d}x, \tag{5.6}$$

where $\mathrm{d}V$ is a volume element. Perhaps more importantly, this implies that the total flux of bacteria entering the catheter lumen within the urine is

$$\begin{aligned} j_{\text{intraluminal}} &= 2\pi \int_0^R \rho u \; r \mathrm{d}r \\ &= \frac{4\lambda\rho}{R^4} \int_0^R \left(R^2 r - r^3\right) \; \mathrm{d}r \\ &= \frac{4\lambda\rho}{R^4} \frac{R^4}{4} = \lambda\rho. \end{aligned} \tag{5.7}$$

Reassuringly, this is the same as the flux of bacteria leaving the bladder (Chapter 4).

5.3 An analytic solution for the bacterial deposition flux

So far, we have been considering the inside of the catheter in isolation, but of course the urine flowing through the catheter lumen comes directly out of the bladder. In fact, this is a boundary condition for Eq. 5.2, as the bacterial density of the urine entering the catheter must be exactly the bacterial density of the urine leaving the bladder: $\sigma(x=0, r, t) = \rho(t)$.

Unlike all other equations introduced earlier within the model (Chapters 2 to 4), the equation for the inside flow (Eq. 5.2) is not (spatially) one dimensional. This makes the model much more complicated, and computationally intensive. However, from a clinical perspective, the nature of the bacterial volume density, $\sigma(x, r, t)$ is not actually important. After all, all the bacteria that remain in the urine flow simply wash out of the system. Then all we really need $\sigma(x, r, t)$ for is to calculate the bacterial deposition flux, $j(x)$, which is itself one dimensional. Therefore, if we can analytically solve for $j(x)$, the model will become more tractable.

Earlier we stated one of the boundary conditions for $\sigma(x, r, t)$: the condition that the flow comes directly out of the bladder, $\sigma(x = 0, r, t) = \rho(t)$. There are of course several other boundary conditions. As stated earlier, we assume that the catheter surface forms a perfectly absorbing boundary. Moreover, since we are working in cylindrical coordinates, we also state that at the centre of the pipe there is no 'real' boundary. Together these three boundary conditions are as

follows:

$$\begin{aligned} \sigma(r, x = 0, t) &= \rho(t) \\ \sigma(r = R, x, t) &= 0 \\ \left.\frac{\partial \sigma}{\partial r}\right|_{r=0} &= 0. \end{aligned} \tag{5.8}$$

As stated earlier, the timescale of the urine flow $\tau_c \sim 7$ s is much shorter than the timescale of bacterial growth $\tau_b \sim 1800$ s. Therefore, over timescales comparable to the timescale of the urine flow, the bladder density can be regarded as constant. Over timescales comparable to the timescale of bacterial growth, the bacterial density profile within the catheter lumen is in a quasi-steady state, with $\frac{\partial \sigma}{\partial t} \approxeq 0$.[1] Thus, Eq. 5.2 reduces to:

$$D_B \left(\frac{\partial^2 \sigma}{\partial r^2} + \frac{1}{r} \frac{\partial \sigma}{\partial r} \right) = \frac{2\lambda}{\pi R^4} \left(R^2 - r^2 \right) \frac{\partial \sigma}{\partial x}. \tag{5.9}$$

We can nondimensionalise Eq. 5.9 by making the change of variables $\tilde{r} = \frac{r}{R}$, $\tilde{x} = \frac{D_B \pi x}{2\lambda}$, resulting in:

$$\frac{\partial^2 \sigma}{\partial \tilde{r}^2} + \frac{1}{\tilde{r}} \frac{\partial \sigma}{\partial \tilde{r}} = (1 - \tilde{r}^2) \frac{\partial \sigma}{\partial \tilde{x}}. \tag{5.10}$$

Eq. 5.10 looks similar to the diffusion equation in cylindrical co-ordinates [126], which has known solutions, so we might naively try to find a change of variables so as to write our equation in that form; however, as we see in §A.3.1 this is not possible. If instead we attempt to use a Laplace transform [19] on Eq. 5.10, we can obtain a 2nd order linear ODE. However, this ODE turns out not to have 'nice' solutions (see §A.3.2). Instead, we will use a method involving a boundary layer theory developed by Levich [69].

Levich's boundary layer theory

Maintaining all the assumptions that brought us to Eq. 5.10, let us add one final assumption: that we are in the 'diffusion inlet region', as defined by Levich [69], such that radial diffusion of bacteria to the intraluminal catheter surface takes place only within a thin boundary layer near the surface. This diffusion inlet region is the region in which the hydrodynamic flow profile has already been

[1] We verify this argument numerically later, in Figure 5.5.

established, but the radial diffusion flow profile of bacteria within the fluid is not yet fully established. We will justify this assumption below for the parameters of our model. Since in this assumption diffusion occurs only close to the surface, we can approximate it as planar, defining $y = 1 - r$ as a small variable. Now we need to solve the planar convection-diffusion equation,

$$v\frac{\partial\sigma}{\partial x} = \frac{\partial^2\sigma}{\partial y^2}, \tag{5.11}$$

where $v = 1 - r^2$. Since y is small, we take v to the first order in y, $v \approx 2y$. Then we can write down

$$2y\frac{\partial\sigma}{\partial x} = \frac{\partial^2\sigma}{\partial y^2} \tag{5.12}$$

with boundary conditions given by

$$\begin{aligned} \sigma &= 0 \qquad \text{at } y = 0 \\ \sigma &= \rho \qquad \text{as } y \to \infty. \end{aligned} \tag{5.13}$$

Introducing a new dimensionless variable

$$\eta = \frac{y}{\sqrt[3]{x}}, \tag{5.14}$$

we obtain

$$\frac{d^2\sigma}{d\eta^2} + \frac{2}{3}\eta^2\frac{d\sigma}{d\eta} = 0, \tag{5.15}$$

which we can then solve, (and do solve, in §A.3.3), to obtain the density profile

$$\sigma(\eta) = \frac{\rho\sqrt[3]{3}}{\Gamma(\frac{1}{3})}\int_0^\eta \mathrm{e}^{-\frac{2}{9}z^3}\, dz, \tag{5.16}$$

where Γ is the Gamma function, and then from there the bacterial deposition flux:

$$\begin{aligned} j(x) &= D_B \left.\frac{\partial\sigma}{\partial y}\right|_{y=0} \\ &= 0.5835 D_B \rho \sqrt[3]{\frac{\lambda}{R^3 D_B}}\frac{1}{\sqrt[3]{x}}. \end{aligned} \tag{5.17}$$

We can check this result for $j(x)$ against a numerical solution of Eq. 5.2, in addition to checking that the assumptions we have made earlier are valid. The fundamental assumption made in Levich's boundary layer theory is that diffusion

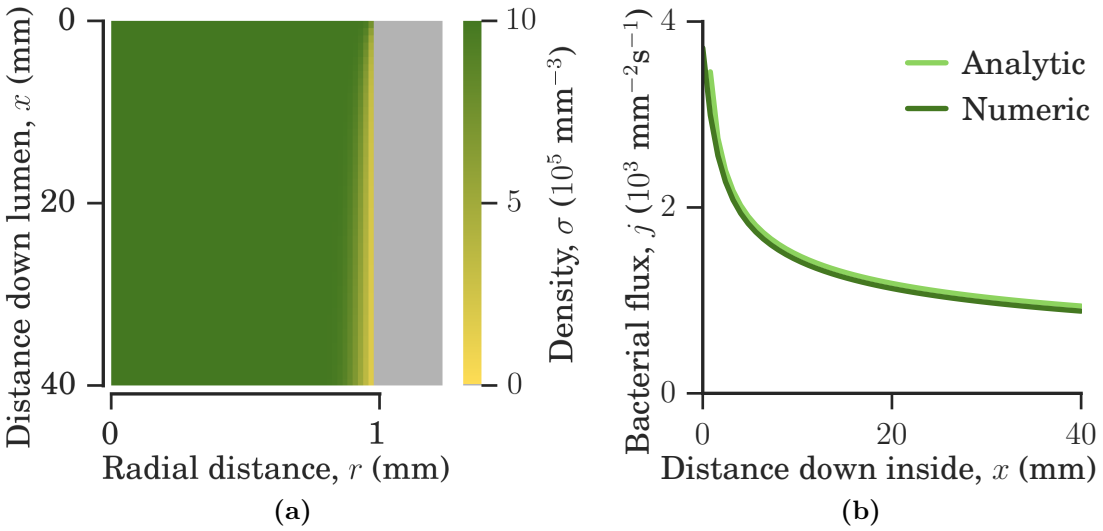

Figure 5.4 *Numerically simulating the intraluminal flow, Eq. 5.2, with parameters as in Table 2.2. [a] The bacterial density within the urine flow in the catheter lumen. [b] Comparing the numerically simulated bacterial deposition flux with the analytic result of Eq. 5.17.*

occurs within a thin boundary layer. To first order we have a relationship between the deposition rate and the boundary layer thickness of $j = D_B\rho/\delta$ (see Levich 2.10 [69]). Therefore, the boundary layer thickness is approximately

$$\delta \approx \frac{\sqrt[3]{x}}{0.5835}\sqrt[3]{\frac{R^3 D_B}{\lambda}}. \tag{5.18}$$

This is thin when $\delta \ll R$, i.e., when $\frac{D_B x}{\lambda} \ll 1$. For this to hold for the entire catheter, we need it to hold for $x = L$, and so we need $\frac{D_B L}{\lambda} \ll 1$. Taking the typical values for these parameters, as presented in Table 2.2, we find $\frac{D_B L}{\lambda} \sim 10^{-4} \ll 1$, well within the regime described by boundary layer theory.

In Figure 5.4, the results of numerical simulations of Eq. 5.2 (§A.3.4) are shown and compared to the analytic result of Eq. 5.17. In Figure 5.4a the existence of a thin boundary layer (yellow) can clearly be seen, while in Figure 5.4b the analytic result for $j(x)$ can be seen to be a good approximation for $x > 0.3$ mm. The $1/\sqrt[3]{x}$ dependence of $j(x)$ predicts higher deposition at the catheter tip than further down towards the outlet, consistent with observations that blockages are typically located near the catheter eyelets [5, 30].

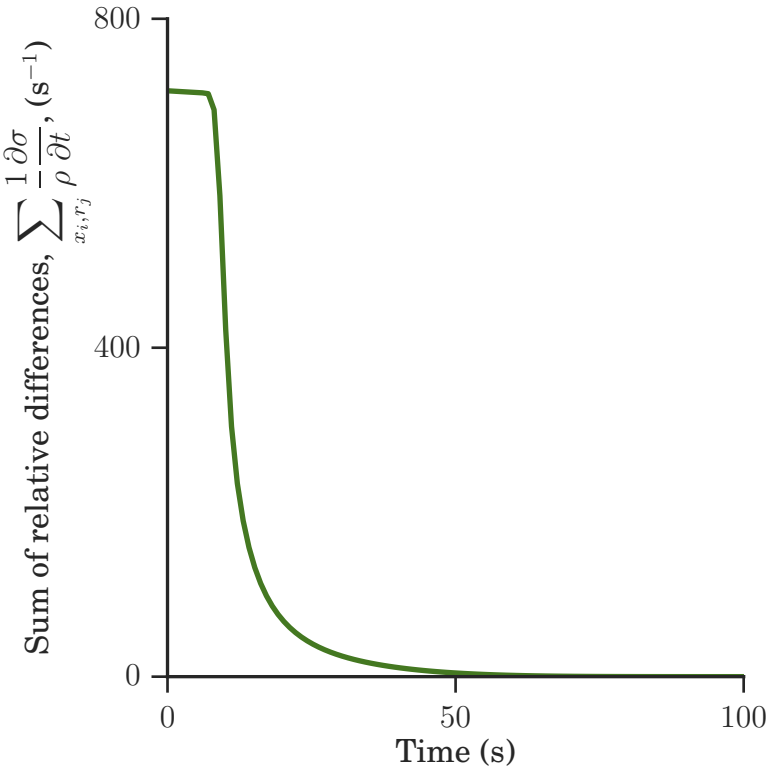

Figure 5.5 *Numerically simulating the system of Eq. 5.4, with parameters as in Table 2.2, and initially uniform conditions ($\sigma(r, x, t=0) = \rho$). We plot the sum over all grid points of the rate of change of the bacterial density, $\frac{\partial \sigma}{\partial t}$, normalised by the bladder population, ρ. The time for these differences to vanish, i.e., for the steady state profile to be achieved, is much less than the timescale of growth in the bladder, as the bacterial doubling time is ~ 30 mins.*

5.4 Summary

Bringing together all the work presented in §5.2 and §5.3, we can now write down the one-dimensional system of equations that describe bacterial transport, deposition and spreading within the inside of the catheter:

$$\begin{aligned} \frac{\partial m}{\partial t} &= D_S \frac{\partial^2 m}{\partial x^2} + r_S m \left(1 - \frac{m}{\kappa_S}\right) + j(x) \\ j(x) &= 0.5835 D_B \rho \sqrt[3]{\frac{\lambda}{R^3 D_B}} \frac{1}{\sqrt[3]{x}}. \end{aligned} \tag{5.19}$$

To get here we have of course made many simplifying assumptions. We have assumed that the catheter has rotational symmetry, which is valid if we exclude the catheter eyelets. As in the model for the extraluminal surface (Chapter 3),

we have assumed that bacteria on the catheter surface spread via diffusion, and hence may be described by a Fisher-Kolmagoroff equation. This is likely to be a significant simplification of what 'really' happens, but it is the simplest possible description. We have also assumed that the rate of flow of urine out of the bladder is constant. In fact, this flow rate varies slowly throughout the day and night [84], however this change is slow and continuous. We describe the urine flow through the catheter as laminar, which is likely to be a good description given the Reynolds number, $Re \approx 6$. We have made the assumption that convective-diffusive effects happen on a much faster timescale than bacterial growth, and thus that when calculating the bacterial flux, we can take the bladder bacterial density as constant. Earlier (§5.2.3), we argued this was justified since the convective timescale is ≈ 7 s, while the bacterial doubling time is 30 mins. To confirm this, in Figure 5.5 we numerically simulate Eq. 5.19 (A.3.5) to show that the rate of change of the bacterial density profile after initial establishment vanishes within 60 s. Finally, we assumed we were within the diffusion inlet region, $h < x \ll H$, where the laminar flow profile is fully established, but diffusion occurs only within a thin boundary layer. This turns out to correspond to the region $0.2 < x \ll 10^5$ mm, which of course catheters, with typical length 40–160 mm, fall well within.

Chapter 6

Implementing the model

6.1 Introduction

In Chapter 2 we outlined a minimal model for bacterial colonisation of a urinary catheter. We saw that this model can be divided into subsystems: the extraluminal surface, the bladder, the urine flow down the catheter lumen, and the intraluminal surface. In Chapters 3 to 5 we then explored these subsystems in detail. We wrote down equations that described the dynamics of the bacterial density in each subsystem:

$$\text{extraluminal surface} \qquad \frac{\partial n}{\partial t} = D_S \frac{\partial^2 n}{\partial x^2} + r_S n \left(1 - \frac{n}{\kappa_S}\right) \tag{6.1}$$

$$\text{bladder} \qquad \frac{d\rho}{dt} = r_B \rho \left(1 - \frac{\rho}{\kappa_B}\right) - k_D \rho \tag{6.2}$$

$$\text{intraluminal surface} \qquad \frac{\partial m}{\partial t} = D_S \frac{\partial^2 m}{\partial x^2} + r_S m \left(1 - \frac{m}{\kappa_S}\right) + j(x) \tag{6.3}$$

$$j(x) = 0.5835 D_B \rho \sqrt[3]{\frac{\lambda}{R^3 D_B}} \frac{1}{\sqrt[3]{x}}. \tag{6.4}$$

Here all the variables and parameters are as defined in Tables 2.1 and 2.2. Note that we have only written explicit equations for the bacterial densities corresponding to the extraluminal surface, bladder, and intraluminal surface. The behaviour of the bacterial density in the intraluminal flow is implicit within the equation for $j(x)$: the solution of the bacterial deposition flux from the intraluminal flow onto the intraluminal surface.

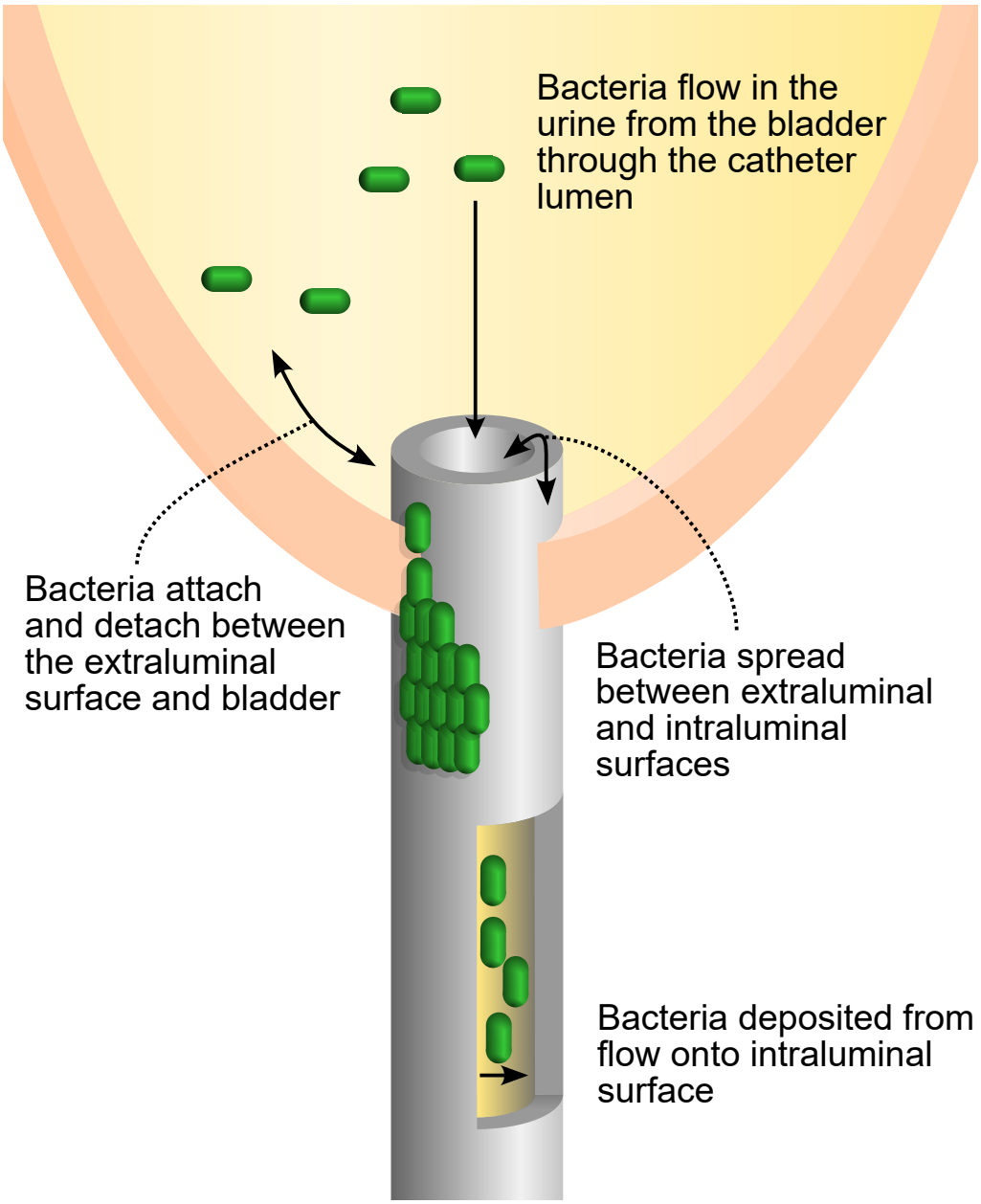

Figure 6.1 *Connecting the different parts of the model. Bacteria transfer between the top of the extraluminal surface and the bladder (§6.2.1). Bacteria transfer between the top of the extraluminal surface and the top of the intraluminal surface(§6.2.2). The intraluminal flow carries bacteria from the bladder (§6.2.3). Bacteria are deposited from the intraluminal flow onto the intraluminal surface (§6.2.4).*

6.2 Coupling the model

We now need to couple these 3 partial differential equations together, into one model (which can then be treated numerically). The different parts of the model are connected through coupling terms which preserve the total bacterial number (Figure 6.1). Briefly, bacteria that reach the top of the extraluminal surface may detach and colonise the bladder. Conversely, bacteria within the bladder may stick to the top of the extraluminal surface and join the biofilm. In this simplified model the extraluminal and intraluminal surfaces of the catheter are directly connected at the top, so bacteria freely diffuse between the two surfaces. The connection between the bladder and intraluminal flow is intuitive: the urine flowing down the catheter lumen is exactly the urine that has been diluted out of the bladder. The intraluminal surface is the absorbing boundary for the intraluminal flow, meaning that bacteria diffuse out of the flow and stick to the surface, but never the reverse – this is $j(x)$, as discussed above. Within the entire system the only bacteria that ever 'come unstuck' are those growing at the tip of the extraluminal surface inside the bladder, which may be thought of as growing directly into the bladder, having run out of catheter surface. The various couplings are illustrated in Figure 6.1 and described in detail in the following sections.

In this process of coupling the sections we must be careful to conserve the number of bacteria. In this model bacteria are 'created' only by growth, and 'destroyed' only by being washed out of the bottom of the catheter. Therefore, the coupling terms must only transport bacteria, without changing the total number. Ensuring that the total bacterial number is conserved requires some care, as our model consists of equations for the bacterial density, not the absolute number. We discuss each of the couplings in more detail in §6.2.1 to §6.2.4.

6.2.1 Connecting the extraluminal surface and bladder

The top of the catheter is located within the bladder and is immersed in urine. Therefore, bacteria may detach from the extraluminal surface of the catheter and join the planktonic population within the bladder. Conversely, bacteria within the urine in the bladder may stick to the extraluminal catheter surface. Within the model, this coupling is incorporated into the extraluminal surface equation

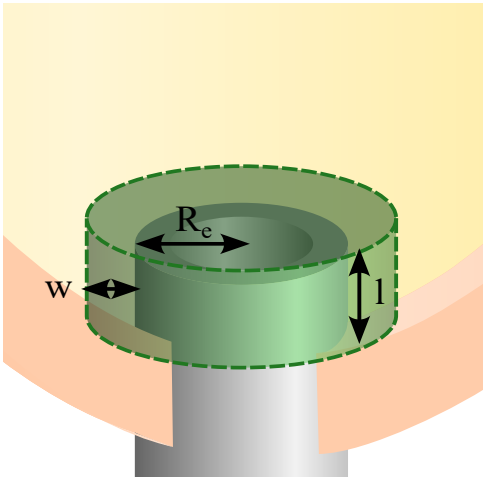

Figure 6.2 *Illustrating the 'contact area' and 'contact volume'. Some bacteria within the bladder are close to the external catheter surface. At the top of the catheter, some bacteria on the surface are immersed in urine. If the catheter protrudes a distance l into the bladder, then there is a total surface contact area on the catheter of $S_c = 2\pi R_e l$. Suppose the bacteria within the bladder are 'in contact' with the catheter if they are within a distance w, and simplify this contact volume to be a cylinder of radius $R_e + w$ and height $l + w$. Then the contact volume is $V_c = \pi(R_e + w)^2(l + w) - \pi R_e^2 l$.*

(Eq. 3.1; as written in Eq. 6.1) as a flux at the top boundary. For the bladder, the coupling takes the form of a source term added to the right-hand side of Eq. 4.3 (Eq. 6.2). The coupling must conserve bacterial number, so the total number of bacteria moving to the bladder must equal the number leaving the catheter surface.

To derive the coupling terms, we consider that only bacteria that are in a region of 'contact' between the extraluminal surface and bladder can migrate. Therefore, we need to define a contact surface (at the top of the catheter) and a contact volume (in the bladder surrounding the catheter) within which bacteria can transfer. Figure 6.2 illustrates how we define these contact geometries. Assuming that a length l of catheter is exposed within the bladder, and that bacteria in the bladder within a distance w have a chance of sticking, we can write down the contact surface area and volume:

$$\begin{aligned} S_c &= 2\pi R_e l \\ V_c &= \pi(R_e + w)^2(l + w) - \pi R_e^2 l. \end{aligned} \tag{6.5}$$

Here R_e is the external catheter radius, and l and w are as shown in Figure 6.2.

Since we need to conserve the bacterial number, we must consider the absolute number of bacteria within the contact regions. $N_s = S_c \cdot n(L,t)$ is the number of bacteria on the catheter surface that are 'in contact' with the bladder, and $N_b = V_c \cdot \rho(t)$ is the number of bacteria in the bladder that are 'in contact' with the catheter. Therefore, the flux of bacteria to the bladder is

$$\underbrace{k_d N_s}_{\text{detaching}} - \underbrace{k_a N_b}_{\text{attaching}} \tag{6.6}$$

where k_d and k_a are respectively the rates at which bacteria detach from and attach to the catheter surface in the presence of urine; and N_s and N_b are the numbers of bacteria at the boundary on the outside of the catheter and in the bladder. To set reasonable values for k_d and k_a we make the following assumptions: any bacteria that are born on the exposed catheter surface detach, so $k_d = r_S$ (recall that r_S is the bacterial growth rate on the catheter surface); and bacteria in the bladder diffuse and stick to the surface irreversibly upon contact, so k_a is the Smoluchowski diffusion-limited rate constant [119].

We can now write down the coupling terms. In the bladder there is a source term for the density,

$$\frac{k_d S_c n(0,t) - k_a V_c \rho(t)}{V}, \tag{6.7}$$

where V is the total residual urine volume of the bladder. At the top of the catheter there is a corresponding surface density flux at the boundary:

$$\frac{k_a V_c \rho(t) - k_d S_c n(0,t)}{S_c}. \tag{6.8}$$

This leads to the full equation for the bladder:

$$\frac{d\rho}{dt} = \underbrace{r_B \rho \left(1 - \frac{\rho}{\kappa_B}\right)}_{\text{growth}} - \underbrace{k_D \rho}_{\text{dilution}} + \underbrace{\frac{k_d S_c n(0,t) - k_a V_c \rho(t)}{V}}_{\text{extraluminal coupling}}. \tag{6.9}$$

6.2.2 Connecting the extraluminal and intraluminal surfaces

Since we do not model the catheter eyelets, we assume that bacteria can spread freely across the top of the catheter between the extraluminal and intraluminal surfaces. This is represented by a continuity condition on the bacterial density,

connecting Eqs. 3.1 and 5.1 (Eqs. 6.1 and 6.3):

$$\begin{aligned} n(x=0,t) &= m(x=0,t), \\ \underbrace{\left.\frac{\partial n}{\partial x}\right|_{x=0}}_{\text{extraluminal}} &= \underbrace{\left.\frac{\partial m}{\partial x}\right|_{x=0}}_{\text{intraluminal}}. \end{aligned} \tag{6.10}$$

6.2.3 Connecting the bladder and intraluminal flow

As urine is generated by the kidneys and enters the bladder, the residual urine inside the bladder is diluted. To ensure continuity of bacterial density in the urine leaving the bladder and entering the lumen, we impose the following coupling between Eq. 4.3 (the bacterial density dynamics in the bladder; Eq. 6.2) and Eq. 5.2 (the bacterial density dynamics in the intraluminal flow, not written explicitly in this chapter):

$$\underbrace{\sigma(r,x=0,t)}_{\text{flow}} = \underbrace{\rho(t)}_{\text{bladder}}. \tag{6.11}$$

In fact, this coupling is implicit within the derivation of the bacterial flux from the urine onto the intraluminal surface, $j(x)$ (Eq. 6.4) in Chapter 5 (Eq. 5.17).

6.2.4 Connecting the intraluminal flow and intraluminal surface

As discussed in Chapter 5, deposition of bacteria from the urine onto the intraluminal surface is incorporated via an absorbing boundary condition for Eq. 5.2, i.e., the catheter wall is assumed to be a perfect sink. The flux of deposited bacteria appears as the source term $j(x)$ for the intraluminal surface in Eq. 5.1 (Eq. 6.3). We found this flux by computing the rate at which bacteria hit the boundary $r = R$ for the longitudinal distance x down the catheter, finding (Eq. 5.3):

$$j(x) = -D_B \left.\frac{\partial \sigma}{\partial r}\right|_{r=R}.$$

This flux can be obtained either by numerical solution of Eq. 5.2 (Eq. 6.3), or by an analytic approximation [69], as we showed in §5.3, which results in (Eq. 5.17):

$$j(x) = 0.5835 D_B \rho \sqrt[3]{\frac{\lambda}{R^3 D_B}} \frac{1}{\sqrt[3]{x}}.$$

Note that this analytic solution for the bacterial deposition flux has no explicit dependence on $\sigma(r, x, t)$, the bacterial volume density within the intraluminal urine flow. Thus, this coupling term (Eq. 5.17) can be viewed as a direct coupling between the bladder and the intraluminal surface, incorporating both Eqs. 6.11 and 5.3. Hence, the full equation for the intraluminal surface is as written in Eqs. 6.3 and 6.4:

$$\frac{\partial m}{\partial t} = \underbrace{D_S \frac{\partial^2 m}{\partial x^2}}_{\text{motility}} + \underbrace{r_S m \left(1 - \frac{m}{\kappa_S}\right)}_{\text{growth}} + \underbrace{0.5835 D_B \rho \sqrt[3]{\frac{\lambda}{R^3 D_B}} \frac{1}{\sqrt[3]{x}}}_{\text{bladder coupling (deposition)}}.$$

6.3 Numerical implementation

Throughout Chapters 3 to 5 we have discussed the results of numerically simulating the governing equations of the model (Eqs. 6.1 to 6.4). Here we discuss the numerical implementation of these simulations, as well as the numerical implementation of the coupling described earlier in this chapter (that will be utilised to obtain the results discussed in Chapter 7).

6.3.1 Extraluminal surface

Recall Eq. 6.1:

$$\frac{\partial n}{\partial t} = D_S \frac{\partial^2 n}{\partial x^2} + r_S n \left(1 - \frac{n}{\kappa_S}\right).$$

This can be discretised with a forward-time centred-space (FTCS) method as:

$$n_p^{k+1} = \frac{D_S \Delta t}{\Delta x^2} \left(n_{p+1}^k - 2n_p^k + n_{p-1}^k\right) + \left(1 + r_S \Delta t\right) n_p^k - \frac{r_S \Delta t}{\kappa_S} \left(n_p^k\right)^2, \qquad (6.12)$$

where n_p^k is the extraluminal bacterial surface density, $n(x, t)$, at the pth discrete position, and the kth time step; Δt is the time step; and Δx is the spatial discretisation. For further details and stability analysis, see §A.1.2.

Since bacteria are free to diffuse between the extraluminal and intraluminal surfaces of the bladder, if there are $N = L/\Delta x$ discrete spatial positions on the lattice along the catheter surface for each of the extraluminal and intraluminal surface, then we can define a ghost point before the first grid point on the extraluminal surface – which is equal to the first grid point on the intraluminal surface: $n^k_{-1} = m^k_0$ (Eq. 6.10). Here, n^k_p is the extraluminal bacterial density, $n(x,t)$ at the pth discrete position, and the kth timestep; and m^k_p is similarly the intraluminal bacterial density, $m(x,t)$.

The extraluminal surface is coupled with the bladder, with flux given by Eq. 6.8, so at the top of the catheter, n_0 is incremented as

$$\begin{aligned} n_0^{k+1} = \frac{D_S \Delta t}{\Delta x^2}\left(m_0^k - 2n_0^k + n_1^k\right) \\ + \left(1 + r_S \Delta t\right) n_0^k - \frac{r_S \Delta t}{\kappa_S}\left(n_0^k\right)^2 \\ + \frac{1}{2\pi R_e \Delta x}\left(k_a V_c \rho^k - k_d S_c n_0^k\right). \end{aligned} \tag{6.13}$$

6.3.2 Bladder

Recall Eq. 6.2:

$$\frac{d\rho}{dt} = r_B \rho \left(1 - \frac{\rho}{\kappa_B}\right) - k_D \rho.$$

Discretising this with a forward Euler method gives

$$\rho^{k+1} = \rho_k + \Delta t \left(\left(r_B - k_D\right)\rho^k - \frac{r_B}{\kappa_B}\left(\rho^k\right)^2 \right), \tag{6.14}$$

where ρ^k is the bladder bacterial volume density at the kth time step, and Δt is the time step. For further details and stability analysis, see §A.2.2.

Instead discretising the coupled bladder equation (Eq. 6.9), again with a forward Euler method, gives

$$\rho^{k+1} = \rho^k + \Delta t \left(\left(r_B - k_D - \frac{k_a V_c}{V}\right)\rho^k - \frac{r_B}{\kappa_B}\left(\rho^k\right)^2 + \frac{k_d S_c}{V} n_0^k \right), \tag{6.15}$$

where ρ^k is the bladder bacterial volume density at the kth time step, and n^k_0 is the extraluminal bacterial density, $n(x,t)$ at the bladder. This is numerically

stable following the same argument as in §A.2.2, requiring

$$\Delta t < 1 \Big/ \left(r_B - k_D - \frac{k_a V_c}{V} + \frac{k_d S_c}{V} \right) \sim 10^4 \text{ s.} \tag{6.16}$$

6.3.3 Intraluminal surface

To simulate bacterial growth and spreading on the inside surface of the catheter, a forward-time centred-space (FTCS) method is used. Recall Eq. 6.3:

$$\frac{\partial m}{\partial t} = D_S \frac{\partial^2 m}{\partial x^2} + r_S m \left(1 - \frac{m}{\kappa_S} \right) + j(x).$$

The bacterial flux, $j(x)$, comes from the deposition of bacteria onto the intraluminal surface from the urine flow out of the bladder. To calculate this numerically requires simulating the intraluminal flow, which is computationally more demanding as it is a 2-dimensional problem, unlike the 1-dimensional surfaces. Instead, here we use the analytic approximation for the bacterial flux, as given by Eq. 6.4,

$$j(x) = 0.5835 D_B \rho \sqrt[3]{\frac{\lambda}{R^3 D_B}} \frac{1}{\sqrt[3]{x}}.$$

This analytic solution is valid for $h < x \ll H$, i.e., the region in which the hydrodynamic flow is established, but the diffusive boundary layer is still small. We can find h by looking for the distance at which the hydrodynamic boundary layer thickness is equal to the catheter radius (§A.3.5). This is $h \sim 0.22$ mm. The behaviour within the early region, $x < h$, would be highly dependent on the exact geometry of the catheter, which is not incorporated into this model. Instead, knowing that the deposition rate must always be finite, we take a zeroth order approximation that the flux for $x < h$ is constant, and $j(x < h) = j(h)$. Since this is only a very small region of the catheter, this approximation has very little impact on the results of the model (see §A.3.5 for further justification).

We can discretise the intraluminal surface in a manner very similar to the

extraluminal surface, using a FTCS method to find

$$m_p^{k+1} = \frac{D_S \Delta t}{\Delta x^2}\left(m_{p+1}^k - 2m_p^k + m_{p-1}^k\right) + (1 + r\Delta t)\, m_p^k - \frac{r\Delta t}{\kappa_S}\left(m_p^k\right)^2 + 0.5835\left(\frac{\lambda D_B^2}{R^3}\right)^{1/3} \Delta t \rho^k (p\Delta x)^{-1/3}, \quad (6.17)$$

where m_p^k is the intraluminal bacterial surface density, $m(x,t)$, at the pth discrete position, and the kth time step; ρ^k is the bacterial volume density in the bladder at the kth time step; Δt is the time step; and Δx is the spatial discretisation. For further details and stability analysis, see §A.3.5.

At the top of the catheter, bacteria can diffuse between the intraluminal surface and the extraluminal surface, so at the top of the catheter we have

$$m_0^{k+1} = \frac{D\Delta t}{\Delta x^2}\left(m_1^k - 2m_0^k + n_0^k\right) + (1 + r\Delta t)\, m_0^t - \frac{r\Delta t}{\kappa_S}\left(m_0^k\right)^2 + 0.5835\left(\frac{\lambda D_B^2}{R^3}\right)^{1/3} \rho^k (\Delta x)^{-1/3}, \quad (6.18)$$

where m_p^k is the intraluminal bacterial density, $m(x,t)$ at the pth discrete position, and the kth timestep, and n_0^k is the extraluminal bacterial density, $n(x,t)$ at the bladder.

6.4 Boundary and initial conditions

In Chapter 2 (following on from §1.3) we discussed four different 'infection pathways' through which colonising bacteria might enter the system. Each of these pathways corresponds within our model to a different set of boundary/initial conditions.

Considering Eqs. 6.1 to 6.4, we see that to fully specify our model we require 4 boundary conditions, as well as the state of the entire system at $t = 0$. In fact, Eq. 6.10 specifies two boundary conditions. Additionally, we take as a default initial condition a 'clean' catheter, with $n(x, t = 0)$, $\rho(t = 0)$, and $m(x, t = 0)$ all zero. Now we must specify a boundary condition for $x = L$ on the extraluminal and intraluminal surfaces, as well as any alternative initial conditions.

1. If the bacteria originate from the skin, this is a Dirichlet boundary condition for the base of the extraluminal surface, $n_N^k = const.$ (the extraluminal base of the catheter is in contact with a reservoir of bacteria), and a Neumann (reflecting) boundary condition for the bottom of the intraluminal surface, $m_{N+1}^k = m_{N-1}^k$ (i.e., we assume that the intraluminal system is closed).

2. If the bacteria come from the drainage bag, this is a Dirichlet boundary condition for the base of the intraluminal surface, $m_N^k = const.$ (the intraluminal base of the catheter is in contact with a reservoir of bacteria), and a Neumann (reflecting) boundary condition for the base of the extraluminal surface, $n_{N+1}^k = n_{N-1}^k$ (i.e., we assume that the skin does not interact with the extraluminal surface).

3. If there is uniform initial contamination across the extraluminal surface, this corresponds to an initial condition $n_p^0 = const.$, with reflecting boundary conditions for both the intraluminal and extraluminal surfaces, $m_{N+1}^k = m_{N-1}^k$ and $n_{N+1}^k = n_{N-1}^k$. Again, the reflecting boundary conditions correspond to the assumption that the catheter-bladder system is 'closed', with no external contamination except the condition explicitly considered.

4. Finally, if the bladder is already contaminated before the catheter is inserted, this corresponds to an initial condition with non-zero bacterial density in the bladder, ρ_0, and again there are reflecting boundary conditions for the catheter surfaces.

We explore all four of these infection scenarios in detail in Chapter 7. When not explicitly stated otherwise, our 'default' assumption is Path 1, bacteria originating from the skin, as the majority of CAUTI are attributed to the extraluminal ascension of bacteria up the catheter [82].

6.5 Characteristic timescales

In developing the model presented in this thesis, we have used timescales to justify assumptions and modelling choices. Here, in Table 6.1, we summarise the timescales presented so far. In Chapters 7 and 8 we will make use of these timescales to predict the timescales of clinical phenomena, including bacteriuria, relating those timescales to the model parameters.

Timescale		Typical value (s)
Clinical		
Short-term catheterisation	≤ 14 days	$\lesssim 10^6$
Long-term catheterisation	> 30 days	$\gtrsim 2 \times 10^6$
Extraluminal surface		
Bacterial growth	$\log(2)/r_S$	4×10^3
Bacterial motility	L^2/D_S	10^{11}
Bacterial ascension	$L/2\sqrt{r_S D_S}$	10^7
Establishment of wave solutions	$\log\left(\frac{\kappa_S}{n_0}\right)/r_S$	10^5
Bladder		
Bacterial growth	$\log(2)/(r_B - k_D)$	10^4
Intraluminal flow		
Bacterial growth	$\log(2)/r_B$	2×10^3
Convective transport	$\pi R^2 L/\lambda$	7
Radial diffusive transport	R^2/D_B	10^4
Longitudinal diffusive transport	L^2/D_B	2×10^7
Response to bladder density fluctuations	1 min	10^2

Table 6.1 *The characteristic timescales of the processes within the model.*

6.6 Summary

The three equations describing the growth dynamics of the bacterial densities – on the extraluminal surface, intraluminal surface, and within the bladder – can be connected via three coupling terms. We can numerically implement the resulting unified model, allowing us to perform a parameter space exploration (Chapter 7), and explore the predictive capabilities of our model (Chapter 8).

Part II

Implications of the model

Chapter 7

Parameter space exploration

7.1 Introduction

While some aspects of catheter associated urinary tract infections are well understood, e.g., the strains of bacteria that are primarily responsible (as discussed in §1.2), comparatively little is known about the factors that determine the timescales and outcomes of these bacterial infections. In Chapters 2 to 6 we constructed a mathematical model for the bacterial colonisation of a urinary catheter and discussed in detail the implications of our modelling choices. This model has 10 physical parameters (and two coupling constants). In Table 2.2, we established the physical significance of these parameters, and briefly discussed values obtained from the literature.

Here, we perform a detailed parameter space exploration, investigating how varying the model parameters alters the dynamics, timescales, and long-time behaviour of the system. This allows us to identify key physical parameters, and show how varying them provides clinical insights. Finally, we discuss our results within the context of the clinical literature, qualitatively linking our model predictions to observed clinical phenomena.

7.2 Results

7.2.1 Urine production rate drives a transition in bacterial density

The rate of urine production by the kidneys is strongly correlated with the fluid intake of the patient. This is a key parameter in our model, since it controls the rate at which bacteria are removed from the bladder by dilution (denoted by k_D; see Eq. 4.3) and the rate of urine flow through the catheter lumen (denoted by λ; see Eq. 5.2), which in turn determines the rate of bacterial deposition on the intraluminal surface. Previous (uncatheterised) micturition models have suggested that there is a critical dependence between the urine production rate and the bacterial growth rate in the bladder [43]. Therefore, we investigated how the behaviour of our model depends on the rate of urine production.

We observed a critical transition upon varying the urine production rate (Figure 7.1). At low production rates, the steady state bacterial population density within the bladder is high since bacteria can grow fast enough to overcome dilution. At high urine production rates, the population density in the bladder falls dramatically, as the dilution rate exceeds the maximal rate at which the bacteria can grow. The transition has a near-linear dependence of the steady state bacterial population density on the urine production rate (Figure 7.1 lower inset); however the time taken to attain the steady state diverges at the critical urine production rate (Figure 7.1 upper inset). A typical value for the urine production rate in humans is 16.7 mm^3s^{-1} (i.e., 1 mL min^{-1}; pink dashed line in Figure 7.1) [31]. This value lies very close to the critical threshold predicted by our model (Figure 7.1), suggesting that individual patients might show dramatically different levels of bacteriuria (bacteria in the urine) depending on their fluid intake. We will further discuss this result, in the context of the population-level variance in urine production rates, in §8.5.1.

This transition is essentially a washout phenomenon, as observed in microbiological continuous culture experiments, where bacteria grow in continuously diluted medium and it is well known that a bacterial population can only be sustained for dilution rates less than the bacterial growth rate [3, 92]. Indeed, when plotted on a linear scale (Figure 7.1 lower inset), the transition in the catheter model appears indistinguishable from washout, with the bacterial density

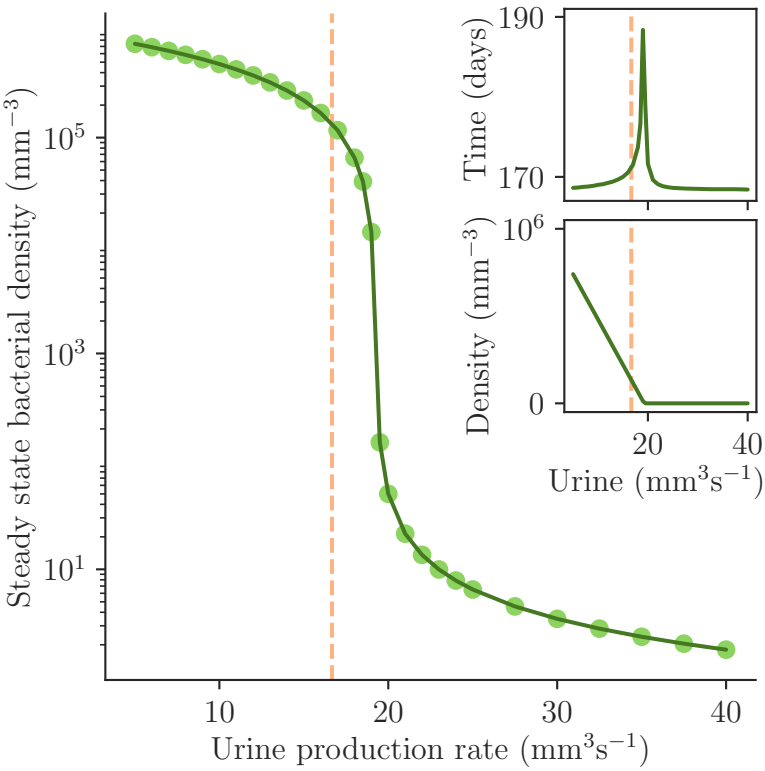

Figure 7.1 *Transition driven by urine production rate. As the rate of dilution of the bladder increases beyond the bacterial growth rate, there is a transition from a high-density bladder state to a "washed out" state. Each point represents a bacterial density obtained from a numerical simulation. A connecting line (▬) is drawn as a guide for the eye. Lower inset shows the same data on a linear scale. Upper inset shows the time taken to attain the maximum density, with a sharp peak at the transition. Also plotted (▬) is the typical urine flow rate in a patient,* 1 *mL min*$^{-1}$ *[31].*

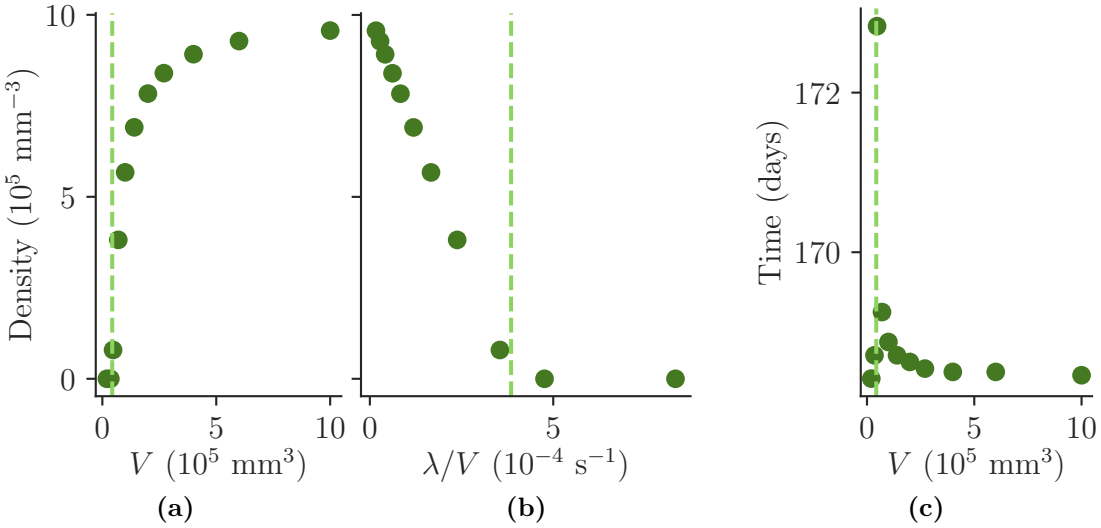

Figure 7.2 *The residual urine volume also determines the dilution rate. (a) The effect of varying the volume of residual urine, V on the steady state bacterial density in the bladder. The vertical line (▬) marks the washout transition, $V = \lambda/r_B$. (b) The same data points as in (a), however the x axis now plots the dilution rate, k_D, where each point was obtained from a simulation with fixed λ but varying V. (c) The effect of varying the residual urine rate on the time taken to steady state bacterial density in the bladder. All parameters other than V are as in Table 2.2. V is varied within the physiologically relevant range: 10 - 1000 mL.*

approaching zero as the urine production rate approaches the bacterial growth rate. However, in the logarithmic plot (Figure 7.1 main), we observe a 'tail' that is due entirely to re-population of the bladder from bacteria that have adhered to the catheter surfaces. Without this bacterial migration from the catheter surface to the residual urine sump, the bacterial density in the urine would fall to zero at the transition (see Figure 4.2 and §4.3.1). The presence of the catheter 'smooths' the transition, such that even at high urine production rates some bacteria are still present in the urine. Hence, the presence of the catheter allows the infecting bacterial population to persist even if the urine production rate is high enough to wash it out of the bladder. Indeed, catheter-associated biofilms are known to act as a bacterial reservoir, leading to persistent re-colonisation of the bladder [9].

As discussed above, and in §4.3.1, the value of the dilution rate k_D (which is related to the urine production rate λ and the bladder volume V via $k_D = \lambda/V$) is critical for the behaviour of our model. In our model, the dilution rate governs both the steady state bacterial density in the bladder, and the timescale over which the steady state is attained (Figure 4.1b). This dependence of the model

on the dilution rate is very similar to the behaviour of other (uncatheterised) micturition models, where there is a critical relationship between the urine dilution rate and the bacterial growth rate [43] (§4.3.2). However, as discussed above, in our model the presence of the catheter means that the bacterial density in the bladder does not go to zero in the high dilution rate 'wash-out' state.

Since the urine production rate is incorporated into the bladder model through the dilution rate ($k_D = \lambda/V$), varying the residual urine sump volume in the bladder, V has similar effects on the bladder dynamics to varying the urine production rate, λ (Figure 7.2). Comparing Figure 7.2b with Figure 7.1 lower inset, the same linear behaviour can be observed. Similarly, comparing Figure 7.2c with Figure 7.1 upper inset, the characteristic spike in timescales of the washout transition (§4.3.1) can be seen. We note, however, that the intraluminal flow dynamics, which control bacterial deposition on the intraluminal catheter surface, are independent of the residual urine sump volume (although they do depend on the urine production rate).

In summary, in §4.3 we established that the form of Eq. 4.3 for the bladder dynamics leads to a washout transition, occurring at $k_D = r_B$, i.e., when the dilution rate equals the growth rate. We now see how this transition is modified within the full coupled model. The dilution rate is defined as $k_D := \lambda/V$, thus the washout transition can be seen when varying either urine production rate (Figure 7.1), or residual urine volume (Figure 7.2). In both cases, the transition is no longer perfectly linear as in Figure 4.2; rather, it is 'smoothed' by bacteria migrating from the catheter surface.

7.2.2 Time to detection of bacteriuria is controlled by movement of bacteria up the catheter

The appearance of bacteria in the urine, bacteriuria (as introduced in §1.2), is an almost inevitable consequence of long-duration catheterisation [123], with an estimated incidence rate of 3–7% per catheter day [71] (bacteriuria is about 10 times more prevalent than CAUTI [48, 82], and is often erroneously treated as CAUTI [18]). By tracking the density of bacteria in the outflowing urine, our model can predict how long after catheter insertion bacteriuria will be detected, assuming a certain detection sensitivity. Here we assume that colonisation is initiated by bacteria on the outside of the catheter, where the urethra meets the

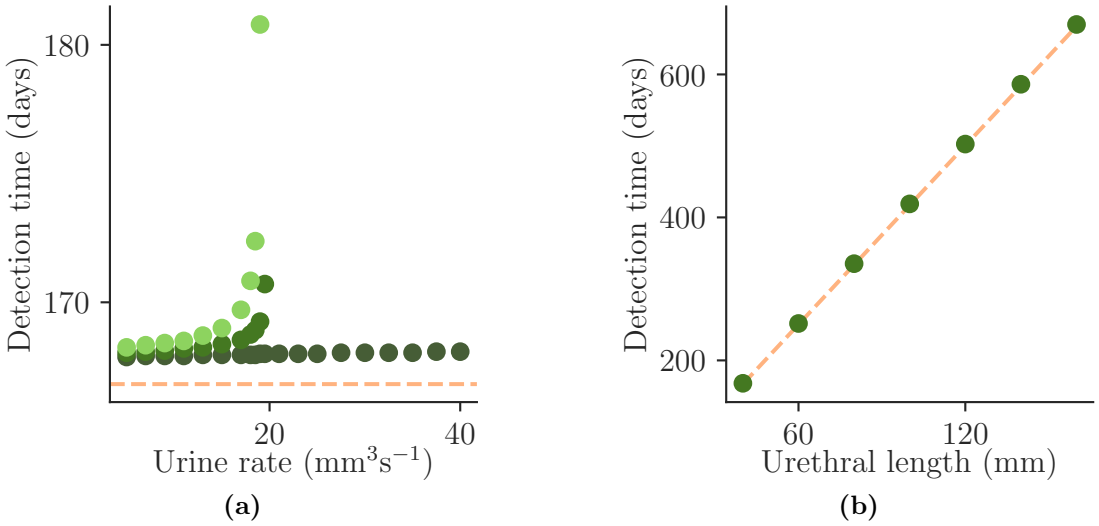

Figure 7.3 *Time to detection of bacteriuria, for tests of varying sensitivities. We plot the times until the bacterial volume density in the urine exceed 10^4 (•), 10^2 (•), and 1 (•) mm^{-3} respectively. Also plotted (▬) is the time for the FKPP wave to spread across the extraluminal surface, $L/2\sqrt{r_S D_S}$ (recall §3.3.3). (a) Varying the urine production rate. (b) Varying the urethral length. Note that in this case there is no significant difference between different testing sensitivities, as the urethral length dominates the timescale. All parameters are as given in Table 2.2.*

skin (Chapter 6).

For high-sensitivity tests (detection at cell counts of 1 mm^{-3}, i.e. 10^3 mL^{-1}), our model predicts that bacteriuria will eventually be detected, no matter how high the urine production rate (Figure 7.3a). This is because, even in the 'washout' regime (Figure 7.1), the presence of the catheter ensures that there are some bacteria in the urine. The time to detection of bacteriuria is almost independent of the urine production rate since the detection time is dominated by the time for bacteria to migrate up the extraluminal surface (see §Bladder-surface regime transition). This implies that early removal of the catheter can prevent occurrence of bacteriuria, since bacteria do not have time to reach the bladder. Since bacterial colonisation can lead to CAUTI, this is consistent with the fact that the duration of catheterisation is the single biggest risk factor for developing CAUTI [48, 71, 99].

In contrast, low sensitivity tests (requiring cell counts $> 10^2$ mm^{-3}, i.e. 10^5 mL^{-1}) will never detect bacteriuria in the high urine production rate regime (Figure 7.3a), even though some bacteria are present in the urine (Figure 7.1).

This is because the steady-state bacterial density is below the detection threshold. Interestingly, some clinical guidelines [48] distinguish different thresholds for diagnosis of CAUTI and bacteriuria. For CAUTI, these guidelines require both clinical symptoms and bacterial counts $> 10^3$ CFU mL^{-1} (equivalent to our high sensitivity threshold; CFU = colony forming units, a proxy for cell count), while a diagnosis of bacteriuria does not require symptoms but does require a higher bacterial count $> 10^5$ CFU mL^{-1} (equivalent to our low sensitivity values). We can interpret this distinction in clinical definitions in the context of our model and the results of Figure 7.3a, as our model predicting that lower sensitivity tests might erroneously return (false) negative results for patients with higher urine production rates suffering from CAUTI – hence the need for higher sensitivity tests to diagnose CAUTI.

The time to detection of bacteriuria depends linearly on the length of the catheter, which corresponds to the length of the urethra (Fig. 7.3b). This is because the timescale of bacterial migration up the extraluminal surface is set by the speed of the FKPP population wavefront (as found in §3.3). The main factor determining urethral length in humans is gender, with a typical length for a woman being 40 mm, and for a man 160 mm [31]. This result is therefore consistent with the fact that biological sex is a well-established risk factor for CAUTI [48, 99]. As we will see later (Chapter 8), the linear dependence of the timescale of bacteriuria on the urethral length is particularly significant in the context of short-term ($\lesssim 14$ days) catheterisation.

7.2.3 Time to formation of a biofilm depends on characteristics of the patient, catheter and infecting bacteria

Catheter blockage is a frequent and serious complication of catheter use. Most commonly, blockage is caused when biofilms of *Proteus mirabilis* form on the catheter surface and increase the urine pH, causing crystals to precipitate [52, 124]. However, non-crystalline biofilms of other uropathogens such as *E. coli* can also disrupt urine flow [30, 111]. Our model cannot directly predict catheter blockage since we do not model biofilm-associated changes in urine flow. However, as a proxy, we predict the time until the value of the surface density of bacteria at any point on the intraluminal surface reaches a threshold of 10^7 bacteria per mm^2 (corresponding roughly to a monolayer), which we term "time to biofilm".

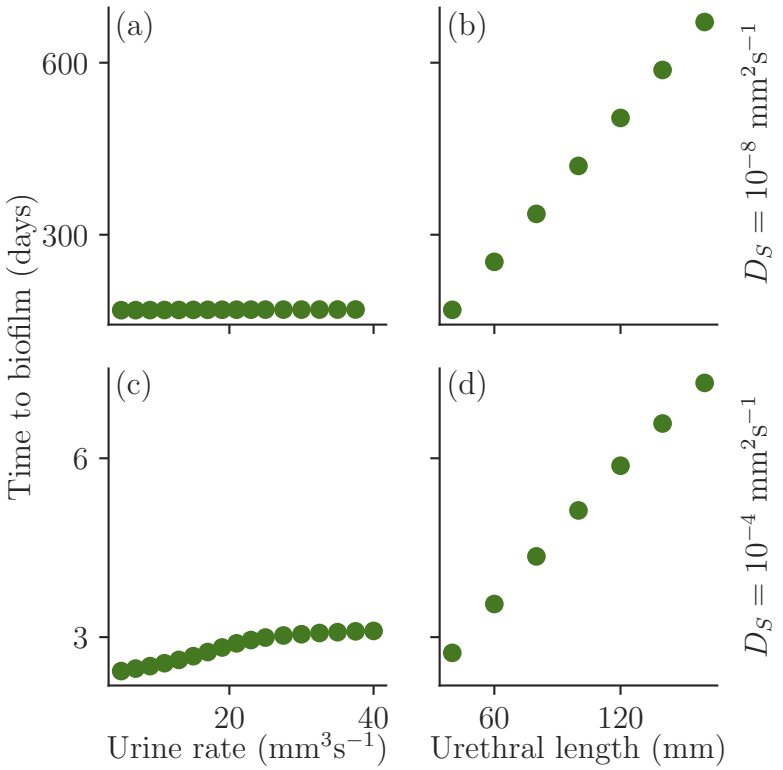

Figure 7.4 *The interplay of physical parameters and bacterial characteristics on the timescale of biofilm formation. We plot the time taken for the maximum bacterial surface density on the catheter lumen to exceed* 10^7 mm^{-2}. *Left, (a) and (c), varying the urine production rate. Right, (b) and (d), varying the urethral length. Upper, (a) and (b), have a bacterial surface diffusivity of* 10^{-8} mm^2s^{-1}. *Lower, (c) and (d), have a bacterial surface diffusivity of* 10^{-4} mm^2s^{-1}. *All other parameters are as given in Table 2.2.*

In our model, the time to biofilm formation depends on the characteristics of the human patient, of the catheter and of the infecting bacteria. Assuming that the infection starts on the external base of the catheter, bacteria must migrate up the catheter before they can populate the intraluminal surface. Bacterial migration up the catheter depends on urethral length and on bacterial surface motility (Eq. 3.1); altering either of these parameters has a drastic effect on the time to biofilm formation (compare Figures 7.4b and 7.4d with bacterial surface diffusion coefficients of 10^{-8} mm^{2}s^{-1} and 10^{-4} mm^{2}s^{-1}).

The urethral length determines the timescale of migration on the extraluminal surface, while the urine production rate determines the timescale of bacterial growth (bacteriuria) in the bladder (recall Table 6.1). The relative contributions of these two timescales to the overall infection timescale are determined by the bacterial characteristics (Figure 7.4; see §Bladder-surface regime transition for a discussion of the dimensionless number). When the bacterial motility is low, the effect of varying the urine rate is negligible (Figure 7.4a) compared to varying the urethral length (Figure 7.4b) – this is the surface dominated regime. But when the bacterial surface motility is higher, varying the urine rate has a significant effect (Figure 7.4c), on a comparable timescale to varying the urethral length (Figure 7.4d) – this is a mixed regime, with both bladder and surface dynamics affecting the overall timescale. Unfortunately, the bacterial surface motility is the model parameter which is least well-defined in the literature. In particular, surface motility is highly dependent on the surface 'wetness' (Table 2.2, §3.2).

Bladder dominated to surface dominated regime transition

The timescale over which bacteriuria or blockages develop is a combination of the time taken for bacteria to ascend the catheter, and the time taken for bacteria to proliferate within the urine. As discussed above, depending on the characteristics of the human host, catheter, and bacteria; there can be three different regimes: a surface dominated regime, a bladder dominated regime, and a mixed regime. The relevant dimensionless number controlling which regime the model is in is the ratio of the two timescales: ascension and proliferation. That is, the ratio of the characteristic time of the FKPP wavefront to ascend the catheter (§3.3.3), and the characteristic time of growth within the bladder (§4.3.1):

$$\alpha = \frac{L}{\sqrt{r_S D_S}} \Big/ \frac{\ln(\kappa_{\text{eff}}/\rho_0)}{r_{\text{eff}}} = \frac{(r_B - k_D)L}{\ln\left(\frac{\kappa_B}{\rho_0}(1 - \frac{k_D}{r_B})\right)\sqrt{r_S D_S}}, \tag{7.1}$$

where κ_{eff} is the effective carrying capacity of the bladder (§4.3.1), r_{eff} is, similarly, the effective bacterial growth rate in the bladder, and ρ_0 is the initial bacterial contamination of the bladder. All other parameters are as defined in Table 2.2.

When $\alpha \gg 1$, our model is in the surface dominated regime, and the urethral length and bacterial surface motility determine the infection timescale. When $\alpha \ll 1$, the model is in the bladder dominated regime, and the bacterial growth rate in the urine, and the urine production rate determine the infection timescale instead. The mixed regime occurs when $\alpha \approx 1$, and all the above properties contribute to the infection timescale. Using the parameter values of Table 2.2, and $\rho_0 = 1$ (since growth in the bladder occurs as soon as a single bacterium is present), $\alpha \approx 100$, and the surface properties dominate the infection timescale, as observed. This is the case for Figures 7.4a and 7.4b. If, as discussed in Chapter 3 (and seen in Figures 7.4c and 7.4d), the bacterial surface motility were as high as $D_S = 10^{-4}$ mm^{2}s^{-1}, we would instead have $\alpha \approx 1$, and be well within the mixed regime.

7.2.4 Different sources of infection produce different patterns of biofilm

As discussed in §1.3, §2.1, and §6.4, most CAUTI are thought to originate extraluminally, for example, from the gastrointestinal tract via the skin of the meatus and perineum [20, 52, 75]. However, bacteria can also contaminate the drainage bag or port and ascend the intraluminal surface of the catheter [75]. A third pathway is contamination during catheter insertion, which is thought to account for around 5% of CAUTI [82]. Sources within the bladder are also possible, either because of a urinary tract infection prior to catheterisation or because of persistent intracellular bacterial communities in the epithelial cells that line the bladder [52, 83]. In our model, different sources of infection lead to different patterns of bacterial density on the extraluminal and intraluminal surfaces of the catheter during colonisation (Figure 7.5) – even though the model always predicts eventual complete coverage of both surfaces by bacteria.

If the bacterial colonisation originates on the outside, at the catheter base (i.e., from the skin), a wave of bacteria spreads up the extraluminal surface. At early times, therefore, the model predicts high bacteria coverage on the lower part of the extraluminal surface only, while the upper extraluminal surface and intraluminal

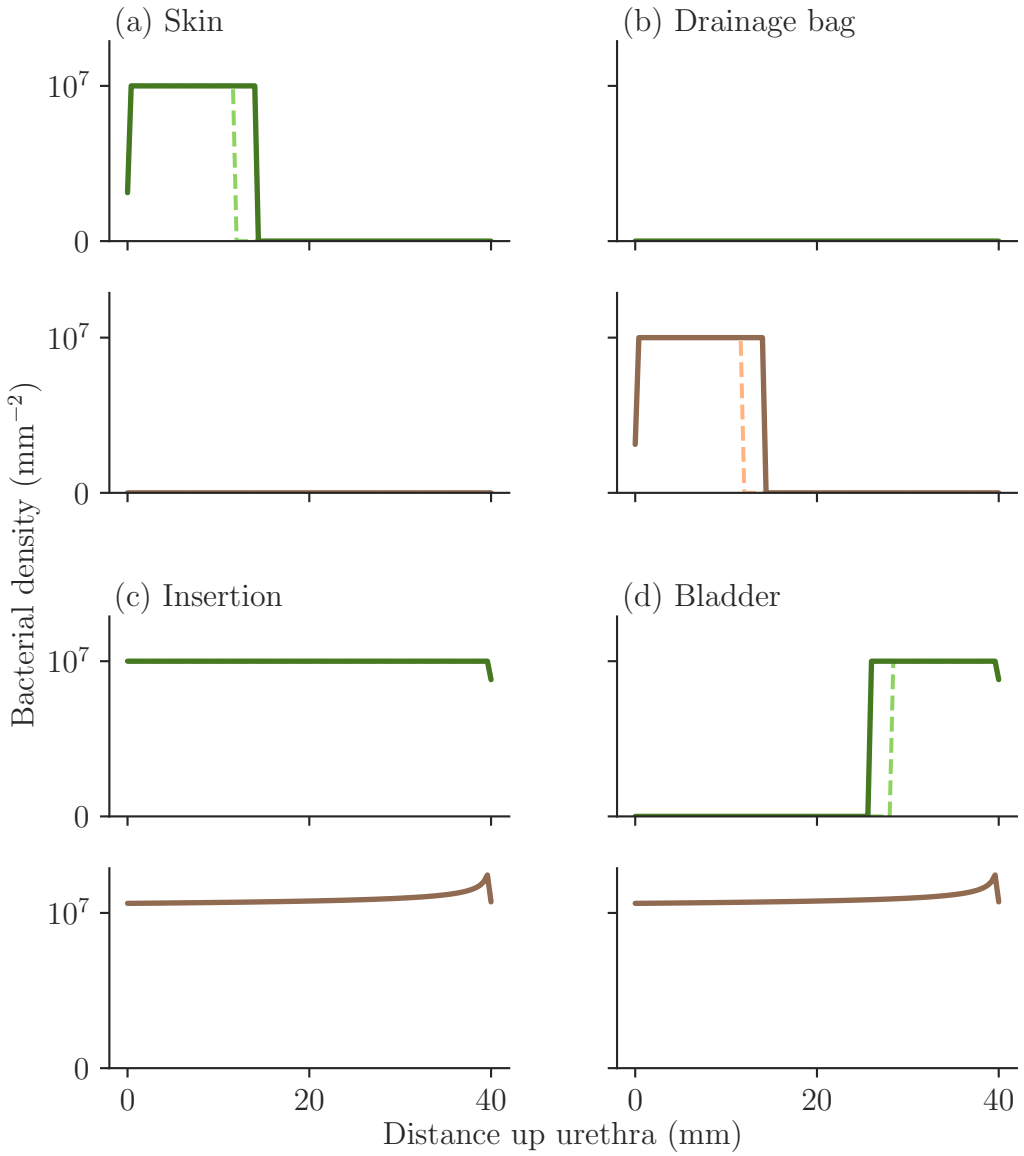

Figure 7.5 *Bacterial density patterns for four different infection scenarios. We plot the bacterial surface density for: the extraluminal surface, after 50 days (--) and 60 days (—); and the intraluminal surface after 50 days (--) and 60 days (—). Here a distance 0 mm up the urethra is the skin or drainage bag boundary, and 40 mm the bladder boundary, all parameters are as given in Table 2.2. Note that within these results we assume the intraluminal surface to be the same length as the urethra; in practice there is an additional length beyond the urethra, connecting to the drainage bag, and we would expect infections ascending from the drainage bag to have longer establishment times than infections from another scenario. (a) The skin acts as a reservoir from which infection can spread. (b) The drainage bag becomes contaminated, and bacteria ascend the catheter lumen. (c) The catheter is inoculated uniformly at time of insertion. (d) Bacteria are already present in the bladder prior to insertion.*

surface are still uncolonised (Figure 7.5a). If the origin is instead at the base of the intraluminal surface (e.g., from the drainage bag), the bacterial wave spreads up the inner surface, so that at early times, bacterial coverage is high only on the lower intraluminal surface (Figure 7.5b). If the colonisation originates in the bladder, the entire intraluminal surface rapidly becomes colonised, and a bacterial wave also propagates down the extraluminal surface from the top (Figure 7.5c). Finally, if the catheter becomes contaminated on insertion, such that bacteria become spread across the extraluminal surface, the model predicts very rapid bacterial growth over the entire extraluminal catheter surface (Figure 7.5d).

Therefore, this model predicts that while catheters that have been in place for long times will show similar patterns of bacterial colonisation, catheters that are examined sooner, before they have been fully colonised, may have qualitatively different spatial distributions of bacterial density, that reflect the source of their colonising bacteria. Measuring patterns of bacterial density on clinical catheter samples might provide a way to test these predictions. This is not commonly assessed, but as we shall discuss in Chapter 8, Wang and Zhang et al. [122, 127] measured the distribution of bacterial density on *in vitro* catheter samples (Figure 8.1), demonstrating that such measurements are feasible. And Raad et al. [96] studied the bacterial density on clinical intravenous catheters, comparing the intraluminal and extraluminal biofilm densities – finding that there was a distinct dependence on duration of catheterisation, with shorter durations of catheterisation corresponding to mostly extraluminal biofilms, while for longer durations the intraluminal biofilms had greater density (compared to the extraluminal biofilms).

7.2.5 Bacterial surface motility determines more than just ascension timescales

In Figure 7.1, we saw that urine production rate has a significant effect on the long-time bacterial density within the bladder – determining if bacteriuria will eventually occur, and the timescale over which it occurs. However, we have also seen (Figures 7.4a and 7.4c) that urine production rate has only a minimal effect on the timescale of biofilm development on the intraluminal catheter surface, and both surface diffusivity and urethral length are more significant parameters. We see this again in Figure 7.6a: the effect on the time to biofilm formation of varying the urine production rate is insignificant compared to the effect of varying the

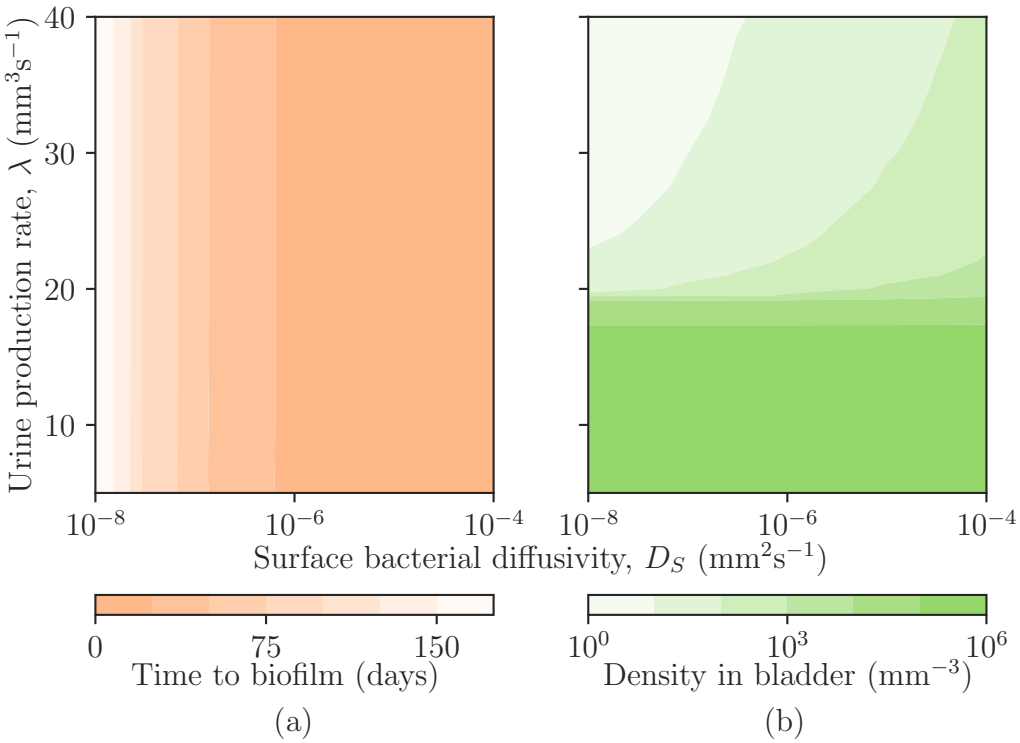

Figure 7.6 *The effects of varying the surface bacterial diffusivity and urine production rate on (a) the time until biofilm formation, and (b) the steady state bacterial density within the bladder. All other parameters as given in Table 2.2.*

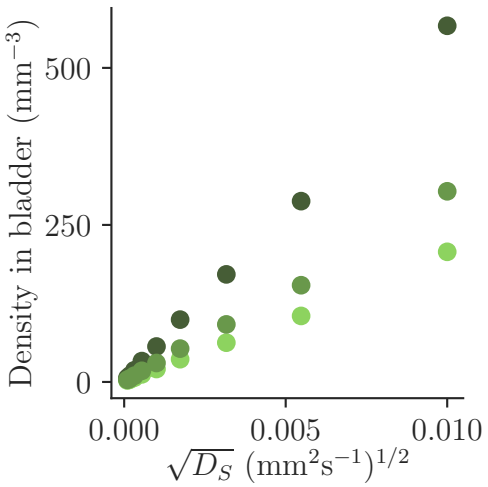

Figure 7.7 *Increasing the surface diffusivity leads to an increased effective coupling between the catheter surface and the bladder. This dependence is determined by the width of the FKPP wave (§3.3), and scales with $\sim \sqrt{D_S}$. Plotted is the steady state bacterial density within the bladder for varying values of the bacterial surface diffusivity, for values of the urine production rate of 25 (●), 30 (●), and 35 (●) mm^{3}s^{-1}. All other parameters are as in Table 2.2.*

surface bacterial diffusivity (when varying the urine production rate, λ, or the surface bacterial diffusivity, D_S, within the physiologically relevant ranges).

Surprisingly, the surface bacterial diffusivity, which we have previously considered as only affecting timescales, can also have significant effect on the outcome of the model: altering the long-time bacterial density within the bladder (Figure 7.6b). In fact, as we discussed in §7.2.1, when the urine production rate is high, $\lambda/V > r_B$, there is a washout-like transition. The non-zero bacterial population within the bladder at high urine production rates is sustained by the coupling with the catheter surface. Thus, in Figure 7.6b, we see how increasing the surface bacterial diffusivity effectively increases the coupling strength, increasing the bacterial density in the 'washed out' state.

The effect of the surface diffusivity on the coupling between catheter and bladder is indirect. The coupling term between the surface and the bladder (§6.2.1) has no explicit dependence on the diffusivity: recall Eq. 6.7,

$$\frac{k_d S_c n(L,t) - k_a V_c \rho(t)}{V}.$$

However, since the steady state bacterial density of the extraluminal catheter surface (Eq. 3.1) is greater than that of the bladder (Eq. 4.3), there is a 'dip' in the bacterial surface density $n(x,t)$ at the catheter tip (e.g. see Figure 7.5c upper). The 'steepness' of this dip is determined by the width of the FKPP wave (§3.3.2), which is $w = 8\sqrt{D_S/r_S}$. Thus, increasing the surface diffusivity effectively increases the area of catheter that is 'in contact' with the bladder, and so increases the effective coupling strength, leading to a higher bacterial density within the bladder (Figure 7.7).

7.3 Discussion

Despite the high prevalence of CAUTI, and its societal and economic costs, much remains to be understood about how bacteria colonise urinary catheters. So far in this thesis, we have formulated a mathematical model that integrates bacterial population dynamics on the catheter surfaces and in the bladder with urine flow. Bacteria migrate on the external catheter surface, populate the bladder, and flow in the urine through the catheter lumen where they can attach to and colonise the surface. The model is consistent with clinical observations that nearly all

long-term catheterisations result in bacteriuria [25, 82], and that catheterisation duration and gender are important risk factors for CAUTI [110, 123].

We have studied in detail how the characteristics of the patient, the catheter and the infecting bacteria influence bacterial density in the bladder, the time to detection of bacteriuria, the time to formation of a biofilm (a proxy for blockage), and the spatial patterns of bacteria on the catheter. The model points to urine production rate as a key parameter controlling a transition between regimes of high and low bacterial density in the bladder. Typical human urine production rates lie close to the predicted threshold (here determined by the growth rate of uropathogenic *E. coli*), suggesting that individual patients might show dramatically different levels of bacteriuria depending on their fluid intake. Drinking more water is known to be protective against urinary tract infections [43, 49, 73, 102]. For CAUTI, previous work suggests that dilution of the urine prevents its alkalisation, and hence crystallisation, by *P. mirabilis* [11]. Our work suggests that increased fluid intake can also delay catheter blockage by decreasing the density of bacteria in the urine and hence slowing down colonisation of the lumen.

Furthermore, our model predicts that reducing the residual urine volume may have similar protective effects as increasing the urine production rate, since the two parameters jointly control the dilution rate. Residual urine volumes are not typically measured within patients, and there is likely to be large variability in volumes patient to patient: values from 10 mL to as high as 500 mL have been measured [40]. Where the urine production rate can be altered by changing nursing/patient practices, the residual urine volume is more likely to be a suitable target for catheter design changes. For example, in 2007 Garcia et al. [40] proposed an alternative design for catheter tubing that reduced residual urine volumes by minimising the disruptions to urine flow that occur when catheter tubing becomes kinked.

The time taken by bacteria to migrate up the catheter is also an important factor, since it dominates the time to detection of bacteriuria and strongly influences the time to formation of a biofilm. Since migration time depends linearly on urethral length, our model predicts that women will develop bacteriuria faster than men. Gender is already a known risk factor for all urinary tract infections, with many reports of greater prevalence in women than in men [36, 59, 110]. Since catheters are typically removed after a fixed time, if the timescale of catheterisation is short (as in many hospital settings), our model would indeed predict a higher incidence

of observed bacteriuria in women than in men.

CAUTI is defined as a symptomatic infection that should be treated by catheter removal and possibly antibiotics; in contrast, asymptomatic bacteriuria may not require treatment [48, 82]. Our model does not describe the human response to bacterial infection, so cannot predict the presence or absence of symptoms such as pain or fever. However, it does make a clear distinction between bacteriuria and bacterial colonisation of the catheter lumen (i.e., biofilm formation). In the model, bacteriuria happens earlier than biofilm formation – suggesting that detection of bacteriuria does not necessarily imply a colonised catheter. Interestingly, the model also predicts that a catheter could become blocked without bacteriuria being detected at all. This happens in the regime of high urine flow, where the bacterial density in the urine is low but the lumen can still become colonised.

Inspecting the spatial patterns of biofilm on infected catheters could provide a way to test our model, as well as a pointer to the origin of an infection. Such measurements are not routinely performed, but intriguingly, a study of central venous catheters [96] observed that while biofilm formation was universal, the extent and location of biofilm formation depended on the duration of catheterization: short-term catheters had greater biofilm formation on the external surface while long-term catheters had more biofilm formation on the inner lumen. These observations are similar to our model predictions, suggesting that closer observation of the nature of the biofilm on infected urinary catheters could be highly informative.

Chapter 8

Predicting outcomes of clinical interventions

8.1 Introduction

In Chapter 2, we laid out the framework for a model for bacterial colonisation of urinary catheters. Then in Chapters 3 to 5 we discussed a specific form of this model, choosing the exact form of equations for the dynamics of the bacterial density. By Chapters 6 and 7, we were even more specific, discussing the form and results of a numerical implementation of this model. In this chapter we return to a broader perspective. We discuss the wider implications of our model and demonstrate how we can use the model to make predictions for the efficacy of prospective clinical interventions for CAUTI.

Our model has 10 parameters (Table 2.2) that together determine the behaviour of the system (Chapter 7). These parameters describe the geometry of the system, and the relevant bacterial and host characteristics. In fact, we can think of the model as a mapping, from 'parameter space' to 'outcome space':

$$\begin{aligned}
\mathcal{M}: &\quad \text{parameters} \rightarrow \text{characteristic timescales},\\
\mathcal{M}: &\quad \text{parameters} + \text{boundary conditions} \rightarrow \text{long-time (steady-state) behaviour},\\
\mathcal{M}: &\quad \text{parameters} + \text{boundary conditions} + \text{initial conditions} \rightarrow \text{dynamics}.
\end{aligned} \tag{8.1}$$

Here, the 'characteristic timescales' of the model include the timescale of bacterial

ascension of the catheter (Chapter 3), the timescale of bacterial proliferation in the bladder (Chapter 4), and the timescale of biofilm development on the intraluminal catheter surface (§7.2.3). Many of these timescales are summarised in Table 6.1. The boundary and initial conditions are as we discussed in §6.4, and reflect the 'infection narrative', e.g., the bacteria originating from the skin, the bladder, or the drainage bag. The steady-state behaviour of the model is the clinical 'outcome', for example bacteriuria, the presence of bacteria in the urine – we saw in §7.2.4 the steady state is independent of the initial condition. Finally, the system dynamics are the full description of the bacterial growth dynamics on the catheter surfaces and within the bladder.

In the model, the behaviour of the system is fully determined by its 10 parameters, boundary conditions, and initial conditions. In this interpretation, we can think of the equations of Chapter 6 as defining the mapping $\mathcal{M}$. In fact, from this perspective, we can think of Chapter 2 as describing a whole class of these mappings (e.g., not specifying the form of the bacterial motility, or the dynamics of bacterial growth on urine). Within this chapter, the majority of our results are specific to this specific mapping $\mathcal{M}$ (the specific model of Chapter 6), however in places we identify properties of the framework of Chapter 2: properties that appear to be intrinsic to the underlying physical system (i.e., independent of the choice of equation(s)).

8.2 Parameter classification

In Chapter 7 we explored the parameter space of our model. Here we use those results to classify the model parameters into three groups, according to their effects on the dynamics, long-time behaviour, and characteristic timescales. This classification is summarised in Table 8.1 and discussed in detail in the following subsections. The following discussion is based on a detailed parameter space exploration, including but not limited to the results presented in Chapter 7. All numerical simulation was performed as detailed in Chapter 6.

Parameter		Timescale significance	Long-time significance
Urethral length	L	✓	
Residual urine volume	V	$\alpha \lesssim 1$	✓
Urine production rate	λ	$\alpha \lesssim 1$	✓
Catheter internal radius	R		
Bacterial surface diffusivity	D_S	✓	
Bacterial bulk diffusivity	D_B		
Catheter surface bacterial growth rate	r_S	✓	
Bacterial growth rate in bladder	r_B	$\alpha \lesssim 1$	✓
Catheter surface carrying capacity	κ_S		
Bladder carrying capacity	κ_B		

Table 8.1 *Classifying the model parameters (Table 2.2) according to their effect on the characteristic timescales and the steady state behaviour of the model. Some parameters have conditionally significant effects on the characteristic timescales, dependent on $\alpha \lesssim 1$, as defined by Eq. 7.1 (i.e., significant only when the timescale of bacterial ascension is comparable to the timescale of bacterial growth in the bladder – requiring highly motile bacteria).*

8.2.1 Parameters with little effect

Four parameters – the catheter radius, bacterial bulk diffusivity, catheter surface carrying capacity, and bladder carrying capacity (R, D_B, κ_S, and κ_B) – have generally negligible effects on the behaviour of the model system.

Catheter radius (R)

The catheter radius only affects the intraluminal urine flow, and intraluminal bacterial growth. Within our model it appears as a dependence for the bacterial deposition flux, $j(x) \sim 1/R$. However, since bacterial deposition happens on a much faster timescale than bacterial growth or bacterial ascension of the catheter, this radial dependence has little impact on the overall infection timescale. It does have a small effect on the predicted long-time bacterial densities over the intraluminal surface, but this effect is small (for example, doubling radius might shift density from 1.2 to 1.1; see the relative size of the spike near 40 mm in Figure 7.5c lower).

Perhaps more importantly, the catheter radius will likely have an effect on the timescale over which catheter blockages occur (which our model does not predict). A greater radius will result in reduced bacterial deposition, since $j(x) \sim 1/R$, however it will also result in reduced wall shear rates (Eq. 1.5), resulting in potentially more favourable conditions for biofilm development. Clinical studies have not found the catheter radius to be significant [31].

Bacterial bulk diffusivity (D_B)

Within the model, the bacterial bulk diffusivity appears in only two places. There is a bulk diffusivity dependence of the bacterial deposition flux, $j(x) \sim D_B^{2/3}$. Therefore, changes in the bulk diffusivity can cause small shifts in the long-time bacterial density over the intraluminal surface. The bacterial bulk diffusivity also appears in the definition of the bacterial attachment rate, $k_a = 4\pi D_B \cdot 1\ \mu\text{m}$, which in turn appears in the coupling of the bladder to the extraluminal surface. Thus, increasing the diffusivity will increase the coupling strength, resulting in a linear shift in the bacterial density on the extraluminal surface at the catheter tip.

Catheter surface carrying capacity (κ_S)

The catheter surface carrying capacity only scales the bacterial surface density in the steady state; it does not affect the dynamics of the system. Therefore, the carrying capacity could have implications for catheter blockages, but otherwise, unless it approaches zero, it will not have significant effects on other outcomes (bacteriuria, CAUTI, etc.).

Bladder carrying capacity (κ_B)

If the bladder carrying capacity is below the threshold for diagnosing bacteriuria, then no bacteriuria can be observed. Beyond this, since the bladder bacterial density appears in the deposition flux, $j(x) \sim \rho$, it will have a scaling effect on the bacterial deposition, resulting in a linear shift in the steady state intraluminal bacterial density, as seen for the catheter radius and bacterial bulk diffusivity.

8.2.2 Parameters affecting characteristic timescales

Three parameters – the urethral length, bacterial surface diffusivity, and catheter surface bacterial growth rate (L, D_S, and r_S) – have a significant impact on one or more of the characteristic timescales (Table 6.1), while having lesser significance for the long-time behaviour of the model.

Urethral length (L)

There is a linear dependence of the timescale of bacterial ascension of the catheter on the urethral length. Therefore, for parameters and initial conditions such that the infection timescale is determined by the ascension time ($\alpha \gg 1$ in Eq. 7.1), doubling the urethral length will roughly double the timescale for bacteriuria to occur. Urethral length does not have any effect on the long-time state of the system.

Bacterial surface diffusivity (D_S)

As we saw in §3.3.2, the FKPP wave speed for the bacterial density on the extraluminal surface scales as $v^* \sim \sqrt{D_S}$. Thus, the timescale of bacterial ascension scales inversely with the square root of the bacterial surface diffusivity. The bacterial surface diffusivity does affect the long-time behaviour of the model as well (§7.2.5). Specifically, it scales the effective coupling of the bladder and the extraluminal catheter surface, reducing the magnitude of the washout transition discussed in §7.2.1. However for a realistic physical range of D_S values (up to 10^{-4} mm^{2}s^{-1}), this effect spans only 2 orders of magnitude in bacterial density (i.e., number of bacteria found within the bladder), much less than the washout transition (~ 6 orders of magnitude).

Catheter surface bacterial growth rate (r_S)

The surface growth rate has similar effects to the surface diffusivity. The FKPP wave speed scales as $v^* \sim \sqrt{r_S}$, leading to an inverse square root dependence of the ascension timescale on the surface growth rate. The growth rate also has an effect on the flux of bacteria from the catheter surface to the bladder, however since the physical range of the bacterial growth rate is much smaller than the range of the surface diffusivity, this has minimal effect on the bladder dynamics.

8.2.3 Parameters which control long-time behaviour

The final three parameters – the residual urine volume, urine production rate, and bacterial growth rate in the bladder (V, λ, and r_B) – significantly affect the long-time behaviour of the model. Under certain circumstances ($\alpha \lesssim 1$, Eq. 7.1; i.e., when the timescale of bacterial ascension of the catheter is comparable to the timescale of bacterial growth in the bladder), these parameters also determine the timescales.

Residual urine volume (V)

Varying the residual volume changes the dilution rate, since $k_D = \lambda/V$. This dilution rate determines both the effective growth rate within the bladder (and hence timescale of bacteriuria), and the steady state bacterial density within the

bladder (§4.3.1; §7.2.1). Recall that within the bladder, the effective growth rate $r_{\text{eff}} = r_B - k_D$ and the effective carrying capacity $\kappa_{\text{eff}} = \kappa(r_B - k_D)/r_B$.

Urine production rate (λ)

As mentioned above, the urine production rate also determines the dilution rate. However, this rate also appears in the expression for the bacterial deposition flux, $j(x) \sim \lambda^{1/3}$, resulting in a small shift in the long-time bacterial density over the intraluminal surface when the urine production rate is varied.

Bacterial growth rate within the bladder (r_B)

We have established that the behaviour of the bladder is determined by the parameter combination $r_{\text{eff}} = r_B - k_D$, and hence the bacterial growth rate is also critical for determining the timescale of bacterial growth within the bladder, and the steady state behaviour of the bacterial density. In particular, for values of the bacterial growth rate less than the dilution rate, the long-time limit (the steady state) for bacterial density within the bladder approaches zero.

8.3 Stationary state analysis

As we saw in Figure 7.5 (and wrote down in Eq. 8.1), the long-time behaviour of the model is independent of the initial conditions: there are no memory effects. We also suggested that there are some properties of the model that appear to be inherent to the underlying physical system. Here we apply a stationary state analysis to one of these properties.

It is well known that the logistic equation has two stationary states [79]: the unstable zero state, and the stable 'full' state, $n = 1$. Since the nonlinear term in the FKPP equation is logistic, the FKPP equation shares this property, with an unstable $n = 0$ state, and stable $n = 1$ state [117]. In fact, our entire model for a urinary catheter shares this property. The 'clean' system, where the catheter and urine are void of bacterial growth, is an unstable state, in which any perturbation (i.e., small contamination) will trigger bacterial growth, ultimately resulting in the 'infected' state. This property has implications for the outcomes of interventions that target CAUTI, bacteriuria, or bacterial colonisation of

catheters. Starting from this perspective, we now consider how altering the parameters of the system affects its stationary state.

All four 'low impact' parameters discussed in §8.2.1 rescale the 'infected' state. The radius (R) and bulk diffusivity (D_B) rescale the density on the intraluminal surface only, the catheter carrying capacity (κ_S) rescales the densities on both the intraluminal and extraluminal surfaces, and the bladder carrying capacity (κ_B) rescales the densities on both the bladder and intraluminal surface. However, for all finite non-zero values, none of the four parameters affect the stability of the stationary state. While in their asymptotic limits they do rescale the relevant 'infected' bacterial density state to zero, resulting in (for the relevant surface/volume) a single stable stationary state at zero, all these asymptotic limits seem physically implausible. For example, in the limit that $R \to \infty$, or $D_B, \kappa_S, \kappa_B \to 0$. Note that the reverse asymptotic limits will have somewhat different behaviour, although they are also physically implausible. $\kappa_S, \kappa_B \to \infty$ has no effect on stationary state stability, while $D_B \to \infty$ or $R \to 0$ violate our modelling assumptions (the assumption of a thin diffusive boundary layer in §5.3).

The three 'timescale' parameters discussed in §8.2.2 have little effect on the stationary states, as these parameters mainly alter the dynamics. The bacterial surface diffusivity (D_S) and catheter surface bacterial growth rate (r_S) do alter the density distribution of the extraluminal surface infected state slightly, and in the case that $r_B < k_D$ (the case of a 'washed out' bladder) they also rescale the density of bacteria in the bladder's infected state.

Finally, the three 'long-time' parameters discussed in §8.2.3 have a significant effect on the stationary state, specifically within the bladder. As observed throughout this thesis, there is a transition, between a 'washed out' low density state and a bacteriuric high density state, at $\lambda/V = r_B$, and for all parameter values such that $\lambda/V \geq r_B$, the only stationary state within the bladder is a stable zero state (or at least near zero). We note that although changing the parameters of §8.2.1 can also in principle lead to zero bacterial density within the bladder, this only occurs in the asymptotic limit, not for realistic parameter values.

8.4 Implications for clinical interventions

Catheter associated urinary tract infections (CAUTI) account for up to 40% of healthcare-acquired infections [82], and so reducing the occurrence of CAUTI is a subject of considerable clinical interest [31]. With this aim, many interventions have been proposed, which can be grouped into two broad categories. The first type of 'interventions' are modifications to healthcare guidelines, targeting hospital protocols and nursing practice. Examples include implementing 'stop' orders, that remind nurses to remove unnecessary catheters [48], or recommending the practice of chlorohexidine cleaning of the skin [28] either before catheterisation or throughout the duration of catheterisation. The second group of 'interventions' involve modified catheter design. The biggest success story of this type was the introduction of closed drainage systems in the 1960s [64], but there have also been numerous other proposals, e.g., silver-coated or antimicrobial catheters [90]. However, many of these interventions have proved ineffective in clinical practice, despite in many cases performing well in laboratory tests. In this section, we apply the model developed in this thesis to draw a new perspective on clinical interventions for CAUTI.

An emergent theme from all the discussion in this chapter is that care must be taken to select an appropriate metric against which to assess an intervention. Over and over (for example, Table 8.1), we have seen that the parameters controlling certain long-time outcomes (for example, bacteriuria is dominated by the relation $r_B > \lambda/V$) are different from the parameters controlling timescales (e.g. the timescale of ascension of the catheter is dominated by bacterial motility). This implies that the appropriate intervention must be selected for the desired outcome. The most obvious example of this is in the difference between an acute care setting (where duration of catheterisation is typically short, and hence the dynamics of the infection are likely relevant), and a long-term care setting (where the duration of catheterisation is longer, and hence outcomes are determined by the long-term behaviour). As we shall see, this has unfortunate implications for the feasibility of evaluating proposed interventions *in vitro*: it is very easy to devise laboratory tests that measure *some* property of a novel catheter, but if that property is not the one determining clinical outcomes, the intervention is unlikely to be successful. Currently, no formal regulations or standard tests exist for assessing the antimicrobial efficacy of urinary catheters *in vitro* [97].

8.4.1 A framework for understanding interventions

The first step in relating a clinical intervention to our model is to consider which parameters the intervention alters (or if it is so fundamental it would alter the equations themselves). For example, interventions relating to antiseptic cleansing likely alter the initial/boundary conditions, whereas an antimicrobial catheter coating would be likely to act through a bacterial death term – which in our model would take the form of a modified bacterial growth rate in the FKPP equation. An example of a 'fundamental' intervention that would alter the structure of our model equations would be intermittent catheterisation, where the catheter is inserted periodically, rather than being indwelling.

The second step is to consider the setting. What is the typical duration of catheterisation? What is the infecting bacterial strain? Are the outcomes being considered long-term or short-term? For example, reducing incidence of bacteriuria in hospitals (where duration of catheterisation is typically short) is a short-timescale problem, while reducing incidence of catheter blockage in care homes (where catheterisation occurs over longer durations) is likely a long-timescale problem. Based on our analysis in section §8.3, we can classify interventions into three types, which we detail below.

Postponement

Interventions which alter 'timescale' parameters (§8.2.2) can delay the occurrence of clinical outcomes (such as bacteriuria or blockage). These interventions can be very effective if they result in the timescale of the primary outcome being longer than the duration of catheterisation – so they are primarily applicable to acute-care settings. Interventions that alter the initial conditions are likely to also fall into this category: for example, antiseptic cleaning of the skin will reduce the extent to which the skin acts as a reservoir, therefore delaying (but not ultimately preventing) the occurrence of infection.

Mitigation

Interventions that rescale the stable stationary state, without altering the stability of the state (parameters in §8.2.1 or parameters in §8.2.3 that still fall below the critical threshold), may be able to reduce bacterial presence down to levels such

that the host immune system can cope. We therefore term these interventions 'mitigation'.

Prevention

Interventions that alter the stability of the stationary states, resulting in a stable zero state, can (in theory) make the expectation value of the primary outcome zero (that is, totally prevent the outcome, in all cases). For example, we would expect incidence of bacteriuria to be zero (where bacteriuria is defined as a bacterial density in the bladder greater than a threshold, e.g., 10^2 mm^{-3}) if the urine production rate is greater than $\lambda = r_B V$. Interventions which alter the governing equations may also fall into this category if they have a stable zero state. For example, not using catheters should result in zero catheter-associated infections. Less trivially, we could consider intermittent catheterisation or tidal drainage in this category.

8.4.2 Evaluating interventions within the modelling framework

New catheter designs, or any other proposed intervention, should clearly identify the outcome that they target. Preventing blockages may require a very different type of intervention to preventing bacteriuria. In short-term care settings, postponement may be equivalent to prevention: this equivalence is unlikely to be the case in long-term care facilities. Here we consider a selection of interventions (that have been proposed in the past) within the framework of our model: relating them to the model parameterisation (Table 2.2 and Table 8.1), and categorising them according to §8.4.1. We summarise this evaluation in Table 8.2 and discuss each intervention in detail below.

Chlorhexidine cleaning

Chlorhexidine is an antimicrobial agent that is commonly used topically in a variety of healthcare settings. In chlorhexidine meatal cleaning, a chlorhexidine solution is applied to the urethral meatus (the skin-urethra interface) immediately prior to catheterisation. This aims to reduce the occurrence of bacterial contamination at time of insertion (as discussed as a possible infection pathway

Intervention	Parameters	Postpone	Mitigate	Prevent
Chlorhexidine cleaning		✓		
Coiled drainage	$V \downarrow$			✓
Hydrogel coating	$\kappa_S \downarrow$, $k_a \downarrow$, $D_S \uparrow$		✓	
Nitrofural-impregnation	$r_S \downarrow$, $r_B \downarrow$	✓		
Silver-alloy coating	$r_S \downarrow$	✓		
Tidal drainage	$\lambda \uparrow$, $V \uparrow$			

Table 8.2 *Evaluating interventions in the model framework, considering effected model parameters to classify interventions, as in §8.4.1. The parameters are as defined in Table 2.2, with ↑ indicating the intervention raises the value of the parameter, and ↓ indicating a decreased value.*

in §1.3), as well as delay onset of bacterial ascension of the catheter (as the skin is initially aseptic and will take time to become colonised again). Thus, we expect chlorhexidine meatal cleaning to result in a postponement effect, with incidence of bacteriuria delayed. Only a few randomised controlled trials have investigated the efficacy of chlorhexidine meatal cleaning. Fasugba et al [28] studied 1642 patients receiving catheterisation in hospital, with mean duration of catheterisation being 4.1 days in the control group, and 2.5 days in the intervention group, and found a 74% reduction in catheter-associated bacteriuria associated with chlorhexidine meatal cleaning. However, as we shall see in §8.5, duration of catheterisation is a very important factor in incidence of bacteriuria (in §8.5, males in the control group who were catheterised for $\geq$ 4 days were $\sim$ 3 times more likely to be bacteriuric than males catheterised for $\leq$ 3 days). Fasugba et al [28] did not control for duration of catheterisation in their analysis, so the true effect size associated with chlorhexidine in that study is unknown.

Coiled drainage

As we discussed early in this thesis (§1.3), the volume of urine residual in the bladder during catheterisation is partly due to kinks in the catheter tubing which prevent full drainage. And we saw in §7.2.1 that since the dilution rate is dependent on the residual volume, $k_D = \lambda/V$, a greater residual urine volume implies a lower dilution rate, and hence increased susceptibility to bacterial

colonisation of the urine (bacteriuria). Garcia et al. [40] proposed a novel catheter design with coiled drainage tubing, that greatly reduces the residual urine volume, V, in catheterised patients. We predict that this style of catheter may reduce incidence of bacteriuria. For example, reducing the mean residual urine volume from 50 mL to 10 mL would lead to a predicted reduction in incidence of bacteriuria from 73% to 6% in females and 69% to 4% in males (resulting in a threshold urine production rate of 0.23 mL/min; analysis as in §8.5.1).

Hydrogel coating

Hydrogel catheters have a coating of insoluble hydrophilic polymers that repulse proteins and bacteria from the surface, theoretically reducing catheter encrustation and biofilm development [107], as well as reducing patient discomfort [31]. Interpreting this from the perspective of our model, we suggest that hydrogel coating reduces the carrying capacity of the catheter surface, κ_S, and the bacterial attachment rate, k_a. However, we would also expect an increase in bacterial motility, D_S, as bacteria are not stuck to the catheter surface. We would not expect a change in bacterial dynamics within the bladder, as hydrogels are not antimicrobial. Thus, our model predicts that hydrogel catheters reduce biofilm formation (since κ_S is reduced), and may reduce blockage, but also reduce the timescale of bacteriuria (since D_S is increased), resulting in higher incidence of bacteriuria in a short-term clinical setting. Clinical trials of hydrogel-coated catheters have been inconclusive [107].

Nitrofural-impregnation

Catheters impregnated with antimicrobial agents, such as nitrofurazone, are in current use in healthcare settings [101]. Nitrofurazone is an antibiotic that is effective against several common uropathogens, including *E. coli*, *S. aureus*, and *S. epidermidis*. [39]. When applied to catheters, it suppresses bacterial growth and adhesion on the catheter surface [24]. It may also have some suppressing effect on bacterial growth in the urine within the bladder, as it leaches from the catheter into the urine. However, multiple studies have found that the efficacy of nitrofural catheters wanes rapidly in time [24, 39], likely due to the concentration of nitrofurazone on the catheter dropping. Gaonkar et al. [39] performed 'zone of inhibition' assays, in which catheter segments were embedded in agar seeded

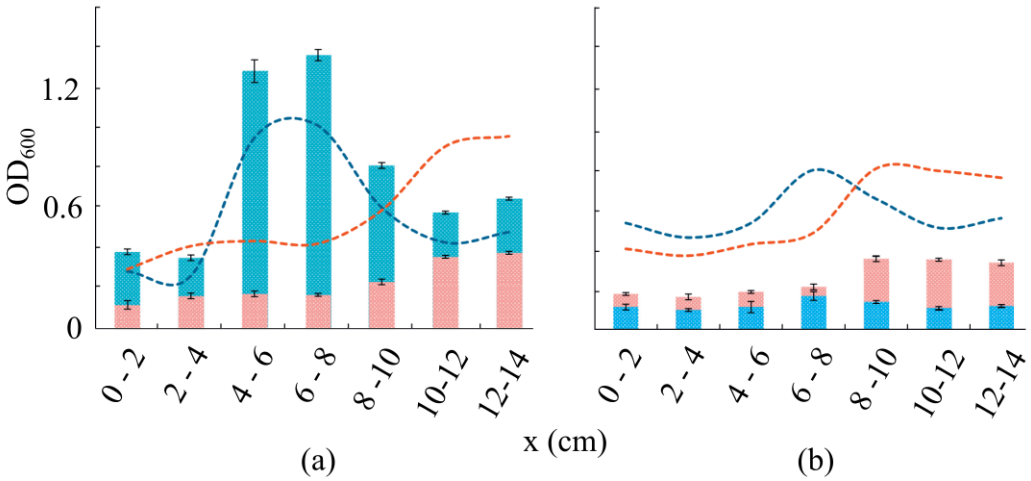

Figure 8.1 *Efficacy of silver-PTFE coating in reducing bacterial ascension of the catheter. The bars are optical density measurements (UV absorbance after crystal violet staining) of the biofilm distribution along the extraluminal surface of silicone (■) catheters, or silver-PTFE coated (■) catheters. Overlaid is the normalised biofilm density distribution over the silicone (- -) and silver-PTFE coated (- -) catheters. (a) Bacterial density at the 'skin' ($x = 13$ cm) was 10^6 cells/mL; 'bacteriuria' occurred after 1.8 days (silicone) or 4 days (silver-PTFE). (b) Bacterial density at the 'skin' ($x = 13$ cm) was 10^2 cells/mL; 'bacteriuria' occurred after 6 days (silicone) or 41 days (silver-PTFE). Figure reproduced with modifications from Wang et al., 2019, Figure 2c–d [121].*

with a high (10^8 CFU/mL) concentration of test organisms and incubated. The diameter of the 'dead zones', where growth was suppressed, was measured. The authors observed the waning efficacy of nitrofural catheters by repeating this assay over multiple days with the same catheter segment. Their results show that within 3 days nitrofural catheters no longer suppress the growth of *E. coli* or *S. aureus*, and the diameter of the inhibition zone for *S. epidermidis* is reduced from 17.5 mm to 4.5 mm (a reduction in area of effect of 93%). Similarly, Desai et al. [24] examined the waning efficacy of nitrofural catheters for preventing bacterial adhesion to the catheter surfaces and found that adhesion of *E. coli* to nitrofural catheters, though reduced, could occur within 3 days of catheter use. In our model, this would result in a time-dependent bacterial surface growth rate (r_S), with a value that is initially zero, but increases with time to approach the bacterial surface growth rate value in the absence of antimicrobials.

Silver-alloy coating

Silver-alloy coated catheters are the most commonly used type of antimicrobial catheter [101]. While silver is less effective at killing microbes than nitrofurazone, silver-alloy catheters do not suffer from rapid waning efficacy in the same manner as nitrofural catheters [101]. Zhang et al. [127] investigated the efficacy of a silver-PTFE coated catheter in preventing *E. coli* ascension up the catheter in an *in vitro* bladder model, in which a catheter was embedded in an agar 'urethra' with an artificial urine growth medium flowing down the catheter from a 'bladder'. The authors measured the biofilm density (via UV absorbance after crystal violet staining) on catheter sections at different positions along the catheter, to obtain bacterial density profiles, similar to those we numerically simulated in Figure 7.5, as well as measuring the time from inoculation until 'bacteriuria' (here defined as $\geq 10^3$ CFU/mL within the 'bladder').

In a separate paper arising from the same *in vitro* study, Wang et al. [121] compared bacterial ascension for a bacterial density at the 'skin' ($x = 13$ cm) of either 10^6 cells/mL, or 10^2 cells/mL (Figure 8.1). The shapes of the observed bacterial density distributions are strikingly similar to the FKPP density wave profiles we discussed in Chapter 3, particularly Figure 3.3a and Figure 3.4a. Specifically, the blue dashed lines (Figure 8.1) are density profiles measured by Wang et al. [121] for an experiment with a 'fixed' boundary at $x = 13$ cm (where Wang et al. [121] placed the catheter in contact with a reservoir of bacteria), and very steep initial conditions (the catheter was initially clean). The peak in the middle results from the nonlinear spreading of the initial condition, which has been overtaken by the linear FKPP wavefront to the left [117].[1] The red dashed lines are characteristic of an FKPP wave with a slower growth term relative to the diffusion term: the non-linear initial conditions relax to the asymptotic waveform (§3.3.3).

Wang et al. [121] determined the time taken to 'bacteriuria' to be 1.8 days (silicone) or 4 days (silver-PTFE), for a 'skin' density of 10^6 cells/mL, and 6 days (silicone) or 41 days (silver-PTFE), for a 'skin' density of 10^2 cells/mL. Assuming FKPP dynamics (as in our model; Chapter 3), we can estimate both r_S and D_S for silver-PTFE catheters, compared to silicone catheters, and calculate a 'wavespeed modifier' that parameterises the efficacy of silver-PTFE coated

[1] The FKPP wavefront is travelling with the linear spreading velocity (recall v^* in §3.3.1) that results from perturbing the initially zero unstable state. Meanwhile, the initial conditions behave according to the non-linear growth dynamics (the reaction term in the FKPP equation).

catheters in delaying bacteriuria compared to silicone catheters:

$$\Delta v = \sqrt{\frac{r_{S;\text{Ag-PTFE}} D_{S;\text{Ag-PTFE}}}{r_{S;\text{silicone}} D_{S;\text{silicone}}}}. \tag{8.2}$$

Here we have four independent measurements (the time to 'bacteriuria' for each case) and four unknown parameters. Our model predicts that the time taken to bacteriuria is the timescale for the asymptotic (FKPP) wavefront to reach the top of the catheter, plus the timescale over which the bacterial density grows to the detection threshold, once the bladder is contaminated:

$$\begin{aligned} \mathcal{T} &= \tau(x{=}0 \to x{=}L) + \tau(N{=}N_0 \to N{=}N_{\text{detect}}) \\ &= \frac{L}{2\sqrt{r_S D_S}} + \frac{1}{r_S} \log\left(\frac{N_{\text{detect}}}{N_0}\right), \end{aligned} \tag{8.3}$$

where N_0 is the initial inoculation density (here either 10^6 cells/mL or 10^2 cells/mL), N_{detect} is the threshold sensitivity (here 10^3 CFU/mL), L is the urethral length (here 13 cm in the laboratory setup), r_S is the bacterial growth rate on the surface, and D_S the bacterial surface diffusion coefficient. By evaluating Eq. 8.3, we find

$$\begin{aligned} r_{S;\text{Ag-PTFE}} &= 0.062 \text{ day}^{-1} & D_{S;\text{Ag-PTFE}} &= 4200 \text{ mm}^2\text{day}^{-1} \\ r_{S;\text{silicone}} &= 0.55 \text{ day}^{-1} & D_{S;\text{silicone}} &= 2400 \text{ mm}^2\text{day}^{-1} \\ \Delta v &= 0.44. \end{aligned} \tag{8.4}$$

Comparing the parameters obtained in Eq. 8.4 with the parameters we assumed in Table 2.2, which were based on observed values in the literature ($r_S = 0.69$ hr^{-1}; $D_S = 10^{-8}$ mm^{2}s^{-1}), we see that, when put in the same units, our calculation (Eq. 8.4) results in values of $D_S \sim 10^{-2}$ mm^{2}s^{-1}, and $r_S = 2 \times 10^{-2}$ hr^{-1}. These describe a bacterial strain that is highly motile and unusually slow growing. Unfortunately, the strain used by Wang et al. [121] was a uropathogenic *E. coli* clinical isolate that has not been well characterised, and Wang et al. [121] did not measure the growth rate of the bacterial strain on the artificial urine medium they utilised within the study. It seems plausible that the artificial urine medium choice was constraining the bacterial growth in their study. As mentioned above, this strain appears to be highly motile,[2] but notably, the motility increases for

[2] *E. coli* is known to exhibit swarming behaviours, with similar motility to as observed by Wang et al. [121], this has been observed particularly for *E. coli* cells confined between agar and a surface [57] – exactly as was the case in the setup of Wang and Zhang et al. [121, 127].

the silver-PTFE coating. This may be a result of the PTFE component of the coating, which is highly hydrophobic.

Tidal drainage

Standard Foley catheters, as discussed throughout this thesis, drain the bladder continuously, resulting in infection dynamics as discussed in Chapter 4, with bacteriuria occurring if the bacterial growth rate exceeds the dilution rate, $r_B > \lambda/V$. Tidally draining catheters instead allow the bladder to fill and empty through raising the height of the drainage tubing or bag, and then intermittently lowering the bag to form a syphon [31], mimicking the natural drainage of the bladder. In this case, the condition on the growth rate for the occurrence of bacteriuria is as found by Gordon and Riley [43] for the case of regular (periodic) micturition (Eq. 4.12):

$$r_B > \log\left(\frac{V_{\max}}{V_{\min}}\right)\frac{\lambda}{V_{\max}-V_{\min}},$$

where $V_{\max}$ is the maximum urine volume in the bladder, and $V_{\min}$ is the minimum urine volume within the bladder. Typical values for $V_{\max} \sim 300$ mL in healthy bladders, and for $V_{\min} \sim 10$ mL [43].

We might interpret this as suggesting that for the same colonising species (for example, a uropathogenic *E. coli* strain, with growth rate ~ 1.4 hr^{-1}), the urine production rate threshold for bacteriuria susceptibility is altered compared to that for the regular Foley catheter configuration. In §8.5.1, we will discuss the natural variability in urine production rates among the population in detail. Our model suggests that for 'standard' Foley catheters, the threshold value of urine production rate, below which bacteriuria occurs, is 1.16 mL/min, which when combined with the population distribution of urine production rates, results in an estimated fraction of 73% of females, and 69% of males who are susceptible to bacteriuria. The remaining individuals in the population have urine production rates that are high enough that our model predicts that they will never develop bacteriuria when catheterised with a standard Foley catheter. However, we find that for tidally draining catheters, the threshold value is 1.97 mL/min, resulting in a higher susceptible fraction of $\sim$ 90% of females, and $\sim$ 89% of males.[3]

[3]To be fair to tidal drainage, we can obtain better results if we drain the bladder more frequently, and do not allow the maximum bladder volume to exceed the typical values seen in 'standard' catheterisation: $V_{\max} = 50$ mL $\rightarrow$ 38% and 30%. However, reducing the residual

We might compare this prediction with the results of an actual study on tidal drainage, where it was found to reduce the rate of infection from 73% to 15% [31], and be surprised, since our prediction is that tidal drainage performs worse. But we should bear in mind that the study quoted on tidal drainage dates to 1943 [98], which predates the introduction of a closed drainage system [64]. Prior to closed drainage, the majority of bacterial colonisation of catheters was intraluminal: today the majority (66%) is extraluminal [82]. And tidal drainage is very effective in flushing bacteria from within the catheter lumen, while leaving the bacteria on the extraluminal surface untouched. Tidal drainage is not commonly used today.

8.5 Case study: predicting the results of a clinical trial

Pickard et al. [90] recruited 7102 UK adults receiving short-term catheterisation (mostly patients undergoing surgical procedures) between 2007 and 2010 for a multicentre randomised control trial[4] investigating the efficacy of antimicrobial catheters in preventing CAUTI. Patients were randomly assigned one of three catheter types: silver-alloy coated latex (referred to throughout this section as 'Silver'), nitrofural-impregnated silicone (referred to as 'Nitro'), or polytetrafluoroethylene-coated latex (the control group; referred to as 'PTFE'). Outcomes data collected included the incidence of symptomatic CAUTI, and the incidence of bacteriuria (bacteria present within the urine). The analysis by Pickard et al. [90] – identifying an absolute reduction of 3.3% in incidence of symptomatic CAUTI as a minimum effect size for clinical relevance – found no statistically significant difference across the randomised groups. The incidence of bacteriuria was regarded as a secondary outcome, and the authors did find a significant reduction in incidence of bacteriuria for nitrofural-impregnated catheters compared to PTFE-coated catheters, but not for silver-alloy catheters compared to PTFE-coated catheters.

The mathematical model developed in this thesis does not predict symptomatic CAUTI, but it does make predictions for catheter-associated bacteriuria. In

volume (for example §Coiled drainage) is significantly more effective.

[4]Randomised control trials (RCT) are "prospective studies that measure the effectiveness of a new intervention or treatment ... randomisation balances participant characteristics (both observed and unobserved) between the groups allowing attribution of any differences in outcome to the study intervention." (Hariton and Locascio, 2018; [45])

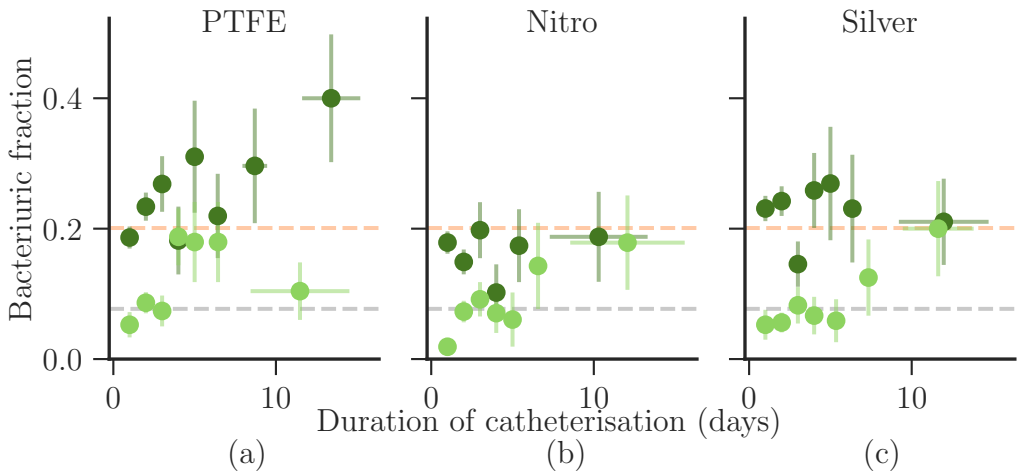

Figure 8.2 *The fraction of patients with a positive CFU result (bacteriuric) for each intervention group, plotted against duration of catheterisation. (a) 1201 females (●) and 762 males (●) received 'PTFE' catheters. (b) 1060 females (●) and 633 males (●) received 'Nitro' catheters. (c) 1078 females (●) and 612 males (●) received 'Silver' catheters. The upper horizontal line (--) is the mean bacteriuric fraction across all patients with a duration of catheterisation > 7 days. The lower horizontal line (--) is the baseline fraction of patients bacteriuric prior to catheterisation. Data has been cleaned and binned according to duration of catheterisation (Table B.1).*

particular, the model predicts the timescale of onset of bacteriuria (§7.2.2), and patient susceptibility to bacteriuria, dependent on physical and biological parameters (§7.2.1). As discussed in §Bladder-surface regime transition, the time before bacteriuria is detected is the sum of the timescale of bacterial ascension of the catheter and the timescale of bacterial proliferation within the bladder. Thus, the model predicts that if a patient is susceptible to bacteriuria (having a urine production rate below the threshold value; §8.5.1), they will develop bacteriuria if catheterised for a duration greater than their timescale of bacteriuria (as determined by their parameterisation within the model). Thus, if we apply the model to a population of such patients, each with a given duration of catheterisation, we can predict the incidence of bacteriuria: i.e., the fraction of patients whose duration of catheterisation is greater than their timescale of bacteriuria.

We can test the predictive capability of the model by applying it to the dataset of Pickard et al. [90], which contains data on both incidence of bacteriuria, and duration of catheterisation. We were able to obtain access from the authors (§B.0.1) to data from the study dataset. For 6394 patients we were provided

data on: the duration of catheterisation, sex, type of catheter received, and a True/False result for 'bacteriuria' (a bacterial count in the urine $> 10^4$ CFU/mL up to 3 days after catheter removal). After cleaning the data to remove patients with missing data entries (§B.1.1), we had data on 5369 patients, who we sorted into groups according to sex and catheter type used, and binned according to their duration of catheterisation (Table B.1; §B.1.2).

The incidence of bacteriuria in this dataset can be seen to differ between males and females (Figure 8.2) – as our model predicts since males and females have very different urethral lengths (§8.5.2). The baseline rate of bacteriuria in patients within the study (i.e., patients for whom bacteria were present in the urine prior to catheterisation) was $7.7 \pm 0.3\%$ (Figure 8.2: grey dashed line). For longer durations of catheterisation (> 7 days), both males and females, for all catheter types, can be seen to converge to the same incidence of bacteriuria: $20 \pm 2\%$ (§B.2.1). Looking at the male data (light green), we see that the bacteriuric fraction transitions between the baseline fraction and the long-time fraction on a timescale between 3 and 10 days, with qualitatively different behaviour for each of the three intervention groups (compare Figures 8.2a, 8.2b, and 8.2c).

As we shall see (§8.5.2), the mean urethral length in males is ~ 7 times longer than in females, so – given that we are observing the timescale of bacteriuria for males to be between 3 and 10 days – we expect the transition in bacteriuric fraction for females to occur on a timeframe $\lesssim 1$ day (as the timescale of bacteriuria scales linearly with urethral length). Thus, as the resolution of the study data is 1 day, we do not expect to see any transition in the bacteriuric fraction for the female data (dark green).

In the following section, we apply the model to predict the efficacy of silver-alloy and nitrofural-impregnated catheters in reducing incidence of bacteriuria in males, and then compare these predictions to the data collected in the study of Pickard et al. [90]. We gather data on population distributions of urine production rate (§8.5.1) and urethral length (§8.5.2) from the literature, as this data was not collected by Pickard et al. [90]. We utilise this distribution data to develop a model fit to the male control data (PTFE), from which we obtain a fitted value[5] for the speed of bacterial ascension of the catheter, v_{asc}

[5]Our model predicts that $v_{\text{asc}} = 2\sqrt{r_S D_S}$ (§3.3.2), but as discussed in Chapter 3, (literature) estimated values for D_S are highly variable, dependent on both bacterial strain characteristics and catheter surface properties, and while r_S is less uncertain, estimating r_S requires knowledge of the colonising bacterial species and strain - which we lack. Thus, in this context, our model is unable to predict the value of v_{asc}, and fitting is appropriate.

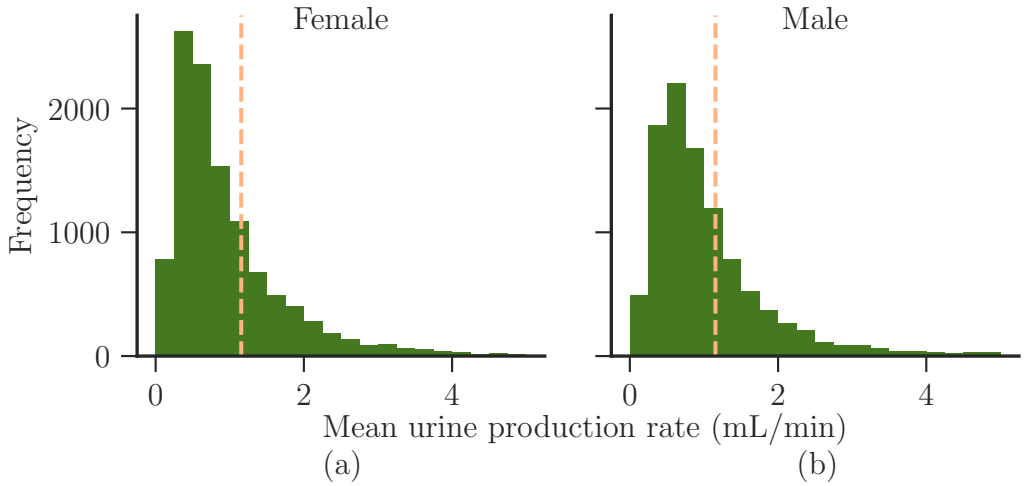

Figure 8.3 *Distribution of average urine production rates in the US population. (a) A sample population of 11011 adult females. (b) A sample population of 10202 adult males. The pink vertical dashed line represents our model estimation of the bacteriuric susceptibility threshold. Patients with higher mean flow rates than this threshold are not predicted to develop bacteriuria, even if catheterised. Patients with lower mean flow rates are predicted to be at greater risk of bacteriuria if catheterised. Data from the CDC National Health and Nutrition Examination Survey, 2009-2014 [81].*

(§8.5.3).Through the exploration of catheter properties and parameterisation of §8.4.2, we obtain predictions for the change in parameterisation for Nitro and Silver catheters, relative to PTFE catheters. This gives rise to model predictions for the dependence of the incidence of bacteriuria on duration of catheterisation for the Nitro and Silver male study groups (§8.5.4). Finally, we apply the model fit (PTFE) and predictions (Nitro and Silver) to the study duration data, to predict the overall incidence of bacteriuria in males in the study and compare these predictions to the outcomes observed in the study (§8.5.5).

8.5.1 Urine production rates in the population

As we saw in Chapter 4 and discussed further in §8.2.2, the urine production rate, λ, is critical in determining the model predictions for catheter-associated bacteriuria. If the dilution rate, $k_D = \lambda/V$ exceeds the bacterial growth rate, 'washout' occurs, and there can no longer be a sustained bacterial population within the urine. In Table 2.2, we established the mean urine production rate (for humans) to be 1 mL/min, and then in §7.2.1, discussed how (assuming the residual urine volume to be 50 mL), this mean rate is close to, but below, the

critical rate, $\lambda = r_B V$.

Of course, not all people have the same urine production rate – within the population there is a distribution of urine production rates, so while the average person falls short of the critical rate, there is a subgroup of the population who exceed it. Our model predicts that these people, with urine production rates exceeding the critical rate, $\lambda > r_B V$, are not susceptible to catheter-associated bacteriuria.

Through the annual *National Health and Nutrition Examination Survey*, the CDC collects health data on a random sample of the US population. This dataset includes the urine production rate and is available online for years from 2009–2020 [81]. Figure 8.3 shows the distribution of urine production rates in the US adult population between 2009 and 2014 (a timeframe comparable to the timeframe of data collection for the study considered in §8.5). Overlaid with a pink dashed line is the critical urine production rate predicted by our model for catheter-associated bacteriuria, assuming parameters as in Table 2.2 (colonisation by uropathogenic *E. coli*). From this we derive an estimate of the susceptible fraction of the population (those with urine production rates less than the threshold value, $\lambda < r_B V = 1.16$ mL/min): $72.9 \pm 0.4\%$ of females, and $68.8 \pm 0.5\%$ of males (§B.2.2). We can also calculate the population mean urine production rate: 1.00 ± 1.15 mL/min in females, and 1.09 ± 1.12 mL/min in males – consistent with the 1 mL/min of Table 2.2.

In our previous discussion (§8.5), the outcome discussed as 'bacteriuria' was defined as a urine culture of $> 10^4$ CFU/mL, up to 3 days after catheter removal. Since the timescale over which bacteriuria occurs is also determined by the urine production rate (§7.2.1), the population who are expected to develop a bacterial count of 10^4 CFU/mL within 3 days of bacterial contamination of the bladder is slightly lower than the total susceptible population. Recalling Eq. 4.8,

$$\rho(t) = \frac{(r_B - k_D)\kappa_B \rho_0 \mathrm{e}^{(r_B - k_D)t}}{(r_B - k_D)\kappa_B + r_B \rho_0 \left(\mathrm{e}^{(r_B - k_D)t} - 1\right)},$$

we can calculate the value of k_D for which $\rho(t = 3 \text{ days}) = 10^4$ CFU/mL, from an initial inoculation of $\rho_0 = 1$ CFU/mL. From this we find the critical urine production rate to be 1.05 mL/min, resulting in an estimate of the susceptible population as $68.9 \pm 0.4\%$ of females, and $63.8 \pm 0.5\%$ of males.

In the study of Pickard et al. [90], $72.1 \pm 0.6\%$ of study participants received

antibiotics prior to surgery. We would not expect these patients to develop bacteriuria within the study duration. This leaves $27.9 \pm 0.6\%$ of the study participants potentially susceptible to bacteriuria. From the discussion above, if we assume the study participants to be similar to the population sampled in Figure 8.3, we estimate the fraction of this population that is susceptible to bacteriuria to be $68.9 \pm 0.4\%$ of the potentially susceptible females, and $63.8 \pm 0.5\%$ of the potentially susceptible males (see preceding paragraph). This results in an estimate of $19.2 \pm 0.4\%$ of females and $17.8 \pm 0.4\%$ males in the study who are susceptible to catheter-associated bacteriuria.[6] This estimate compares favourably to the $20 \pm 2\%$ of the study participants who were catheterised for a duration of 7 days or more who were observed to have positive urine culture (bacteriuric; Figure 8.2). To test if this is coincidence or a true explanation would require urine production rate data for the study participants, which unfortunately Pickard et al. [90] did not collect. Unfortunately, we also did not obtain data on which patients in the dataset had been treated with antibiotics (although such data might be available on further request).

Increasing fluid intake is known to be protective against urinary tract infections (UTI) [43, 49, 73, 102], and several studies have linked increased fluid intake with lower rates of catheter encrustation and blockages [11, 13]. In Chapter 4, we proposed a mechanism through which increased fluid intake (which is correlated with urine production rate) can be directly protective against catheter-associated bacteriuria, since this rate governs a washout transition within the bladder. Using the data fits presented here, we can now quantify the reduction in risk of catheter-associated bacteriuria that is associated with a (modest) increase in fluid intake (Table 8.3; §B.2.2). In the study by Pickard et al. [90], we estimate only $27.9 \pm 0.6\%$ of study participants to be potentially susceptible to bacteriuria. If we look for a 3.3% reduction in absolute incidence of bacteriuria (as Pickard et al. [90] calculated to be required for clinical significance), our model predicts this could be obtained by increasing the mean urine production rate of study participants (ie increasing their fluid intake) by ~ 400 mL/day.[7]

[6] $0.279 \times 0.689 = 0.192 \ldots$

[7] For example, for males: $68.8 - 3.3/27.8 = 57.0$ %, which we see from Table 8.3 is attained with an increase of ~ 400 mL/day.

Increase in urine production rate	Predicted susceptibility		Relative risk adjustment	
	Female	Male	Female	Male
(mL/day)	(%)	(%)	(%)	(%)
0	72.9 ± 0.4	68.8 ± 0.5	-	-
100	70.4 ± 0.4	65.5 ± 0.5	-3.4 ± 0.8	-4.7 ± 0.9
200	67.3 ± 0.4	62.2 ± 0.5	-7.7 ± 0.8	-9.6 ± 0.9
300	63.6 ± 0.5	58.4 ± 0.5	-12.7 ± 0.8	-15.1 ± 0.9
400	60.1 ± 0.5	53.6 ± 0.5	-17.6 ± 0.8	-22.1 ± 0.9
500	55.7 ± 0.5	48.6 ± 0.5	-23.6 ± 0.8	-28.3 ± 0.9

Table 8.3 *Our model predicts that increasing fluid intake decreases susceptibility to catheter-associated bacteriuria. An increase in urine production rate of 100 mL/day is equivalent to 0.07 mL/min.*

8.5.2 Urethral lengths in the population

Urethral length, L, determines the timescale for bacterial ascension of the catheter (Chapter 3), and as discussed in §8.2.2, for $\alpha \gg 1$ (surface-dominated behaviour), the overall timescale of bacterial colonisation scales roughly linearly with urethral length. In Table 2.2, we took the urethral length as 40 mm in females, and 160–200 mm in males – a common assumption in the literature [31]. In fact, as we shall see below, urethral length is normally distributed within the population.

Pomian et al. [94] measured the urethral lengths of 927 Caucasian adult females, and found the urethral lengths to be normally distributed, with mean 30.1 mm, and standard deviation 4.2 mm. Kohler et al. [60] measured the urethral lengths of 109 American adult males, and similarly observed a normal distribution, with mean 223 mm, and standard deviation 24 mm. From this we see that the sex disparity in urethral lengths is even greater than we previously assumed, and for males the variance in urethral lengths is substantial. In particular, we expect bacteriuria to occur in females ~ 7 times faster than in the average male (as the mean female urethra is ~ 7 times shorter than the mean male urethra), and we expect $\sim 20\%$ difference in the time to bacteriuria for males with shorter urethras vs. males with longer urethras.

8.5.3 Fitting the model to find $v_{\mathbf{asc}}$

As discussed in §8.5, in Figure 8.2 we saw that the timescale of bacterial colonisation in females seems to be less than 1 day (the resolution of the study data for duration of catheterisation). As a result, we are unable to meaningfully compare the model predictions to the study data for females. Hence, in the following subsections we focus only on male data.

We assume males within the study of Pickard et al. [90] to have urethral lengths normally distributed, with mean 223 mm, and standard deviation 24 mm, in line with the population data of Kohler et al. [60] (§8.5.2). Our model predicts that a patient will develop bacteriuria if they have been catheterised for a duration that exceeds the timescale for bacteria to ascend their catheter. Here we neglect to include the timescale of bacterial proliferation within the bladder, as this is typically $\sim$ 2.1 days (for parameter values as in Table 2.2), which is less than the 3 day window post-catheterisation in which Pickard et al. [90] tested for the occurrence of bacteriuria (in other words, we expect almost all patients who were catheterised for a duration greater than the ascension timescale to have a positive CFU result). As we discussed in §3.3.2, the characteristic timescale of ascension is $L/v_{\text{asc}} = L/2\sqrt{r_S D_S}$. The model prediction for the dependence of bacteriuric fraction on catheterisation duration is then a cumulative function: the fraction of patients for whom the predicted timescale of ascension is less than the catheterisation duration. Since urethral lengths are normally distributed, the model prediction for the bacteriuric fraction takes the form of a sigmoid (error) function [29], with mean L_μ/v_{asc}, and width L_σ/v_{asc} (where L_μ is the mean urethral length, here taken to be 223 mm, and L_σ is the standard deviation on the mean urethral length, here taken as 24 mm):

$$\begin{aligned} f(T; v_{\text{asc}}) &= f_0 + \frac{f_{\text{sus}}}{2}\left[1 + \text{erf}\left(\frac{T v_{\text{asc}} - L_\mu}{\sqrt{2} L_\sigma}\right)\right] \\ &= 0.077 + 0.10\left[1 + \text{erf}\left(\frac{T v_{\text{asc}} - 223 \text{ mm}}{24\sqrt{2} \text{ mm}}\right)\right], \end{aligned} \tag{8.5}$$

where $f(T)$ is the fraction of patients catheterised for duration T who have positive CFU result, f_0 is the baseline bacteriuric fraction (§8.5), and f_{sus} is the total fraction of the population susceptible to bacteriuria (for example, not taking antibiotics, with urine production rate below the washout threshold; §8.5.1), L_μ is the mean urethral length, L_σ is the standard deviation of the urethral length distribution (§8.5.2), and erf is the error function. Here we take $f_{\text{sus}} = 20\%$,

the mean bacteriuric incidence for catheterisations > 7 days (as in §8.5). An alternative modelling choice would be to take $f_{\text{sus}} = 17.8\%$, the (model) predicted bacteriuric susceptibility in the male study participants (§8.5.1). This alternative choice would result in a slightly lower prediction of the overall bacteriuric fraction but does not significantly alter the fit for v_{asc}. In fact, as we can see in Figure 8.4, the fit we obtain from Eq. 8.5 (green dashed line) is excellent. We discuss this fit further below.

We fit Eq. 8.5 to the control group data, to determine the wavespeed, v_{asc} for the PTFE catheter group (Figure 8.4). We obtain a fitted value $v_{\text{asc}} = 61.2 \pm 7.7$ mm/day, corresponding to a mean ascension time of 3.65 ± 0.46 days. In principle we can compare this to the parameter space exploration we performed in §7.2.3 by assuming a value of r_S as typical of *E. coli* (as in Table 2.2), and taking $v_{\text{asc}} = 2\sqrt{r_S D_S}$ to estimate $D_S \sim 6 \times 10^{-4}$. This is similar to the value we previously took as an upper estimate for D_S (§3.2), which was the active diffusion coefficient of *E. coli* swimming freely in a bulk medium (water). We might interpret this as suggesting that in this context, bacterial migration up the catheter is primarily a swimming motility mode (perhaps through the mucosal layer), rather than a slower surface (biofilm) growth-mediated spread, or faster swarming behaviour (§3.2).

In the discussion above we have used the model predicted wavespeed, arising from the FKPP equation, $2\sqrt{r_S D_S}$. However, ascertaining the bacterial surface diffusion coefficient, D_S from the literature is challenging, as it depends on both bacterial strain-specific characteristics, and on catheter surface properties – both material-specific properties and surface 'wetness'. In fact, as we saw in Chapter 3, in the literature we find an estimated range of values for D_S that spans many orders of magnitude. Additionally, while the bacterial growth rate, r_S is better defined, it is also strain-specific. In the context of this study, we do not know the colonising bacterial species, and so we can estimate neither r_S or D_S.

It is common in the literature to assume a linear increase in bacteriuric incidence with duration of catheterisation – indeed this assumption is made by Pickard et al. [90] in their analysis. Our model suggests a sigmoidal fit (Eq. 8.5) should be more appropriate than a linear fit. We can compare a linear fit (Figure 8.4 grey dotted line) with our model sigmoidal fit, for example by calculating the residual sum of squares (RSS). We find RSS = 0.011 for the sigmoidal fit, a better result than RSS = 0.018 for the linear fit (§B.2.3).[8] Furthermore, the sigmoidal fit is a

[8] If, as we discussed above, we fit our sigmoidal function (Eq. 8.5) with $f_{\text{sus}} = 17.8\%$, rather

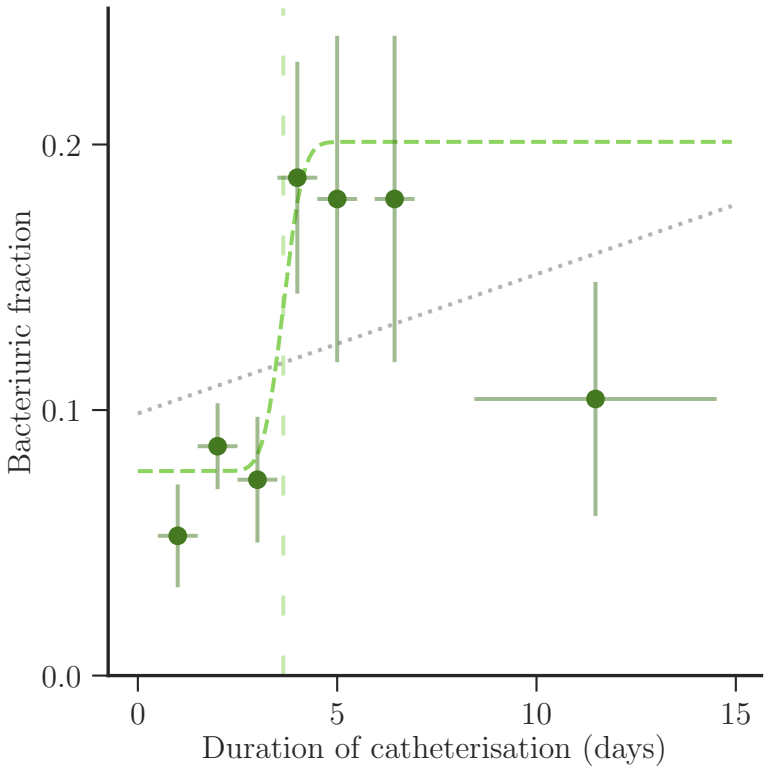

Figure 8.4 *Fitting the model to control group data. Plotted is the fraction of patients who have a positive CFU count, for males receiving PTFE catheters, against the duration of catheterisation. The model prediction is a sigmoid function (Eq. 8.5), with a mean duration of L_μ/v_{asc}, and a width of L_σ/v_{asc}. This prediction has been fit to the data (- -) to obtain an estimate of $v_{asc} = 61.2 \pm 7.7$ mm/day (a mean ascension time of 3.65 ± 0.46 days – shown with a vertical dash line (- -)). It is common within the literature to assume a linear increase in bacteriuric fraction with duration of catheterisation (····). Comparing the residual sum of squares for the two fits, the sigmoidal fit ($RSS = 0.011$) is a better fit than the linear fit ($RSS = 0.018$).*

single parameter fit, while the linear fit is a two-parameter fit: if we constrain the linear fit (for example requiring that the bacteriuric fraction at 0 days is 7.7%), it performs even worse, RSS = 0.021. Figure 8.4 shows both fits, with the sigmoidal fit (green dashed line) visually (qualitatively) more convincing than the linear fit (grey dotted line).

8.5.4 Predicting the bacteriuric fraction

The intervention groups in the study of Pickard et al. [90] received one of two catheter types: nitrofural-impregnated silicone (Nitro), or silver-alloy coated latex (Silver). These antimicrobial catheters have different parameterisations within the model (§8.4.2). We can make model predictions for these intervention groups by considering how the altered growth rate, r_S, results in either a slower ascension speed, v_{asc} (§Silver-alloy coating corresponds to a constant reduction in bacterial growth rate), or a delayed onset of bacterial colonisation on the catheter (§Nitrofural-impregnation corresponds to a time-dependent reduction in bacterial growth rate, due to the waning efficacy). We estimate the wavespeed of bacterial ascension on a silver-alloy catheter to be ~ 2.3 times slower than on a PTFE catheter (a 'wavespeed modifier' of $\Delta v = 0.44$; Eq. 8.2), while the initially high antimicrobial activity (with rapid waning) of the nitrofural-impregnated catheters leads to an estimated 3 day lag in the bacterial ascension compared to a PTFE catheter.

In Figure 8.5, we compare these model predictions for the dependence of the bacteriuric incidence on duration of catheterisation, to the incidence observed for the two interventions within the study. The predicted sigmoid functions take the form

$$\begin{aligned} f_{\text{silver}}(T) &= f(T; 0.44 v_{\text{asc}}) \\ f_{\text{nitro}}(T) &= f(T - 3 \text{ days}; v_{\text{asc}}). \end{aligned} \tag{8.6}$$

where $f(T; v_{\text{asc}})$ is as defined in Eq. 8.5. We see (Figure 8.5) that these predictions are qualitatively plausible when compare with the data (note that these are *not* fits, rather they are model predictions using literature values), particularly in the predicted mean ascension times (6.65 ± 0.46 days for Nitro, 8.4 ± 1.1 days for Silver), however there is insufficient data to assess the quality of the fit. For

than $f_{\text{sus}} = 20\%$, we in fact obtain an even better fit, with $RSS = 0.007$, while the fitted value of the ascension velocity does not significantly shift ($v_{\text{asc}} = 63.0 \pm 8.6$ mm/day).

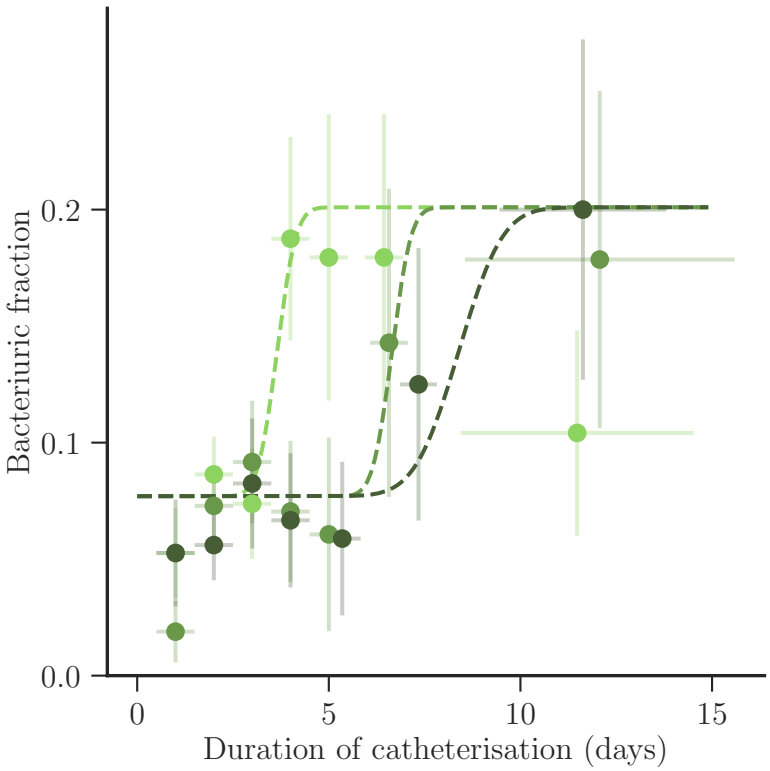

Figure 8.5 *The ascension time of bacteria varies with catheter type. Plotted is the fraction of patients with a positive CFU count against the duration of catheterisation, for males with a PTFE catheter (●), males with a nitrofural-impregnated catheter (●), and males with a silver-coated catheter (●). A sigmoid function has been fitted to the PTFE group (--; Figure 8.4), obtaining an estimate of* $v_{asc} = 61.2 \pm 7.7$ *mm/day. We predict sigmoid functions (Eq. 8.6) for the Nitro group (--) and the Silver group (--). This gives rise to predicted mean ascension times of* 6.65 ± 0.46 *days for the Nitro group, and* 8.4 ± 1.1 *days for the Silver group.*

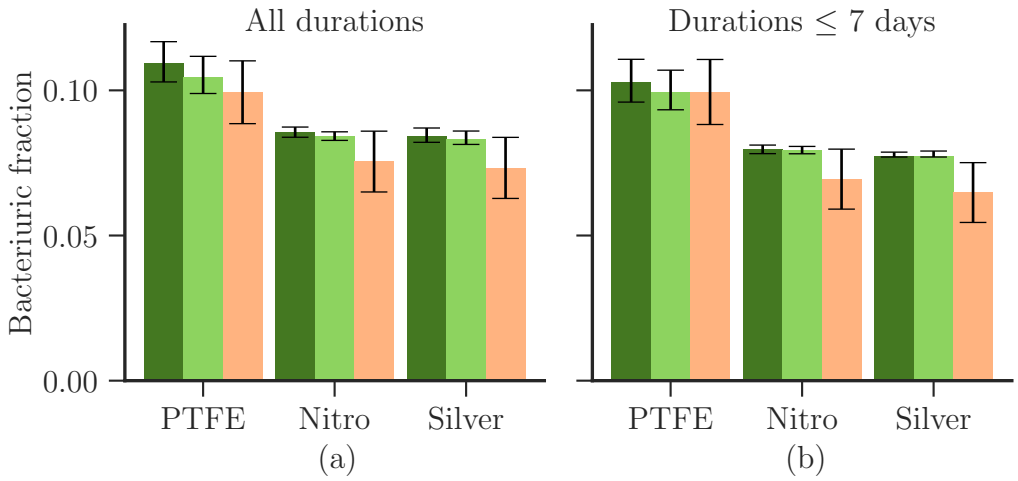

Figure 8.6 *Comparing the model predicted bacteriuric fraction with a fitted bacteriuria susceptibility, $f_{sus} = 20\%$(■) and a model predicted bacteriuria susceptibility, $f_{sus} = 17.8\%$ (■) with the observed incidence of bacteriuria (■), across all males within the study. (a) Comparing across all catheterisation durations. (b) Sampling only catheterisation durations up to one week.*

example there are only 89 males in the Nitro group who were catheterised for 5 days or longer, and 113 males in the Silver group who were catheterised for 5 days or longer (Table B.1) – so we are unable to resolve the data sufficiently to compare the steepness of the transition between baseline and maximum bacteriuric fraction.

8.5.5 Comparing the model predictions to observed results

The model allows us to predict the risk of developing bacteriuria for a patient catheterised for a given duration. Applying this risk function to the catheterisation duration distribution and taking the mean results in a prediction for the total fraction of patients who will have a positive CFU result in the study (Figure 8.6; §B.2.4), i.e., the incidence of bacteriuria.[9] Comparing these model predictions to the outcomes observed in the study by Pickard et al. [90], again the predictions seem qualitatively plausible, but the relative lack of data for durations > 7 days limits the ability of the model to distinguish between nitrofural-impregnated catheters and silver-alloy coated catheters.[10] The consistent overestimation of

[9] We plot the model predictions for both of the values of f_{sus} previously discussed. We see that although the model predicted susceptibility leads to a better fit for PTFE, it does not significantly alter the model predictions for Silver or Nitro.

[10] The errorbars quoted on the model predictions in Figure 8.6 should be interpreted as a measure of the certainty of the model to predict the study outcomes, assuming all modelling

bacteriuric fraction which we observe in Figure 8.6 is likely due in part to an overestimation of the baseline bacteriuric fraction, f_0. The value taken, $f_0 = 7.7\%$, throughout this analysis is a statistic calculated across all patients within the study, male and female; however, it is well known that females have much higher incidence of both UTIs [36, 110] and recurrent UTIs [59] (in the absence of catheterisation) than males, so we would expect the true value of f_0 across males within the study to be lower. For future work, we can request access to the individual patient data for pre-existing bacteriuria, to explore this further.

For both the model predictions and the observed outcomes, we see a significant decrease in incidence of bacteriuria in males for antimicrobial catheters, compared to the control PTFE catheter group. Our model predicts a decrease in absolute incidence of bacteriuria of 2.4% and 2.5% for Nitro and Silver catheters respectively, while in the data we observe a decrease in absolute incidence of bacteriuria of 2.4% and 2.6% respectively. This is particularly notable, since Pickard et al. [90] did not observe any decrease in bacteriuria associated with Silver catheters in their analysis. This is because Pickard et al. [90] controlled for sex but did not analyse separately the male and female data. Using the perspective gained from our model, we could predict that antimicrobial catheters should be more effective in males (due to their greater urethral lengths). Once analysed with this perspective in mind, the data of Pickard et al. [90] indeed shows a substantial decrease in bacteriuria for antimicrobial catheters used for males – hence our model has led us to an improved analysis of the data and a new result.

8.5.6 Discussion

Our model predicts the long-time bacteriuria incidence within the study of Pickard et al [90] to be $19.2 \pm 0.4\%$ for females and $17.8 \pm 0.4\%$ for males – which compares favourably to the $20 \pm 2\%$ incidence of bacteriuria for the study participants who were catheterised for a duration of 7 days. The model predicts that the time before bacteriuria occurs depends linearly on the urethral length. Applying this to the underlying normal distribution of urethral lengths within the male population results in a predicted sigmoidal function for the dependence of the incidence of bacteriuria on the duration of catheterisation.

assumptions to be true. Quantifying the uncertainty due to parameter estimation (§8.4.2) or modelling assumptions (Chapters 2 to 6) would require more data, not currently available in the literature.

This sigmoidal prediction provides a much more convincing fit (both qualitatively and quantitatively) than the linear fits common within the literature. We parameterised the interventions (silver-alloy and nitrofurazone) within our model to predict the mean ascension times for the intervention groups, resulting in qualitatively convincing predictions, compared to the observed data. Finally, we predicted the overall incidence of bacteriuria for each intervention group within the study of Pickard et al [90], again finding a qualitatively convincing comparison with the study data. Particularly notably, the model predicted a decrease in incidence of bacteriuria associated with the use of silver-alloy catheters, which was present in the dataset yet not reported by Pickard et al. [90].

It is known that in long-term catheterisation, polymicrobial infections develop, with number of colonising species increasing with duration of catheterisation [123]. The analysis conducted in this section does not consider polymicrobial infections explicitly: our model would predict that the incidence for each colonising species will take the form of a sigmoid, with wavespeed determined by the bacterial characteristics (growth and motility). Since individual species were not distinguished within the study by Pickard et al. [90], it is not possible to confirm this.

In Figure 8.2, we saw that incidence of bacteriuria across all the subgroups appeared to converge to the same value for longer durations of catheterisation (> 7 days): all except one group. For the group receiving PTFE catheters, the incidence of bacteriuria in females seems to increase with duration of catheterisation - despite our model prediction (as discussed in §8.5) that the transition from baseline to maximum incidence of bacteriuria happens rapidly, in $\lesssim 1$ day. It is possible that this is attributable to the end of the surgery-related course of antibiotics being taken by some of the patients finishing, leading to an increase in the total susceptible population. If, for example, the length of time that patients take antibiotics for varies across the group, then this would lead to the type of spread-out increase in bacteriuric fraction seen in Figure 8.2a. However, we do not currently have access to data concerning the antibiotic treatment of patients within the study, so we cannot evaluate this.

Also, in Figure 8.2 we took the baseline bacteriuric fraction to be 7.7%, as calculated across all patients within the study. We discussed briefly in §8.5.5 why this may be an overestimate for the baseline bacteriuric fraction in males. However, in Figure 8.2, comparing (a), (b), and (c), we see that the distribution of the 'pre-transition' datapoints around the baseline, regardless of the value,

differs across the subgroups. In particular, in Figure 8.2b, the first data point – males catheterised with Nitro catheters for 1 day – reflects a bacteriuric incidence of $\sim$ 2%, well below the baseline incidence, prior to catheterisation. This suggests that the antimicrobial activity of the nitrofural catheters immediately after insertion may be sufficient to kill the bacterial population within the urine in the bladder, as well as on the catheter surface. However, this effect is lost by the second day of catheterisation – a rapid waning in the antimicrobial activity – suggesting that the effect seen on day 1 may only apply to the planktonic bacterial population, not the underlying recurrent population (likely intracellular populations). In contrast, in Figure 8.2c, all but one of the male datapoints 'pre-transition' lie beneath the baseline. This may reflect a consistent small antimicrobial activity from the silver catheters in the urine within the bladder.

In the absence of study-specific data on urine production rates or urethral lengths, we took distributions from other studies in the literature, and assumed a similar population. For urethral lengths (§8.5.2) this may not be too unreasonable. Making this similarity assumption for urine production rates (§8.5.1) is more problematic. In particular, the patients within the study of Pickard et al. [90] were inpatients in a hospital, generally undergoing a surgical procedure. This is likely to significantly disrupt normal habits, including fluid intake, so it is unclear what the true distribution of urine production rates should be for these patients. It is also possible that fluid intake behaviour would vary significantly with duration of catheterisation, for example behaviour immediately before or after surgery is likely to be different to behaviour in recovery.

When we discussed antibiotic usage in the study (§8.5.1), we assumed a flat figure of 72%. However, as we began to discuss above, it is likely that many patients took antibiotics for only a portion of the time they spent catheterised. Some patients also began taking antibiotics subsequent to being catheterised, either to treat catheter-associated infection, or for unrelated reasons [90]. Moreover, it is likely that antibiotic usage is correlated with duration of catheterisation, as patients undergoing catheterisation for longer periods are correspondingly in hospital for a longer time – and longer duration of stay in hospital is associated with increased antibiotic usage [116]. This is a possible explanation for the unexpectedly low value of bacteriuria incidence in males in the PTFE group undergoing catheterisation for 8–20 days (Figure 8.2a).

The greatest uncertainty in our model predictions likely comes from estimating the parameter change for Nitro or Silver, relative to PTFE (§8.5.4). As

discussed in §8.4.2, *in vitro* studies of catheter properties are limited, with the majority assessing only bacterial adhesion, or 'zone of inhibition' antimicrobial activity. Neither of these properties can be used to determine the bacterial ascension wavespeed - for that we need growth and motility assays. Where studies have measured bacterial ascension of catheters, for example using an artificial bladder/urethra setup, these authors have focused on specific (novel) catheters, and normally compared them to only one other catheter, often silicone [39, 101, 121, 127].

The wavespeed adjustment we utilise in Eq. 8.6, a factor $\Delta v = 0.44$, is more correctly the adjustment for a silver-alloy coated latex hydrogel catheter, compared to a silicone catheter (§8.4.2;[121, 127]). But the silver-alloy coated latex catheters in the study of Pickard et al. [90] were not hydrogel coated, and the control group received PTFE-coated latex catheters, not silicone catheters. It is difficult to say how these factors alter the wavespeed adjustment: hydrogel likely increases bacterial motility, latex catheters are associated with slightly lower bacterial adhesion than silicone catheters, and the action of PTFE on catheters is difficult to predict. By reducing friction with the urethra and bladder [31], the deposition of fibrinogen is likely reduced, possibly reducing bacterial adhesion, growth or motility, but conversely, PTFE has been linked to increased biofilm formation compared to silicone [66].

In addition, the data supporting the assumption of a 3 day lag in bacterial ascension in nitrofural-impregnated catheters (Eq. 8.6) is very weak. Two studies found that nitrofural catheters completely suppressed bacterial growth on first exposure (i.e., straight 'out of the packet'), but that by 3 days of exposure nitrofural catheters were no longer able to prevent bacterial growth. Desai et al. found that after 3 days the catheters still displayed some antimicrobial activity [24], while Gaonkar et al. found no antimicrobial activity after 3 days [39]. Neither study made observations for intervals between 0 and 3 days, and, as we discussed above, Figure 8.2b suggests that the waning effect may be significant by 2 days. It is highly unlikely that the effect of nitrofural-impregnation on bacterial growth is discontinuous (as we assumed when writing Eq. 8.6) – instead, it is more likely that the antimicrobial activity wanes continuously after insertion, with the majority of the effect lost by 3 days.

In discussing our results in §8.5.5, we highlight how our model predicts that the efficacy of antimicrobial catheters in preventing catheter-associated bacteriuria should depend strongly on urethral length, and thus be more significant in males.

We also saw that this effect was present within the study data, for both nitrofural and silver-alloy catheters. We mentioned that Pickard et al. [90] did not note this effect, as they did not conduct separate analyses for male data and female data. In fact, this seems to be a common phenomenon in the literature. Some studies are conducted only on male patients, or only female patients, or have different sex breakdown for the control group compared to the intervention group, or even neglect to collect sex data entirely [101]. In light of our model, it seems likely that this is a major factor muddying the waters when evaluating efficacy of antimicrobial catheters. In particular, for silver-alloy catheters, there have been many studies that find them highly effective in reducing bacteriuria or CAUTI in short-term catheterisation, but there have also been many studies (including Pickard et al. [90]), that have found them to have no effect. In our analysis presented here, we have shown that silver-alloy catheters are effective in preventing bacteriuria specifically in males undergoing short-term catheterisation, and not in females.

8.6 Summary

We can interpret the model presented within this thesis as a mapping from 'parameter space' to 'outcome space' (Eq. 8.1). By classifying the model parameters according to their effect on the characteristic timescales and steady state behaviour of the model (Table 8.1), we identify parameters that are particularly critical in determining the outcomes in short-term catheterisation (urethral length, bacterial surface diffusivity, and catheter surface bacterial growth rate), and in long-term catheterisation (residual urine volume, urine production rate, and bacterial growth rate within the bladder).

We use a stationary state argument to conclude that the 'clean' catheter state is an unstable state, in which any small contamination leads to bacterial growth. Thus, we come to understand that interventions with the goal of preventing bacterial colonisation long-term must act on the stationary states of the system. Conversely, interventions that modify the dynamics may reduce bacterial colonisation within short-term settings. We can classify clinical interventions according to their action on the parameters, stationary state, and dynamics – leading to a classification of postponement, mitigation, or prevention (Table 8.2).

While considering clinical interventions, we apply the model to find new

perspectives on both *in vitro* and *in vivo* studies. Of particular note, the only study to investigate the spatial distribution of bacterial biofilms on extraluminal catheter surfaces found distributions highly suggestive of FKPP dynamics (Figure 8.1). We finish by demonstrating how the model can predict outcomes of clinical trials of catheter interventions, applying insights from the model to a multicentre randomised control trial investigating the efficacy of antimicrobial catheters [90]. We find that the model predicts a sigmoidal dependence of incidence of bacteriuria on duration of catheterisation, and that this sigmoidal shape is a much better fit than the linear dependence typically assumed in the literature (Figure 8.5). The model predictions for overall incidence of bacteriuria are qualitatively plausible and identify an outcome (reduced incidence associated with silver-alloy catheters in males) that was present in the data but not discussed in the original study.

This comparison to the CATHETER trial (§8.5) is a case study in how the model might be applied. As we discussed, in this case the extraluminal surface emerged as the relevant part of the model. However, the model could also be applied to other clinical studies. For example, if the model were applied to a study focussing on intraluminal biofilm development/blockage, the intraluminal surface and flow could be expected to play a larger role. And for studies evaluating the origin of CAUTI, for example by examining biofilm distribution across catheters, the entire coupled model might be necessary.

Further work

As we have seen, the model presented in this thesis captures all the phenomena described in the clinical literature. However, as we discussed in detail within each chapter, we made many simplifying assumptions, some more justified than others. Moreover, the results presented within Chapters 7 and 8 raise a number of further questions. Here I discuss some possible modifications to the model and potential avenues for further study.

Mathematical modelling

In Chapter 3, we modelled bacterial ascension on the extraluminal surface of the catheter with an FKPP equation. We commented that this inherently reduces the number of modes of bacterial motility to one: an active diffusion term. In Chapter 8, we discussed experimental results suggestive of FKPP-like dynamics for the bacterial ascension on the extraluminal surface, and saw how data from the CATHETER trial by Pickard et al. [90] led to estimates for the active bacterial diffusion coefficient consistent with the motility of bacteria swimming in bulk medium. However, we might ask what is the 'real' nature of bacterial motility ascending the catheter? We know that the bacteria are moving in a region between the catheter surface and the uroepithelial cells that line the urethral wall. This region contains a mucosal layer consisting of urine, fibrinogen, and other proteins. It would be interesting to model bacterial motility in such an environment in more detail. Perhaps the model for this extraluminal surface ascension should be compartmental, for example with separate compartments for the catheter surface, the mucosal layer, and the epithelial cells. Alternatively, perhaps the model should allow for multiple motility modes, for example rapidly moving 'swarming' cells, randomly swimming motile cells, and slow-moving cells adhered to the catheter surface.

In Chapter 4, we discussed how the logistic growth model that we used for the bladder dynamics has no physical justification, but it is a convenient way to add a physical bound to exponential growth. We briefly discussed how an alternative approach might be to use a chemostat model, where bacterial growth is nutrient-limited, and the steady state is controlled by the dilution rate. However, to construct such a model we need to ask what is the dynamics of bacterial growth on urine? Urine is a complex medium, with carbon sources mainly in the form of amino acids: the subject of how bacteria grow on multiple scarce carbon sources is a topic of current research [86, 87].

However, this modelling approach describes only the planktonic bacterial population. A recent topic of interest in UTI modelling has been intracellular bacterial communities (IBC; bacteria that persist inside the epithelial cells that line the bladder), as it is believed these are a mechanism for recurrent UTIs [17]. It is unclear what role IBC play in catheter-associated infections, and to what extent IBC models developed for UTIs would need modification for catheters, for example to account for catheter-induced uroepithelial cell damage. If considering the role of the epithelial cells, it is likely that the host immune system also plays some role in regulating bacterial growth within the bladder and would need to be included in future models. Thus, a more sophisticated model for bacterial colonisation of the bladder might also need to be compartmental, perhaps with a chemostat model describing the planktonic population, and an IBC model describing the sustained bacterial population and the host immune response.

When developing the model of Chapter 5 for the intraluminal dynamics, for simplicity we neglected to consider the effect of biofilm development on the surface on the flow profile. To be able to predict catheter blockages this would need to be included, and the fluid dynamics treated more carefully, likely requiring computational fluid dynamics simulations (for example, software such as OpenFOAM). We also assumed the dilution rate to be constant: in fact, urine production rate varies periodically, with reduced rates overnight [84]. A topic of considerable interest in the biophysics community is 'upstream swimming', whereby the flow orients bacteria near the pipe surface to swim upstream against the flow, attaining upstream velocities of $\sim 20\ \mu\text{ms}^{-1}$ [55]. Previous authors have suggested that this may be relevant to catheter-associated bacteriuria/infections. Assuming these reported rates of upstream swimming, bacteria might migrate from the drainage bag to the bladder on a timescale of 5 hrs. Within this thesis we neglected upstream swimming as: the majority (66%) of CAUTI is attributable

to extraluminal bacteria ascension; after placement urinary catheters are rapidly coated in a sticky conditioning film, not accounted for within upstream swimming models; and since urinary catheters rely solely on gravity for drainage, backflow is likely to be a common and frequent occurrence, which is likely to be a much more significant mode of transport of bacteria from the drainage bag to the bladder. A future model would however do well to consider the occurrence of backflow and its role in the development of bacteriuria.

Other modelling considerations for future work might include the action of antibiotics in the treatment of CAUTI, for example the role of catheter biofilms in determining treatment efficacy, since biofilms are notoriously difficult to eradicate with antibiotics. From a nutrient-limitation perspective, we might ask if people with abnormal urine (for example diabetics have higher sugar concentrations) experience UTIs or CAUTIs differently. Finally, we might wonder if there is a better modelling approach for estimating the strength of coupling between the different parts of our model. For example, within this work we assumed that all bacteria that come into contact with the catheter surface stick – this is unlikely to be the case. We might also ask how the coupling strengths vary with bacterial and catheter specific properties.

Experimental biophysics

The experimental results of Wang and Zhang et al. [122, 127] (who constructed an artificial bladder/urethra system to investigate bacterial ascension of urinary catheters) are highly supportive of a reaction-diffusion (FKPP) style description of bacterial ascension of the extraluminal surface of catheters (Figure 8.1). It would be very interesting to see further studies conducted with a similar experimental setup to ascertain the nature of bacterial ascension of the extraluminal surface, for example investigating other bacterial strains and catheter coatings. A complementary experimental study might apply the same staining, imaging, and analysis to analyse bacterial density patterns on catheters obtained from clinical use. If data on duration of catheterisation was also collected, then – assuming the existence of a bacterial wavefront – the position of the wavefront could be correlated with the duration of catheterisation, and potentially a wavespeed could be determined. Ideally, such a study would measure bacterial densities on both surfaces of the catheter: extraluminal and intraluminal. However, conducting such measurements on the intraluminal surface is more challenging, due to the

high surface curvature, and the need to image 'through' the catheter (which, as we discussed briefly in Chapter 5, fluoresces brightly with excitation/emission wavelengths similar to many stains). Avoiding such microscopy via standard microbiology methods of culturing and counting colonies is unlikely to be viable, due to the presence of many 'unculturable' cells in catheter biofilms [125].

In our model, colonisation by multiple bacterial species would be assumed to be independent, with the timescale of colonisation determined by the wavespeed of the bacterial front for each species. Thus we expect that in an artificial catheter/urethra/bladder setup, if we exposed the end of the system (the 'skin-urethra interface') to a reservoir containing multiple bacterial species, we would detect those species in the 'bladder' after times determined by the bacterial strain characteristics: $L/2\sqrt{r_S D_S}$, where L is the 'urethral length', r_S is the bacterial strain growth rate in the 'urethra' and D_S is the bacterial strain surface motility (active diffusion coefficient). This would be interesting in comparison to clinical observations of incidence of bacteriuria for durations of catheterisation between 14 days and 30+ days – and in comparison to rates of polymicrobial bacteriuria.

Clinical studies

In this thesis, urine production rate emerged as a critical parameter, determining if bacteriuria is possible, or if the bladder is instead in a 'washed out' state with bacteria being diluted out faster than they grow. Clinical studies of fluid intake and urinary catheters have focused mostly on catheter encrustation, urine pH, and the activity of *P. mirabilis*. Our model predicts a universal effect, with increasing urine production rate resulting in reduced incidence of bacteriuria, regardless of bacterial strain. This is a prediction that could be tested in a clinical study, linking fluid intake with incidence of catheter-associated bacteriuria. Similarly, dilution rate is also determined by the residual urine volume within the bladder. Currently, little data exists on the population distribution of residual urine volumes with catheterisation, particularly outside of intensive care units. It would be interesting to determine what the form of this distribution is, and if, in an observational study, there is any correlation between mean residual urine volume and incidence of bacteriuria – as our model predicts there will be.

Kohler et al [60] measured urethral lengths in men via use of a Foley catheter: inserting a catheter, marking on the catheter where it exited the urethra, and then

measuring the length of catheter that had been inserted. Thus, measurements of urethral lengths seem a natural addition to studies investigating urinary catheters. In Chapter 8, we saw that urethral length determines the timescale of bacterial colonisation, and hence, in short-term catheterisation, urethral length determines incidence of bacteriuria. A clinical study could directly confirm this link, identifying urethral length as a risk factor for catheter-associated bacteriuria. This might identify men with shorter urethral lengths as having a greater risk of catheter-associated bacteriuria, as well as determining the extent to which differing incidence of bacteriuria between males and females might be attributable to urethral length.

Catheter design

Finally, we suggest that our model, with its identification of critical parameters for different outcomes, might guide the development of a testing framework for new catheter design. Our model predicts how changing the parameters of the system alters the outcomes, timescales, and dynamics (Chapter 8). If a testing framework can determine the parameterisation of a given catheter design or intervention, then the model can be applied to predict the outcomes in a clinical setting.

Conclusions

The primary aim of this thesis was exploratory: to identify topics in which biophysics may contribute to understanding the bacterial colonisation of urinary catheters. To accomplish this, I constructed a minimal mathematical model, following the 'infection story' described to me by clinical collaborators. This 'narrative-driven' modelling approach is common across ecology, epidemiology, and population dynamics – but also across physics. In writing only the maths necessary to tell the story, I constructed a 'least-wrong' model, elucidating the fundamental mechanisms of the system, without obfuscation by small-scale complex processes.

To do so, I made many simplifying assumptions and reductions, as highlighted throughout this thesis. Yet, as also discussed throughout, and especially within Chapter 8, this minimal model is already sufficient to explain all the phenomena I encountered within the literature. One conclusion from this is that in sufficiently complex systems, even 'obvious' or 'trivial' statements can have many consequences and deeper significance. For example, within this thesis, the 'trivial' statement that if bacteria are diluted faster than they grow then there will not be a sustained population within the urine (washout), leads to predictions for the susceptibility to bacteriuria within a population.

A second conclusion is that while it is possible to build 'perfect' *in vitro* setups, which capture all sorts of complex physical behaviours (e.g., upstream swimming), and that we might also describe with beautiful physics, these behaviours are typically 'fragile solutions' to the system. Outside of the idealised laboratory conditions, in the inherently noisy conditions of life, these solutions are rarely seen. We can consider this as a parallel to the wavespeed solutions of the FKPP equation. It is possible to construct intricate initial conditions, resulting in many possible theoretical wavespeeds, yet, in a numerical or experimental setting, these almost invariably collapse to the asymptotic solution. We can also draw a second

parallel, to ordering in statistical physics, where low temperature ordering is lost as temperature rises.

The above argument seems to imply that we should expect a sufficiently complex system to collapse to its 'story'. This is uncomfortable, but we can take a more 'physics-based' understanding by considering emergent phenomena. When we combine sufficiently large numbers of microscopic systems (whether atoms, or bacteria, or fish, ...), the resultant macroscopic system has properties and phenomena of its own, that the individual constituents do not possess. When a clinician observes a patient, they are observing properties of the macroscopic system – so the 'story' they tell is the emergent phenomenon. Here I am claiming that this is an emergent phenomenon not only from the vast numbers of individual cells (human and bacterial) interacting, but also from the high numbers of processes and interactions involved. Biophysics phenomena, like biofilms and upstream swimming, are emergent phenomena resulting from the interactions of large numbers of living organisms (here bacteria) with their environments. The clinician's *narrative* then is the emergent phenomenon from all of the underlying biophysics processes.

The corollary to the 'story' is that context matters. If we alter the narrative, then the mathematical description – the model – also changes, and hence the results we obtain differ. This is the argument we made in Chapter 8. If we wish to design an intervention that mitigates or prevents a specific outcome, we must consider that specific outcome in the design and testing of our intervention. And an intervention may be highly effective in one context (e.g., short-term catheterisation in hospital), yet have no effect in another context (e.g., long-term care in the community).

Biophysics is a rich and beautiful field; however, we must be wary when we draw conclusions from phenomena studied in isolation. Life is noisy and complicated, and phenomena rarely occur in isolation. When it comes to biophysical modelling for clinical applications, perhaps simple is best.

Appendices

Appendix A

Methods, proofs and derivations

A.1 Chapter 3: Modelling the extraluminal surface

A.1.1 Linear spreading velocity of the FKPP equation

As referred to on pages 32, 33.

We can find the linear spreading velocity of the FKPP equation (Eq. 3.1 or Eq. 3.3) by linearising the equation about the unstable (zero) state [117]. Van Saarloos [117](p38–42) demonstrates this method for the dimensionless FKPP equation (Eq. 3.3), showing that the linear spreading velocity $v^* = 2$, and the asymptotic spatial decay rate $\lambda^* = 1$. Here we apply this method to our model for bacteria on a catheter surface, recalling Eq. 3.1:

$$\frac{\partial n}{\partial t} = D_S \frac{\partial^2 n}{\partial x^2} + r_S n \left(1 - \frac{n}{\kappa_S}\right).$$

We linearise Eq. 3.1 about the unstable state $n(x,t) = 0$, to find

$$\frac{\partial n}{\partial t} = D_S \frac{\partial^2 n}{\partial x^2} + r_S n. \tag{A.1}$$

We obtain the dispersion relation by substituting a Fourier mode, $\mathrm{e}^{-i\omega t + ikx}$, into Eq. A.1:

$$\omega(k) = i(r_S - D_S k^2). \tag{A.2}$$

Following van Saarloos [117], we solve for the saddle point k^* by solving

$$\left.\frac{d\omega}{dk}\right|_{k^*} = \frac{\Im[\omega(k^*)]}{\Im[k^*]}, \tag{A.3}$$

finding

$$k^* = i\sqrt{\frac{r_S}{D_S}}. \tag{A.4}$$

We can then write down the linear spreading velocity:

$$v^* = \frac{\Im[\omega(k^*)]}{\Im[k^*]} = 2\sqrt{r_S D_S}, \tag{A.5}$$

and the asymptotic spatial decay rate

$$\lambda^* = \Im[k^*] = \sqrt{\frac{r_S}{D_S}}. \tag{A.6}$$

A.1.2 Numerical implementation of the extraluminal surface

As referred to on pages 30, 69.

Recall Eq. 3.1:

$$\frac{\partial n}{\partial t} = D_S \frac{\partial^2 n}{\partial x^2} + r_S n \left(1 - \frac{n}{\kappa_S}\right).$$

This can be discretised with a forward-time centred-space (FTCS) method as:

$$n_p^{k+1} = \frac{D_S \Delta t}{\Delta x^2}\left(n_{p+1}^k - 2n_p^k + n_{p-1}^k\right) + \left(1 + r_S \Delta t\right) n_p^k - \frac{r_S \Delta t}{\kappa_S}\left(n_p^k\right)^2, \tag{A.7}$$

where n_p^k is the extraluminal bacterial surface density, $n(x,t)$, at the pth discrete position, and the kth time step; Δt is the time step; and Δx is the spatial discretisation.

To check for stability, we can apply von Neumann stability analysis while freezing a coefficient [1]. We take an error ansatz $n(x,t_k) = \mathrm{e}^{i\phi x}$, and calculate the amplification factor, which for stability must be less than one: $\left|\frac{n(x,t_{k+1})}{n(x,t_k)}\right| \leq 1$. Then by freezing $\left(n_p^k\right)^2 = n_p^k \left|\max[n(x,t)]\right| = n_p^k \kappa_S$, we have

$$\begin{aligned}\frac{n(x,t_{k+1})}{n(x,t_k)} &= \frac{D_S \Delta t}{\Delta x^2}\left(\mathrm{e}^{i\phi\Delta x} - 2 + e^{-i\phi\Delta x}\right) + (1 + r\Delta t) - r\Delta t \\ &= 1 - \frac{4 D_S \Delta t}{\Delta x^2}\sin^2\left(\frac{\phi \Delta x}{2}\right).\end{aligned} \tag{A.8}$$

So we require

$$-1 \leq 1 - \frac{4D_S\Delta t}{\Delta x^2} \underbrace{\sin^2\left(\frac{\phi\Delta x}{2}\right)}_{\in[0,1]} \leq 1 \qquad \forall\ \phi\Delta x \in [-\pi, \pi] \tag{A.9}$$

Which is just the 'normal' stability condition $\Delta t < \frac{\Delta x^2}{2D_S}$.

Due to the existence of travelling wave solutions, we also have a condition on Δx: the step size must be less than the width of the travelling wavefront. This is necessary to avoid shock behaviour. If the spatial discretisation is coarser than the width of the travelling wavefront, then the shock wave will propagate through the numerical solution at a speed of $\Delta x/\Delta t$, rather than the correct speed of $2\sqrt{r_S D_S}$. Thus, we have a shock condition of $\Delta x < 8\sqrt{\frac{D_S}{r_S}}$. More accurate numerical results are obtained [1] with a step size slightly smaller than the stability conditions, so in this thesis the values chosen for the step sizes were:

$$\begin{aligned} \Delta x &= \frac{1}{2}\sqrt{\frac{D_S}{r_S}} \\ \Delta t &= \frac{\Delta x^2}{20 D_S} \end{aligned} \tag{A.10}$$

which for the parameter values given in Table 2.2 are $\Delta x = 0.003$ mm, and $\Delta t = 45$ s.

A.1.3 Experimental methods for Figure 3.1

As referred to on page 27.

Sample preparation

E. coli strain MG1665 was cultured in LB growth medium at 37°C overnight. The culture was diluted 1:10 in M63 growth medium, for a total volume of 10 mL. An 8 cm segment of catheter was sterilised with alcohol, placed in a petri dish, and covered in the cell culture solution. The dish was then covered and incubated at 30°C for 72 hrs. The sample was then rinsed in PBS twice to remove unattached cells, fixed with formaldehyde, and stained with DAPI.

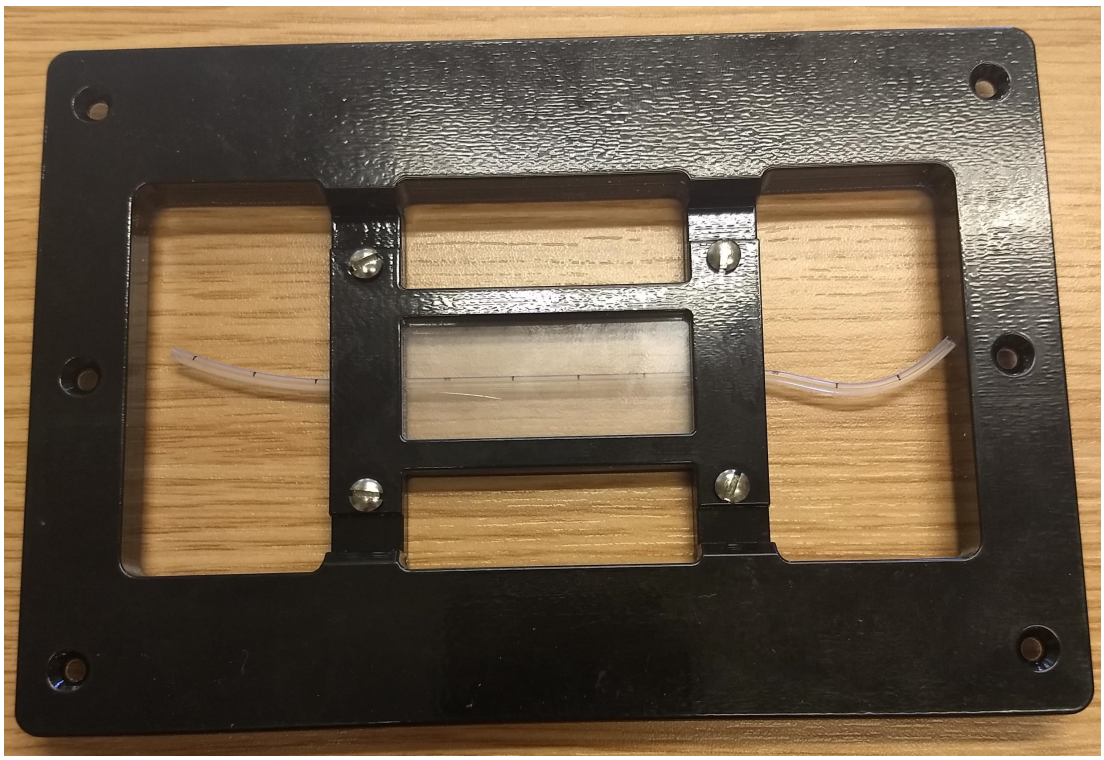

Figure A.1 *A frame designed to hold a section of catheter flat between cover slides. This allows the use of a microscope to image along the length of the catheter.*

Imaging

In order to image bacteria along the length of the catheter we designed a custom microscope stage, which frames a 5cm section of catheter between two cover slides (Figure A.1). This design holds the catheter completely flat/taut, minimising the distortion, and also results in least 'wastage' as very little of the catheter is obscured by the frame.

Utilising this frame, epi-fluorescence images of the sample were taken, with a DAPI filter cube, at both 10x (Figure 3.1a) and 60x (Figure 3.1b) magnification.

A.2 Chapter 4: Modelling the bladder

A.2.1 Solution to the logistic equation

As referred to on pages 43, 46.

We can solve the logistic equation (Eq. 4.2) through separation of variables. For ease of writing, we take a change of variable $\tilde{N} = N/\kappa$, to write

$$\frac{d\tilde{N}}{dt} = r\tilde{N}(1-\tilde{N}). \tag{A.11}$$

Separating variables results in

$$rdt = \frac{d\tilde{N}}{\tilde{N}(1-\tilde{N})} = \frac{d\tilde{N}}{\tilde{N}} + \frac{d\tilde{N}}{1-\tilde{N}}, \tag{A.12}$$

which can then be integrated to find

$$\log\tilde{N} - \log(1-\tilde{N}) = rt + c, \tag{A.13}$$

where c is the constant of integration. We can rearrange this to obtain

$$\tilde{N}(t) = \frac{A\mathrm{e}^{rt}}{1 + A\mathrm{e}^{rt}}, \tag{A.14}$$

where $A = \mathrm{e}^c$. Applying the initial condition $\tilde{N}(0) = N_0/\kappa$, we find $A = N_0/(\kappa - N_0)$, and hence

$$N(t) = \frac{N_0\kappa\mathrm{e}^{rt}}{\kappa + N_0\left(\mathrm{e}^{rt}-1\right)}. \tag{A.15}$$

A.2.2 Numerical implementation of the bladder

As referred to on pages 41, 70, 70.

Recall Eq. 4.3:

$$\frac{d\rho}{dt} = r_B\rho\left(1 - \frac{\rho}{\kappa_B}\right) - k_D\rho.$$

Discretising this with a forward Euler method gives

$$\rho^{k+1} = \rho_k + \Delta t\left(\left(r_B - k_D\right)\rho^k - \frac{r_B}{\kappa_B}\left(\rho^k\right)^2\right), \tag{A.16}$$

where ρ^k is the bladder bacterial volume density at the kth time step.

The stability can be evaluated by comparison with the logistic map, as follows. Rewriting Eq. A.16 as

$$\rho^{k+1} = (1 + A\Delta t)\rho^k + \frac{r_B \Delta t}{\kappa_B} \left(\rho^k\right)^2, \tag{A.17}$$

where $A = r_B - k_D$, and making a change of variables $u^k = -\frac{r_B \Delta t}{\kappa_B (1+A\Delta t)} \rho^k$, gives

$$u^{k+1} = (1 + A\Delta t)\, u^k (1 - u^k), \tag{A.18}$$

which stably converges to its non-zero equilibrium (see Murray, Chapter 2.3 [79]) for $1 < 1 + A\Delta t < 2$, i.e.

$$\Delta t < \frac{1}{r_B - k_D}. \tag{A.19}$$

For the parameters in Table 2.2, this gives $\Delta t \lesssim 10^4$ s. Within simulations the time steps chosen are of the order $\Delta t \sim 10^2$ s, satisfying the stability condition.

A.3 Chapter 5: Modelling the intraluminal flow & surface

A.3.1 Appealing to a parallel with the diffusion equation

As referred to on page 58.

Recall Eq. 5.10, the dimensionless form of our stationary state equation for the bacterial density transport and diffusion:

$$\frac{\partial^2 \sigma}{\partial r^2} + \frac{1}{r}\frac{\partial \sigma}{\partial r} = (1 - r^2)\frac{\partial \sigma}{\partial x}.$$

As we noted in §5.3, Eq. 5.10 has parallels with the diffusion equation in cylindrical co-ordinates [126]:

$$\frac{1}{\rho}\frac{\partial}{\partial \rho}\left(\rho \frac{\partial \psi}{\partial \rho}\right) = \frac{\partial \psi}{\partial t}, \tag{A.20}$$

which has solutions of the form

$$\psi(\rho, t) = \frac{1}{t} \exp\left(\frac{-\rho^2}{4t}\right). \tag{A.21}$$

Ideally we would like to change variables $r \to \rho = f(r)$ to write Eq. 5.10 in the form of Eq. A.20. Making this substitution gives

$$\left(\frac{1}{r}f' + f''\right)\frac{\partial\sigma}{\partial\rho} + (f')^2\frac{\partial^2\sigma}{\partial\rho^2} = \left(1 - r^2\right)\frac{\partial\sigma}{\partial x}. \tag{A.22}$$

But, equating the terms of Eq. A.22 and Eq. A.20, we would need to have this system of equations:

$$\begin{aligned} f'' + \frac{1}{r}f' &= (1 - r^2)f \\ (f')^2 &= 1 - r^2 \end{aligned} \tag{A.23}$$

which is inconsistent and not solvable.

A.3.2 Attempting method of Laplace transform

As referred to on page 58.

Again recall Eq. 5.10:

$$\frac{\partial^2\sigma}{\partial r^2} + \frac{1}{r}\frac{\partial\sigma}{\partial r} = (1 - r^2)\frac{\partial\sigma}{\partial x}.$$

This time we instead attempt to solve Eq. 5.10 by using a Laplace transform [19], as follows:

$$\int_0^\infty \mathrm{e}^{-pz}\frac{1}{r}\frac{\partial}{\partial r}\left(r\frac{\partial\sigma}{\partial r}\right)\,\mathrm{dz} = \int_0^\infty \mathrm{e}^{-pz}(1 - r^2)\frac{\partial\sigma}{\partial z}\,\mathrm{dz}, \tag{A.24}$$

which leads to the following ODE:

$$\frac{d^2\tilde{\sigma}}{dr^2} + \frac{1}{r}\frac{d\tilde{\sigma}}{dr} = p(1 - r^2)\tilde{\sigma}. \tag{A.25}$$

Now we have a 2nd order linear ODE and we would like to find a 'nice' solution to it. That is, we would like to have a closed form solution, otherwise known as a Liouvillian solution. As we have already seen (§A.3.1), it is not straightforward to see how to find this solution, nor is it obvious whether such a solution exists. The Kovacic algorithm is one way to find such a solution, and in fact if it fails

then there is no such closed form solution [26, 62]. The Kovacic algorithm is implemented within Mathematica's DSolve function, meaning that if that function fails to solve our equation, then no such solution exists.

Using DSolve in Mathematica to solve Eq. A.25 gives solutions of the form:

$$\tilde{\sigma} = \sqrt{2}\exp\left[\frac{i\sqrt{p}r^2}{2}\right]\Big(AU\left[\ldots\right] + B_1F_1\left[\ldots\right]\Big) \tag{A.26}$$

where U and ${}_1F_1$ are confluent hypergeometric functions, and A and B are constants of integration. To proceed with this approach we would next take the inverse Laplace transform of Eq. A.26. Instead we shall choose a different approach, as described in §A.3.3.

A.3.3 Levich boundary layer theory

As referred to on page 59.

To calculate the bacterial flux, we follow the path laid out by Levich in his book, *Physiochemical hydrodynamics* [69]. In particular, we use the approach laid out in Chapter 2.20, *Diffusion in laminar flow in a tube*. We first summarise the approach and the requisite assumptions, before working through the full solution in detail.

Summary

The maximal deposition of particles on the surface of a pipe is given by

$$j(x) = D\left.\frac{\partial\sigma}{\partial y}\right|_{y=0} = 0.5835D\sigma_0\sqrt[3]{\frac{\lambda}{R^3D}}\frac{1}{\sqrt[3]{x}}. \tag{A.27}$$

This holds when $Re < 2500$ and $L \ll \lambda/D$. Here $j(x)$ is the particle flux to the surface, D is the particle bulk diffusivity, σ_0 is the initial particle concentration, λ is the volume flow rate, R is the pipe radius, x is the longitudinal displacement, Re is the Reynolds number, and L is the pipe length. Also, $\sigma(x, y)$ is the particle concentration (i.e., bacterial density) within the fluid, and y is the perpendicular displacement from the surface (i.e., a planar approximation of the radial co-ordinate).

On a catheter we have typical values as given in Table A.1, so Eq. A.27 can be

Parameter	Value
D	10^{-4} mm^{2}s^{-1}
λ	16.7 mm^{3}s^{-1}
R	1 mm
Re	6
L	100 mm

Table A.1 *Typical parameter values for CAUTI, as taken from Table 2.2, and Eq. 1.2.*

seen to be valid: $L = 10^2$ mm and $\lambda/D = 10^5$ mm, so $L \ll \lambda/D$, and $Re = 6$, so $Re < 2500$. Hence, we can calculate the typical deposition rate to be

$$j(x) \approx 0.003 \frac{\sigma_0}{\sqrt[3]{x}}.$$

Assumptions

1. All particles that contact the surface stick, i.e. the 'perfect sink' assumption. This is an absorbing boundary condition, and leads to a maximal estimation for the deposition flux.

2. There are no external forces, except for the pressure differential driving the flow. This is the so-called 'Smoluchowski-Levich' assumption [14].

3. The flow within the pipe is laminar. This requires $Re < 2500$, and that we must be beyond the initial hydrodynamic inlet region, $x > h \sim R \cdot Re/27$. For our model catheter, $Re \sim 6$, and so $h \sim 0.2$ mm. Since the length of a catheter is $40 - 160$ mm, the majority of our modelled catheter is in the laminar flow regime.

4. The diffusion profile is not fully established, and so there exists a thin diffusion boundary layer. The diffusion profile is fully established at a distance $H \sim \lambda/D$ down the pipe. Then for $x \ll H$, the boundary layer is extremely thin, and can be approximated as planar. So, for the catheter we need $L \ll \lambda/D$.

Solution

The full convection-diffusion equation to be solved in the case of a catheter is as follows [70, 112]:

$$\begin{aligned} \frac{\partial \sigma}{\partial t} &= D\left(\frac{\partial^2 \sigma}{\partial r^2} + \frac{1}{r}\frac{\partial \sigma}{\partial r}\right) - u(r)\frac{\partial \sigma}{\partial x} \\ u(r) &= \frac{2\lambda}{\pi R^4}\left(R^2 - r^2\right). \end{aligned} \tag{A.28}$$

Here $\sigma(r, x, t)$ is the bacterial volume density, D is the diffusivity of bacteria within urine, and $u(r)$ is the (Poiseuille) flow profile. Within the description of the flow, λ and R are, respectively, the rate of urine production and the internal radius of the catheter.

Since the convective-diffusion processes take place over a timescale much shorter than that of bacterial growth, we assume that the concentration of bacteria across the top of the catheter is constant, and we are in steady state, $\frac{\partial \sigma}{\partial t} = 0$. Then the boundary conditions are as follows:

$$\begin{aligned} \sigma(r, x = 0, t) &= \sigma_0 \\ \sigma(r = R, x, t) &= 0 \\ \left.\frac{\partial \sigma}{\partial r}\right|_{r=0} &= 0. \end{aligned} \tag{A.29}$$

Now Eq. A.28 becomes

$$D\left(\frac{\partial^2 \sigma}{\partial r^2} + \frac{1}{r}\frac{\partial \sigma}{\partial r}\right) = \frac{2\lambda}{\pi R^4}\left(R^2 - r^2\right)\frac{\partial \sigma}{\partial x}. \tag{A.30}$$

If $h < x \ll H$, we are in the diffusion inlet region, and diffusion takes place within a thin boundary layer near the surface. Hence we have $\sigma(r) \approx \sigma_0$ when far from the walls, i.e. when $R - r$ is large. Therefore, it makes sense to consider a new (small) variable $y = R - r$, with $\sigma \to \sigma_0$ as $y \to \infty$. Now the boundary conditions become

$$\begin{aligned} \sigma &= \sigma_0 \qquad \text{at } x = 0 \\ \sigma &= 0 \qquad \text{at } y = 0 \\ \sigma &= \sigma_0 \qquad \text{as } y \to \infty, \end{aligned} \tag{A.31}$$

and the velocity becomes

$$\begin{aligned} u(r) &= \frac{2\lambda}{\pi R^4}\left(R^2 - r^2\right) \\ &\simeq \frac{4\lambda}{\pi R^3} y \qquad \text{to first order.} \end{aligned} \tag{A.32}$$

Since $\delta \ll R$, that is since the region of interest (the boundary layer, δ) is small compared to the radius of curvature, we can approximate the system as planar, and Eq. A.30 becomes

$$D\frac{\partial^2 \sigma}{\partial y^2} = \frac{4\lambda}{\pi R^3} y \frac{\partial \sigma}{\partial x}. \tag{A.33}$$

For brevity, we define $\varepsilon = \frac{4\lambda}{\pi R^3 D}$, (which has dimensions of length^{-2}), and write

$$\frac{\partial^2 \sigma}{\partial y^2} = \varepsilon y \frac{\partial \sigma}{\partial x}. \tag{A.34}$$

Now we will proceed by following the similarity method laid out by Levich in Chapter 2.14 (a variant on the more familiar method of characteristics [69]). We look for a transformation under which Eq. A.34 is unchanged:

$$y \to a y' \qquad x \to b x', \tag{A.35}$$

which turns out to require $b = a^3$. We can see that this transformation does not alter our boundary conditions, and hence that the solution is invariant under the transformation:

$$\sigma(y, x) = \sigma(ay, a^3 x). \tag{A.36}$$

Then we can look for a combination $\eta(y, x)$ such that η is unchanged under this transformation and proceed essentially as in the method of characteristics.

$$\eta = \frac{\varepsilon^{1/3} y}{x^{1/3}}, \tag{A.37}$$

$$\begin{aligned} \frac{\partial \sigma}{\partial x} &= -\frac{\varepsilon^{1/3} y}{3x^{4/3}} \frac{d\sigma}{d\eta}, \\ \frac{\partial^2 \sigma}{\partial y^2} &= \frac{\varepsilon^{2/3}}{x^{2/3}} \frac{d^2 \sigma}{d\eta^2}, \end{aligned} \tag{A.38}$$

and Eq. A.34 becomes

$$\begin{aligned}\frac{d^2\sigma}{d\eta^2} &= -\frac{\varepsilon^{2/3}y^2}{3x^{2/3}}\frac{d\sigma}{d\eta} \\ &= -\frac{1}{3}\eta^2\frac{d\sigma}{d\eta}.\end{aligned} \tag{A.39}$$

To solve this, we define an intermediary variable, $v = \frac{d\sigma}{d\eta}$, and then solve the first order ODE:

$$\begin{aligned}\frac{dv}{d\eta} + \frac{1}{3}\eta^2 v &= 0, \\ v &= C_1 \mathrm{e}^{-\frac{1}{9}\eta^3}.\end{aligned} \tag{A.40}$$

And then we see that $\sigma(\eta)$ is given by

$$\sigma(\eta) = C_1 \int_0^\eta \mathrm{e}^{-\frac{1}{9}z^3}\, dz + C_2 \qquad\qquad \eta = \frac{\varepsilon^{1/3}y}{x^{1/3}}, \tag{A.41}$$

where C_1 and C_2 are constants of integration. Now we can apply the boundary conditions given in Eq. A.31:

1. At $y = 0$, i.e. at $\eta = 0$, $\sigma = 0$. So $C_2 = 0$.
2. As $y \to \infty$, $\eta \to \infty$, we have $\sigma \to \sigma_0$. Therefore,

$$C_1 = \frac{\sigma_0}{\int_0^\infty \mathrm{e}^{-\frac{1}{9}z^3}\, dz} \tag{A.42}$$

And so we find

$$\sigma(\eta) = \frac{\sigma_0 \int_0^\eta \mathrm{e}^{-\frac{1}{9}z^3}\, dz}{\int_0^\infty \mathrm{e}^{-\frac{1}{9}z^3}\, dz}. \tag{A.43}$$

We can evaluate $\int_0^\infty \mathrm{e}^{-\frac{1}{9}z^3}\, dz$ using Gamma functions. The Gamma function is defined by $\Gamma(z) = \int_0^\infty x^{z-1}e^{-x}\, dx$. Making a change of variables, $u = \frac{1}{9}z^3$, so that $du = \frac{1}{3}z^2 dz$ and $dz = 3^{-1/3}u^{-2/3}du$, we write

$$\begin{aligned}\int_0^\infty \mathrm{e}^{-\frac{1}{9}z^3}\, dz &= \int_0^\infty 3^{-\frac{1}{3}}u^{-\frac{2}{3}}\mathrm{e}^{-u}\, du \\ &= \frac{\Gamma(\frac{1}{3})}{\sqrt[3]{3}}.\end{aligned} \tag{A.44}$$

Then finally we find an expression for σ,

$$\sigma(y,x) = \frac{\sigma_0 \sqrt[3]{3}}{\Gamma(\frac{1}{3})} \int_0^{\sqrt[3]{\frac{4\lambda}{\pi R^3 D}} \frac{y}{\sqrt[3]{x}}} \mathrm{e}^{-\frac{1}{9}z^3}\, dz. \tag{A.45}$$

And hence we can find the deposition rate

$$\begin{aligned} j(x) &= D\left(\frac{\partial \sigma}{\partial y}\right)_{y=0} \\ &= D\left(\frac{\sigma_0 \sqrt[3]{3}}{\Gamma(\frac{1}{3})} \mathrm{e}^{-\frac{1}{9}\eta^3} \sqrt[3]{\frac{\varepsilon}{x}}\right)_{y=0} \\ &= \frac{D\sigma_0}{\Gamma(\frac{1}{3})} \sqrt[3]{\frac{12\lambda}{\pi R^3 D}} \frac{1}{\sqrt[3]{x}} \\ &= 0.5835 D\sigma_0 \sqrt[3]{\frac{\lambda}{R^3 D}} \frac{1}{\sqrt[3]{x}}, \end{aligned} \tag{A.46}$$

where the constant prefactor 0.5835 is obtained by numerical evaluation of $\frac{1}{\Gamma(1/3)} \sqrt[3]{12/\pi}$.

Finally, we check the boundary layer thickness. To first order we have a relationship between the deposition rate and the boundary layer thickness of $j = D\sigma_0/\delta$ (see Levich Chapter 2.10 [69]). Therefore, the boundary layer thickness is approximately

$$\delta \approx \frac{\sqrt[3]{x}}{0.5835} \sqrt[3]{\frac{R^3 D}{\lambda}}, \tag{A.47}$$

and this is thin when $\delta \ll R$, i.e., when $\frac{Dx}{\lambda} \ll 1$.

A.3.4 Numerical implementation of the intraluminal flow

As referred to on page 60.

Recall Eq. 5.2:

$$\frac{\partial \sigma}{\partial t} = D_B \left(\frac{\partial^2 \sigma}{\partial r^2} + \frac{1}{r}\frac{\partial \sigma}{\partial r}\right) - \frac{2\lambda}{\pi R^4}\left(R^2 - r^2\right)\frac{\partial \sigma}{\partial x}.$$

For convenience, we nondimensionalise with the following transform: $\tilde{r} = r/R$, $\tilde{x} = D_B \pi x / 2\lambda$, and $\tilde{t} = D_B t / R^2$, to write

$$\frac{\partial \sigma}{\partial \tilde{t}} = \left(\frac{\partial^2 \sigma}{\partial \tilde{r}^2} + \frac{1}{\tilde{r}} \frac{\partial \sigma}{\partial \tilde{r}} \right) - \left(1 - \tilde{r}^2\right) \frac{\partial \sigma}{\partial \tilde{x}}. \tag{A.48}$$

We discretise this with a forward time, centred r space, and backward x space scheme, to obtain:

$$\sigma_{pq}^{k+1} = \sigma_{pq}^{k} + \Delta t \left[\frac{\sigma_{pq+1}^{k} - 2\sigma_{pq}^{k} + \sigma_{pq-1}^{k}}{\Delta r^2} + \frac{1}{q\Delta r} \left(\frac{\sigma_{pq+1}^{k} - \sigma_{pq-1}^{k}}{2\Delta r} \right) - \left(1 - (q\Delta r)^2\right) \left(\frac{\sigma_{pq}^{k} - \sigma_{p-1q}^{k}}{\Delta x} \right) \right], \tag{A.49}$$

where σ_{pq}^{k} is the intraluminal bacterial volume density, $\sigma(r, x, t)$, at the pth discrete longitudinal position, qth discrete radial position, and the kth time step; Δt is the time step; Δr is the longitudinal radial discretisation; and Δx is the longitudinal spatial discretisation. Here we have chosen a backward (upstream) scheme for x as it allows us to neglect the downstream boundary at the end of the catheter.

We can analyse Eq. A.49 for stability using von Neumann analysis, with the following error ansatz: $\sigma(r, x, t_k) = \mathrm{e}^{i\psi x} \mathrm{e}^{i\phi r}$. This results in an equation for the amplification factor:

$$\frac{\sigma_{pq}^{k+1}}{\sigma_{pq}^{k}} = 1 + \frac{\Delta t}{\Delta r^2} \underbrace{\left(\left(2 + \frac{1}{q}\right) \cos(\phi \Delta r) - 2 \right)}_{\in \left[-5,1\right]} + \frac{\Delta t \left(1 - (q\Delta r)^2\right)}{\Delta x} \underbrace{\left(\mathrm{e}^{-i\psi\Delta x} - 1 \right)}_{\in \left[-2,0\right]}. \tag{A.50}$$

For numerical stability we require $\left| \frac{\sigma_{pq}^{k+1}}{\sigma_{pq}^{k}} \right| \leq 1$. That is, we require

$$-1 \leq 1 - \frac{5\Delta t}{\Delta r^2} - \frac{2\Delta t}{\Delta x} \tag{A.51}$$

and

$$1 + \frac{1}{q} \frac{\Delta t}{\Delta r^2} \leq 1. \tag{A.52}$$

From Eq. A.51 we obtain a stability condition on the time step, which we can redimensionalise:

$$\Delta t \leq \left(\frac{5 D_B}{2\Delta r^2} + \frac{2\lambda}{R^2 \pi \Delta x} \right)^{-1}. \tag{A.53}$$

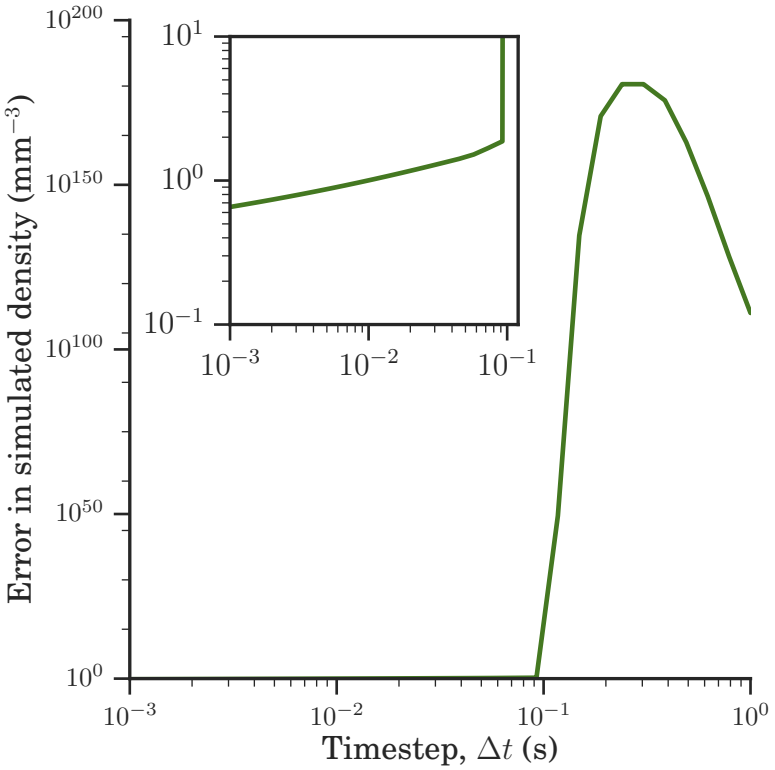

Figure A.2 *Convergence of the numerical scheme for the bacterial density within the intraluminal flow (Eq. A.49). Plotted is the difference in simulated density between a simulation run with a timestep* Δt*, and a run with a timestep* 1.25 *times larger. Each simulation was run with parameters as in Table 2.2,* $\Delta x = 0.8$ *mm, and* $\Delta r = 0.02$ *mm. Inset is a zoomed view, showing numerical stability for timesteps* $\Delta t \lesssim 0.1$ *s.*

Evaluating this for the parameter values of Table 2.2, with $\Delta x = 0.8$ mm and $\Delta r = 0.02$ mm, would imply that we require $\Delta t \lesssim 10^{-4}$ s. However, from Eq. A.52, we see that there is no value for the timestep that can ensure the stability of this scheme, as q, Δr, and Δx are all strictly positive, and hence this condition is always violated.

However, all is not lost. So far we have only considered one of our boundaries (the downstream, $x = L$, 'open' boundary). In fact we also have Dirichlet boundary conditions, both at the upstream ($x = 0$) boundary, where the bacterial density is fixed by the density within the bladder ($\sigma(x{=}0, r, t) = \rho(t)$), and at the catheter surface ($r = R$) boundary, where bacteria stick to the surface ($\sigma(x, r{=}R, t) = 0$). These absorbing boundary conditions effectively 'damp' errors: as we can see in Figure A.2, this scheme actually converges at timesteps closer to 0.1 s. For the figures within this chapter, a timestep of 0.05 s was used.

A.3.5 Numerical implementation of the intraluminal surface

As referred to on pages 61, 71, 71, 72.

To simulate bacterial growth and spreading on the inside surface of the catheter, a forward-time centred-space (FTCS) method is used. Recall Eq. 5.1:

$$\frac{\partial m}{\partial t} = D_S \frac{\partial^2 m}{\partial x^2} + r_S m \left(1 - \frac{m}{\kappa_S}\right) + j(x).$$

The bacterial flux, $j(x)$, comes from the deposition of bacteria onto the intraluminal surface from the urine flow out of the bladder. To calculate this numerically requires simulating the intraluminal flow, which is computationally more demanding as it is a 2-dimensional problem, unlike the 1-dimensional surfaces. Instead, here we use the analytic approximation for the bacterial flux, as given by Eq. 5.17,

$$j(x) = 0.5835 D_B \rho \sqrt[3]{\frac{\lambda}{R^3 D_B}} \frac{1}{\sqrt[3]{x}}.$$

This analytic solution is valid for $h < x \ll H$, i.e., the region in which the hydrodynamic flow is established, but the diffusive boundary layer is still small. We can find h by looking for the distance at which the hydrodynamic boundary layer thickness is equal to the catheter radius. From Levich [69], defining the

hydrodynamic boundary layer thickness as the thickness at which the flow speed is 90% of the main flow speed, this is

$$R \sim 5.2\sqrt{\frac{\nu h}{U_0}}$$
$$h \sim \frac{1}{27}\frac{\lambda}{\pi\nu} \sim \frac{Re \cdot R}{27} \sim 0.22 \text{ mm}.$$

The behaviour within the early region, $x < h$, would be highly dependent on the exact geometry of the catheter, which is not incorporated into this model. Instead, knowing that the deposition rate must always be finite, we take a zeroth order approximation that the flux for $x < h$ is constant, and $j(x < h) = j(h)$. Since this is only a very small region of the catheter, this approximation has very little impact on the results of the model (as can be seen in Figure 5.4b).

We can discretise the intraluminal surface in a manner very similar to the extraluminal surface, using a FTCS method to find

$$m_p^{k+1} = \frac{D_S \Delta t}{\Delta x^2}\left(m_{p+1}^k - 2m_p^k + m_{p-1}^k\right) + (1 + r\Delta t)\, m_p^k - \frac{r\Delta t}{\kappa_S}\left(m_p^k\right)^2 + 0.5835\left(\frac{\lambda D_B^2}{R^3}\right)^{1/3} \Delta t \rho^k (p\Delta x)^{-1/3}, \quad \text{(A.54)}$$

where m_p^k is the intraluminal bacterial surface density, $m(x,t)$, at the pth discrete position, and the kth time step; ρ^k is the bacterial volume density in the bladder at the kth time step; Δt is the time step; and Δx is the spatial discretisation. Eq. A.54 is numerically stable with the same condition as the extraluminal surface, provided that the conditions discussed prior hold for the validity of $j(x)$. That is, $L \ll 10^5$ mm.

Recalling §A.1.2, the discretisation is stable provided

$$\Delta x < 8\sqrt{\frac{D_S}{r_S}}$$
$$\Delta t < \frac{\Delta x^2}{2D_S}. \quad \text{(A.55)}$$

We find that the best results are obtained with a slightly smaller step size:

$$\Delta x < \frac{1}{2}\sqrt{\frac{D_S}{r_S}}$$
$$\Delta t < \frac{\Delta x^2}{20D_S}. \quad \text{(A.56)}$$

A.3.6 Experimental methods for Figure 5.1

As referred to on page 51.

Sample preparation

Sample 1 was used for Figures 5.1a and 5.1b. *E. coli* strain AD51, which constitutively expresses green fluorescent protein (GFP), was cultured in LB growth medium at 37°C overnight. The culture was diluted 1:10 in M63 growth medium, for a total volume of 5 mL. An 8 cm segment of a (veterinary) urinary catheter was injected with culture, then placed in a petri dish with a DI water trough (to avoid excess evaporation), covered and incubated at 30°C for 24 hrs. The sample was then fixed by injection with formaldehyde.

Sample 2 was used for Figures 5.1c and 5.1d. *E. coli* strain RJA002, which contains a constitutively expressed yellow fluorescent reporter gene (YFP), was cultured in LB growth medium at 37°C overnight. The culture was diluted 1:10 in M63 growth medium, for a total volume of 5 mL. An 8 cm segment of catheter was injected with culture, then placed in a petri dish with a DI water trough (to avoid excess evaporation), covered and incubated at 30°C for 24 hrs. The sample was then fixed by injection with formaldehyde.

Before fixing the samples, I checked that injecting catheters with formaldehyde does not lead to biofilm detachment. In the literature it is established that biofilm detachment occurs for flow speeds above 3 ms^{-1} [16, 106]. The maximum flow speed obtained when injecting formaldehyde into a urinary catheter is $\sim$ 0.3 ms^{-1}, as above this speed the pressure is sufficient to dislodge the syringe connector. Thus, it is unlikely that fixing samples by formaldehyde injection leads to significant biofilm detachment.

Imaging

Both samples were imaged with the Mesolens setup by Gail McConnell and her group at the University of Strathclyde. Mesolens is a giant microscope that has a numerical aperture of 0.47 with a magnification of 4x [76]. This allows for the imaging of 6 mm samples to resolutions ~ 1 μm.

Strain AD51 expresses green fluorescent protein, and strain RJA002 expresses yellow fluorescent protein. Epi-fluorescence images were taken with excitation

wavelength 490 nm. Epi-fluorescence images of both samples were also taken at 385 nm. Significant background auto-fluorescence and debris could be seen at 385 nm. During image processing this background fluorescence was subtracted, resulting in the images seen in Figure 5.1.

Appendix B

Data access and data analysis

B.0.1 Data access

As referred to on page 110.

We obtained limited access to data from the CATHETER trial [91]. We received data on duration of catheterisation, sex, type of catheter received, and a True/False result for 'bacteriuria' – a bacterial count in the urine $> 10^4$ CFU/mL up to 3 days after catheter removal. No patient-identifying information was provided.

B.1 Data processing

B.1.1 Cleaning data

As referred to on page 110.

We received data on 6394 patients in the study. Of these, 146 were missing duration data, with a further 791 missing outcome data. Removing data points with cross catheterisation (whereby multiple types of catheters were used for one patient), left 5369 patients with complete data entries. Of these, 1703 received nitrofural-impregnated catheters, 1695 received silver-alloy coated catheters, and 1971 received PTFE-coated catheters.

The median duration of catheterisation was 2 days for all patient groups. Plotting

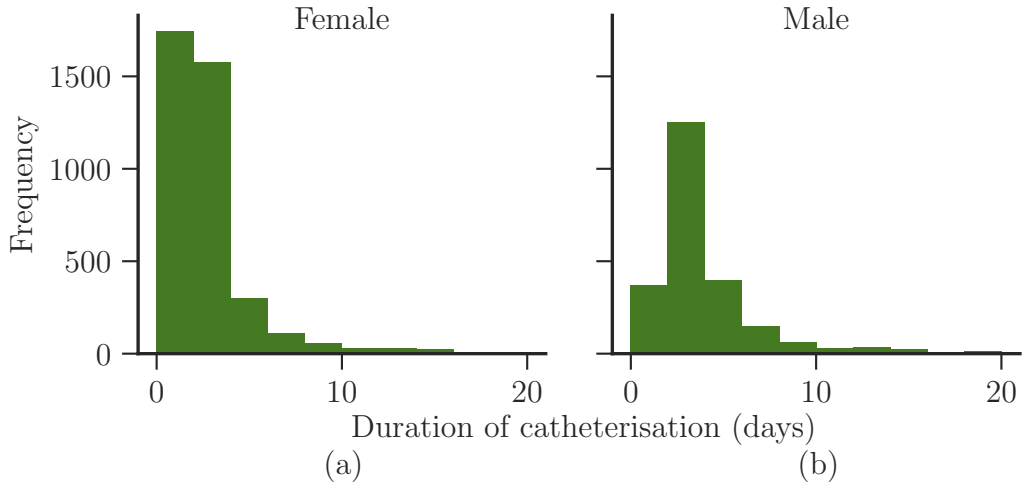

Figure B.1 *Breakdown by sex of the durations of catheterisation for patients in the study (Pickard et al., 2012 [90]), excluding 32 patients with durations greater than 20 days. (a) Distribution of duration of catheterisation for 3897 females. (b) Distribution of duration of catheterisation for 2351 males.*

the distribution of catheterisation durations for females (Figure B.1a) and males (Figure B.1b), we see that most patients were catheterised for ≤ 7 days, however catheterisation up to 20 days was not uncommon. 32 patients were catheterised for durations greater than 20 days (maximum duration 65 days): these patients have been excluded from further analysis. We see that the distribution of durations for female patients differs from the distribution for male patients, with many more female patients undergoing catheterisation of duration ≤ 2 days. This likely represents an underlying sex-based difference in the reason for patient hospital stays.

B.1.2 Binning data

As referred to on page 110.

To obtain the bacteriuric fraction, we binned the data points into duration bins of size ≥ 25 patients, and defined the bacteriuric fraction as the number of patients with a positive urine culture, divided by the total number of patients in the bin. The binned data is available in Table B.1. The choice of a minimum bin size of 25 represents a compromise between the duration resolution of the data, and the accuracy of the bacteriuric fraction. The bacteriuric fraction for longer durations (where data was sparser) was $\sim 20\%$, so with a bin size of 25 patients we expect 5 occurrences of bacteriuria per bin.

Duration (days)	Number of patients	Bacteriuric fraction
Females with PTFE catheters		
1	531	0.186 ± 0.017
2	385	0.234 ± 0.022
3	108	0.269 ± 0.043
4	55	0.182 ± 0.052
5	29	0.310 ± 0.086
6–7	41	0.212 ± 0.075
8–10	27	0.296 ± 0.088
11–20	25	0.400 ± 0.098
Females with Nitrofural catheters		
1	498	0.179 ± 0.017
2	349	0.149 ± 0.019
3	86	0.198 ± 0.043
4	49	0.102 ± 0.043
5–6	46	0.174 ± 0.056
7–20	32	0.188 ± 0.067
Females with Silver-alloy catheters		
1	472	0.231 ± 0.019
2	355	0.242 ± 0.023
3	103	0.146 ± 0.035
4	58	0.259 ± 0.057
5	26	0.269 ± 0.087
6–7	26	0.231 ± 0.083
8–20	38	0.211 ± 0.066
Males with PTFE catheters		
1	133	0.052 ± 0.019

Table B.1 *Cleaned and binned study data. Table continues on next page.*

Duration (days)	Number of patients	Bacteriuric fraction
2	301	0.086 ± 0.016
3	122	0.074 ± 0.024
4	80	0.188 ± 0.044
5	39	0.179 ± 0.061
6–7	39	0.179 ± 0.061
8–20	48	0.104 ± 0.044
Males with Nitrofural catheters		
1	106	0.019 ± 0.013
2	247	0.073 ± 0.017
3	120	0.092 ± 0.026
4	71	0.070 ± 0.030
5	33	0.061 ± 0.042
6–7	28	0.143 ± 0.066
8–20	28	0.179 ± 0.072
Males with Silver-alloy catheters		
1	95	0.053 ± 0.023
2	232	0.056 ± 0.015
3	97	0.082 ± 0.028
4	75	0.067 ± 0.029
5–6	51	0.059 ± 0.033
7–8	32	0.125 ± 0.058
9–20	30	0.200 ± 0.073

Table B.1 *Cleaned and binned study data. After removing missing data entries, the data points were binned into bins of* ≥ 25 *patients. The bacteriuric fraction is defined as the fraction of patients with a positive CFU result (a bacterial count* $> 10^4$ *CFU/mL up to 3 days after catheterisation). The error is the sample standard deviation,* $\sqrt{p(1-p)/n}$*, where* p *is the bacteriuric fraction, and* n *the bin size (the number of patients).*

B.2 Data analysis

B.2.1 Bacteriuric fraction for each intervention group

As referred to on page 111.

In Figure 8.2, we plot the data points as described in Table B.1, and overlay the baseline bacteriuric fraction, and the mean bacteriuric fraction for patients with duration of catheterisation > 7 days. The bacteriuric fraction is defined as the fraction of patients with a positive CFU result (a bacterial count $> 10^4$ CFU/mL up to 3 days after catheterisation). The (y) error is the sample standard deviation, $\sqrt{p(1-p)/n}$, where p is the bacteriuric fraction, and n the bin size (the number of patients). The data points are located at the mean duration of the bin, and the (x) error is the standard deviation in the durations within the bin, $\sqrt{\sum(x-\bar{x})^2/n}$, where x is the duration, $\bar{x}$ is the mean duration, and n the bin size. The baseline bacteriuric fraction is 469/6123 ($7.7 \pm 0.3\%$), as reported by Pickard et al. [90]. The mean fraction for durations > 7 days was calculated as the number of patients catheterised for > 7 days with positive urine cultures: 56/278 ($20 \pm 2\%$).

B.2.2 Urine production rates in the population

As referred to on pages 113, 114.

Data was obtained from the CDC National Health and Nutrition Examination Survey [81], 2009-2014, on the mean urine production rates of 21313 American adults and plotted in Figure 8.3. We define the susceptible fraction as those with urine production rates less than a threshold value, and give the error on the susceptible fraction as the sample standard deviation, $\sqrt{p(1-p)/n}$, where p is the susceptible fraction, and n the number of patients. When we calculate the population mean urine production rate, we give the standard deviation on the mean, $\sqrt{\sum(x-\bar{x})^2/n}$.

In Table 8.3 we calculate the change in susceptible fraction corresponding to a given increase in mean urine production rate. That is, if $F(\lambda)$ is the distribution of urine production rates, then the susceptible fraction is $F(\lambda < \lambda^*)$, where λ^* is the critical urine production rate (generally $\lambda^* = r_B V$); and the susceptible fraction given an increased mean urine production rate is $F(\lambda+\Delta\lambda < \lambda^*)$, where $\Delta\lambda$ is the increase in urine production rate. We calculate the relative risk adjustment

as

$$\frac{F(\lambda+\Delta\lambda<\lambda^*)-F(\lambda<\lambda^*)}{F(\lambda<\lambda^*)}, \tag{B.1}$$

with the resultant error then being

$$\sqrt{\left[\frac{\text{Error}_{F(\lambda+\Delta\lambda<\lambda^*)}}{F(\lambda<\lambda^*)}\right]^2+\left[\frac{F(\lambda+\Delta\lambda<\lambda^*)\text{Error}_{F(\lambda<\lambda^*)}}{(F(\lambda<\lambda^*))^2}\right]^2}. \tag{B.2}$$

B.2.3 Fitting the model to find v_{asc}

As referred to on page 117.

In Figure 8.4, we fitted our sigmoidal model (Eq. 8.5) to the control group (PTFE) data and compared it to a linear fit. The sigmoid function was fitted using least-squares minimisation (`scipy.optimize.curve_fit`), and the linear fit by a linear regression (`scipy.stats.linregress`). We compared the two fits by comparing the residual sum of squares: $\text{RSS} = \sum(x-y)^2$, where x is the study data, and y is the model predicted value.

B.2.4 Making predictions

As referred to on page 121.

Eq. 8.6 defines the model prediction for the bacteriuric incidence dependence on duration of catheterisation. We used this to calculate the mean ascension times: 6.65 ± 0.46 days for Nitro, 8.4 ± 1.1 days for Silver. Since Nitro represents a time-translation in the model prediction, the error for Nitro is equal to the model for PTFE. The predicted effect of Silver amounts to a stretch factor 2.3, hence the error for Silver is 2.3 times the error for PTFE.

In Figure 8.5, we presented the model predictions for the total incidence of bacteriuria for males in the study. These predictions were calculated as follows:

$$\frac{\sum_T f(T; v_{\text{asc}})}{N}, \tag{B.3}$$

where $f(T; v_{\text{asc}})$ is the modelled bacteriuric risk function (Eq. 8.5), T are the durations of catheterisation recorded in the study, and N is the total number of patients.

The errors on the predictions then arise from two source: the errors in the fit

used to find v_{asc}, and from the patient variability in the dataset:

$$\sqrt{\left[\text{Error}_{v_{\text{asc}}}\right]^2 + \left[\text{Error}_T\right]^2}. \tag{B.4}$$

We determined $\text{Error}_{v_{\text{asc}}}$ by propagating the uncertainty on the fit for v_{asc} through Eq. B.3. We determined Error_T through bootstrapping with replacement, using `sklearn.utils.resample`.

Bibliography

[1] K. M. Agbavon, A. R. Appadu, and M. Khumalo. On the numerical solution of Fisher's equation with coefficient of diffusion term much smaller than coefficient of reaction term. *Advances in Difference Equations*, 2019(146), 2019.

[2] E. M. Ahmed. Hydrogel: Preparation, characterization, and applications: A review. *Journal of Advanced Research*, 6(2):105–121, 2015.

[3] R. J. Allen and B. Waclaw. Bacterial growth: A statistical physicist's guide. *Reports on Progress in Physics*, 82(1), 2019.

[4] M. J. Andersen and A. L. Flores-Mireles. Urinary catheter coating modifications: The race against catheter-associated infections. *Coatings*, 10(23), 2020.

[5] L. R. Band, L. J. Cummings, S. L. Waters, and J. A. Wattis. Modelling crystal aggregation and deposition in the catheterised lower urinary tract. *Journal of Mathematical Biology*, 59(6):809–840, 2009.

[6] A. Be'er and G. Ariel. A statistical physics view of swarming bacteria. *Movement Ecology*, 7(1), 2019.

[7] H. C. Berg. *E. coli in motion*. Springer, New York, 2004.

[8] F. Biering-Sørensen, H. V. Hansen, P. N. Nielsen, and D. Looms. Residual urine after intermittent catheterization in females using two different catheters. *Scandinavian Journal of Urology and Nephrology*, 41(4):341–345, 2007.

[9] T. Bjarnsholt. The Role of Bacterial Biofilms in Chronic Infections. *APMIS*, 121(SI):1–58, 2013.

[10] H. Bremer and P. P. Dennis. Modulation of Chemical Composition and Other Parameters of the Cell at Different Exponential Growth Rates. *EcoSal Plus*, 3(1), 2008.

[11] R. J. Broomfield, S. D. Morgan, A. Khan, and D. J. Stickler. Crystalline bacterial biofilm formation on urinary catheters by urease-producing

urinary tract pathogens: A simple method of control. *Journal of Medical Microbiology*, 58(10):1367–1375, 2009.

[12] F. Bull, S. Tavadodd, N. Bommer, M. Perry, C. Brackley, and R. J. Allen. Urine production rate is critical in a model for catheter-associated urinary tract infection. *bioRxiv*, 2022. doi: 10.1101/2022.10.31.514508.

[13] R. G. Burr and I. M. Nuseibeh. Urinary catheter blockage depends on urine pH, calcium and rate of flow. *Spinal Cord*, 35:521–525, 1997.

[14] H. J. Busscher and H. C. Van Der Mei. Microbial adhesion in flow displacement systems. *Clinical Microbiology Reviews*, 19(1):127–141, 2006.

[15] M. E. Cates. Diffusive transport without detailed balance in motile bacteria: does microbiology need statistical physics? *Reports on progress in physics. Physical Society (Great Britain)*, 75(4):042601, 2012.

[16] T. E. Cloete, D. Westaard, and S. J. Van Vuuren. Dynamic response of biofilm to pipe surface and fluid velocity. *Water Science and Technology*, 47(5):57–59, 2003.

[17] M. S. Conover, M. Hadjifrangiskou, J. J. Palermo, M. E. Hibbing, K. W. Dodson, and S. J. Hultgren. Metabolic requirements of Escherichia coli in intracellular bacterial communities during urinary tract infection pathogenesis. *mBio*, 7(2), 2016.

[18] N. W. Cortes-Penfield, B. W. Trautner, and R. L. Jump. Urinary Tract Infection and Asymptomatic Bacteriuria in Older Adults. *Infectious Disease Clinics of North America*, 31(4):673–688, 2017.

[19] J. Crank. *The mathematics of diffusion*. Oxford University Press, 2nd edition, 1975.

[20] R. Daifuku and W. E. Stamm. Association of Rectal and Urethral Colonization With Urinary Tract Infection in Patients With Indwelling Catheters. *JAMA: The Journal of the American Medical Association*, 252 (15):2028–2030, 1984.

[21] N. C. Darnton, L. Turner, S. Rojevsky, and H. C. Berg. Dynamics of bacterial swarming. *Biophysical Journal*, 98(10):2082–2090, 2010.

[22] M. G. J. De Vos, M. Zagorski, A. McNally, and T. Bollenbach. Interaction networks, ecological stability, and collective antibiotic tolerance in polymicrobial infections. *Proceedings of the National Academy of Sciences of the United States of America*, 114(40):10666–10671, 2017.

[23] K. H. Dellimore, A. R. Helyer, and S. E. Franklin. A scoping review of important urinary catheter induced complications. *Journal of Materials Science: Materials in Medicine*, 24(8):1825–1835, 2013.

[24] D. G. Desai, K. S. Liao, M. E. Cevallos, and B. W. Trautner. Silver or nitrofurazone impregnation of urinary catheters has a minimal effect on uropathogen adherence. *Journal of Urology*, 184(6):2565–2571, 2010.

[25] R. M. Donlan. Biofilms and device-associated infections. *Emerging Infectious Diseases*, 7(2):277–281, 2001.

[26] A. Duval and M. Loday-Richaud. Kovacic's algorithm and its application to some families of special functions. *Applicable Algebra in Engineering, Communication and Computing*, 3(3):211–246, 1992.

[27] J. Elgeti, R. G. Winkler, and G. Gompper. Physics of microswimmers - Single particle motion and collective behavior: A review. *Reports on Progress in Physics*, 78:056601, 2015.

[28] O. Fasugba, A. C. Cheng, V. Gregory, N. Graves, J. Koerner, P. Collignon, A. Gardner, and B. G. Mitchell. Chlorhexidine for meatal cleaning in reducing catheter-associated urinary tract infections: a multicentre stepped-wedge randomised controlled trial. *The Lancet Infectious Diseases*, 19(6):611–619, 2019.

[29] W. Feller. *An Introduction to Probability Theory and Its Applications*, volume 2. Wiley, New York, 2nd edition, 1971.

[30] R. C. L. Feneley, C. M. Kunin, and D. J. Stickler. An indwelling urinary catheter for the 21st century. *BJU International*, 109:1746–1749, 2011.

[31] R. C. L. Feneley, I. B. Hopley, and P. N. T. Wells. Urinary catheters: history, current status, adverse events and research agenda. *Journal of Medical Engineering & Technology*, 39(8):459–470, 2015.

[32] L. Ferrières, V. Hancock, and P. Klemm. Specific selection for virulent urinary tract infectious Escherichia coli strains during catheter-associated biofilm formation. *FEMS Immunology and Medical Microbiology*, 51(1): 212–219, 2007.

[33] R. A. Fisher. The wave of advance of advantageous genes. *Annals of Eugenics*, 7(4):355–369, 1937.

[34] A. L. Flores-Mireles, J. N. Walker, M. G. Caparon, and S. J. Hultgren. Urinary tract infections: Epidemiology, mechanisms of infection and treatment options. *Nature Reviews Microbiology*, 13(5):269–284, 2015.

[35] V. S. Forsyth, C. E. Armbruster, S. N. Smith, A. Pirani, A. C. Springman, M. S. Walters, G. R. Nielubowicz, S. D. Himpsl, E. S. Snitkin, and H. L. T. Mobley. Rapid growth of uropathogenic Escherichia coli during human urinary tract infection. *mBio*, 9(2):1–13, 2018.

[36] B. Foxman. Urinary tract infection syndromes. Occurrence, recurrence, bacteriology, risk factors, and disease burden. *Infectious Disease Clinics of North America*, 28(1):1–13, 2014.

[37] R. S. Friedlander, H. Vlamakis, P. Kim, M. Khan, R. Kolter, and J. Aizenberg. Bacterial flagella explore microscale hummocks and hollows to increase adhesion. *Proceedings of the National Academy of Sciences*, 110 (14):5624–5629, 2013.

[38] H. Gage, M. Avery, C. Flannery, P. Williams, and M. Fader. Community prevalence of long-term urinary catheters use in England. *Neurourology and Urodynamics*, 36(2):293–296, 2017.

[39] T. A. Gaonkar, L. A. Sampath, and S. M. Modak. Evaluation of the Antimicrobial Efficacy of Urinary Catheters Impregnated With Antiseptics in an In Vitro Urinary Tract Model. *Infection Control & Hospital Epidemiology*, 24(7):506–513, 2003.

[40] M. M. Garcia, S. Gulati, D. Liepmann, G. B. Stackhouse, K. Greene, and M. L. Stoller. Traditional Foley Drainage Systems-Do They Drain the Bladder? *Journal of Urology*, 177(1):203–207, 2007.

[41] A. Gelimson, K. Zhao, C. K. Lee, W. T. Kranz, G. C. L. Wong, and R. Golestanian. Multicellular Self-Organization of P. aeruginosa due to Interactions with Secreted Trails. *Physical Review Letters*, 117(17), 2016.

[42] H. Godfrey. Living with a long-term urinary catheter: Older people's experiences. *Journal of Advanced Nursing*, 62(2):180–190, 2008.

[43] D. M. Gordon and M. A. Riley. A theoretical and experimental analysis of bacterial growth in the bladder. *Molecular Microbiology*, 6(4):555–562, 1992.

[44] C. V. Gould, C. A. Umscheid, R. K. Agarwal, G. Kuntz, and D. A. Pegues. Guidelines for prevention of catheter-associated urinary tract infections. *Infection Control and Hospital Epidemiology*, 31(4):319–326, 2010.

[45] E. Hariton and J. J. Locascio. Randomised controlled trials – the gold standard for effectiveness research: Study design: randomised controlled trials. *BJOG: An International Journal of Obstetrics and Gynaecology*, 125 (13):1716, 2018.

[46] J. Henrichsen. Bacterial Surface Translocation: a Survey and a Classification. *Bacteriological Reviews*, 36(4):478–503, 1972.

[47] J. Hill, O. Kalkanci, J. L. McMurry, and H. Koser. Hydrodynamic Surface Interactions Enable Escherichia Coli to Seek Efficient Routes to Swim Upstream. *Physical Review Letters*, 98(6):068101, 2007.

[48] T. M. Hooton, S. F. Bradley, D. D. Cardenas, R. Colgan, S. E. Geerlings, J. C. Rice, S. Saint, A. J. Schaeffer, P. A. Tambayh, P. Tenke, and L. E. Nicolle. Diagnosis, Prevention, and Treatment of Catheter-Associated Urinary Tract Infection in Adults: 2009 International Clinical Practice Guidelines from the Infectious Diseases Society of America. *Clinical Infectious Diseases*, 50(5):625–663, 2010.

[49] T. M. Hooton, M. Vecchio, A. Iroz, I. Tack, Q. Dornic, I. Seksek, and Y. Lotan. Effect of Increased Daily Water Intake in Premenopausal Women with Recurrent Urinary Tract Infections. *JAMA Internal Medicine*, 178 (11):1509–1515, 2018.

[50] J. L. Ingraham, O. Maaloe, and F. C. Neidhardt. *Growth of the Bacterial Cell*. Sinauer Associates, Sunderland (Massachusetts), 1983.

[51] B. A. Inman, W. Etienne, R. Rubin, R. A. Owusu, T. R. Oliveira, D. B. Rodriques, P. F. Maccarini, P. R. Stauffer, A. Mashal, and M. W. Dewhirst. The impact of temperature and urinary constituents on urine viscosity and its relevance to bladder hyperthermia treatment. *International Journal of Hyperthermia*, 29(3):206–210, 2013.

[52] S. M. Jacobsen, D. J. Stickler, H. L. T. Mobley, and M. E. Shirtliff. Complicated Catheter-Associated Urinary Tract Infections Due to Escherichia coli and Proteus mirabilis. *Clinical Microbiology Reviews*, 21 (1):26–59, 2008.

[53] L. Jerram. *E. coli*. National Museum of Scotland, 2022. `https://www.nms.ac.uk/exhibitions-events/past-exhibitions/ecoli-by-luke-jerram/` [Accessed 19 April 2023].

[54] B. V. Jones, R. Young, E. Mahenthiralingam, and D. J. Stickler. Ultrastructure of Proteus mirabilis swarmer cell rafts and role of swarming in catheter-associated urinary tract infection. *Infection and Immunity*, 72 (7):3941–3950, 2004.

[55] T. Kaya and H. Koser. Direct upstream motility in Escherichia coli. *Biophysical Journal*, 102(7):1514–1523, 2012.

[56] K. A. Kazmierska, R. Thompson, N. Morris, A. Long, and T. Ciach. In vitro multicompartmental bladder model for assessing blockage of urinary catheters: Effect of hydrogel coating on dynamics of proteus mirabilis growth. *Urology*, 76(2):515.e15–515.e20, 2010.

[57] D. B. Kearns. A field guide to bacterial swarming motility. *Nature Reviews*, 8(9):634–644, 2010.

[58] I. Klapper and J. Dockery. Mathematical Description of Microbial Biofilms. *SIAM Review*, 52(2):221–265, 2010.

[59] R. D. Klein and S. J. Hultgren. Urinary tract infections: microbial pathogenesis, host–pathogen interactions and new treatment strategies. *Nature Reviews Microbiology*, 18(4):211–226, 2020.

[60] T. S. Kohler, M. Yadven, A. Manvar, N. Liu, and M. Monga. The length of the male urethra. *International Braz J Urol*, 34(4):451–454, 2008.

[61] A. Kolmogorov, I. Petrovsky, and N. Piskunov. Etude de l'equation de la diffusion avec croissance de la quantitedematiere et son application a un probleme biologique. *Bulletin of Moscow State University Series A: Mathematics and Mechanics*, 1:1–25, 1937.

[62] J. J. Kovacic. An algorithm for solving second order linear homogeneous differential equations. *Journal of Symbolic Computation*, 2(1):3–43, 1986.

[63] J. Krebs, P. Bartel, and J. Pannek. Residual urine volumes after intermittent catheterization in men with spinal cord injury. *Spinal Cord*, 51(10):776–779, 2013.

[64] C. M. Kunin. Can we build a better urinary catheter? *New England Journal of Medicine*, 319(6):365–366, 1988.

[65] E. Lauga and T. R. Powers. The hydrodynamics of swimming microorganisms. *Reports on Progress in Physics*, 72(9):096601, 2009.

[66] J. Leech, S. Golub, W. Allan, M. J. Simmons, and T. W. Overton. Non-pathogenic Escherichia coli biofilms: effects of growth conditions and surface properties on structure and curli gene expression. *Archives of Microbiology*, 202(6):1517–1527, 2020.

[67] A. S. Letica-Kriegel, H. Salmasian, D. K. Vawdrey, B. E. Youngerman, R. A. Green, E. Y. Furuya, D. P. Calfee, and R. Perotte. Identifying the risk factors for catheter-associated urinary tract infections: A large cross-sectional study of six hospitals. *BMJ Open*, 9(2), 2019.

[68] V. Levering, Q. Wang, P. Shivapooja, X. Zhao, and G. P. López. Soft robotic concepts in catheter design: An on-demand fouling-release urinary catheter. *Advanced Healthcare Materials*, 3(10):1588–1596, 2014.

[69] V. G. Levich. *Physicochemical hydrodynamics*. Prentice-Hall, Englewood Cliffs, N.J., 1962.

[70] M. J. Lighthill. Initial development of diffusion in poiseuille flow. *IMA Journal of Applied Mathematics (Institute of Mathematics and Its Applications)*, 2(1):97–108, 1966.

[71] E. Lo, L. E. Nicolle, S. E. Coffin, C. V. Gould, L. L. Maragakis, J. A. Meddings, D. A. Pegues, A. M. Pettis, S. Saint, and D. S. Yokoe. Strategies to Prevent Catheter-Associated Urinary Tract Infections in Acute Care Hospitals: 2014 Update. *Infection Control & Hospital Epidemiology*, 35 (05):464–479, 2014.

[72] J. Long, S. W. Zucker, and T. Emonet. Feedback between motion and sensation provides nonlinear boost in run-and-tumble navigation. *PLoS Computational Biology*, 13(3):1–25, 2017.

[73] Y. Lotan, M. Daudon, F. Bruyère, G. Talaska, G. Strippoli, R. J. Johnson, and I. Tack. Impact of fluid intake in the prevention of urinary system diseases: a brief review. *Current Opinion in Nephrology and Hypertension*, 22(SUPPL.1):S1–S10, 2013.

[74] S. S. Magill, J. R. Edwards, W. Bamberg, Z. G. Beldavs, G. Dumvati, M. A. Kainer, R. Lynfield, M. Maloney, L. McAllister-Hollod, J. Nadle, S. M. Ray, D. L. Thompson, L. E. Wilson, and S. K. Fridkin. Multistate Point-Prevalence Survey of Health Care–Associated Infections. *New England Journal of Medicine*, 370(13):1198–1208, 2014.

[75] S. Mathur, N. A. Sabbuba, M. T. Suller, D. J. Stickler, and R. C. Feneley. Genotyping of urinary and fecal Proteus mirabilis isolates from individuals with long-term urinary catheters. *European Journal of Clinical Microbiology and Infectious Diseases*, 24(9):643–644, 2005.

[76] G. McConnell, J. Trägårdh, R. Amor, J. Dempster, E. Reid, and W. B. Amos. A novel optical microscope for imaging large embryos and tissue volumes with sub-cellular resolution throughout. *eLife*, 5:1–15, 2016.

[77] J. A. Meddings, M. A. M. Rogers, M. Macy, and S. Saint. Systematic Review and Meta-Analysis: Reminder Systems to Reduce Catheter-Associated Urinary Tract Infections and Urinary Catheter Use in Hospitalized Patients. *Clinical Infectious Diseases*, 51:550–560, 2010.

[78] J. A. Meddings, M. A. M. Rogers, S. L. Krein, M. G. Fakih, R. N. Olmsted, and S. Saint. Reducing unnecessary urinary catheter use and other strategies to prevent catheter-associated urinary tract infection: an integrative review. *BMJ Qual Saf*, 23:277–289, 2014.

[79] J. D. Murray. *Mathematical Biology: I: An Introduction*. Springer-Verlag, New York, 3rd edition, 2002.

[80] R. W. Nash, R. Adhikari, J. Tailleur, and M. E. Cates. Run-and-tumble particles with hydrodynamics: Sedimentation, trapping, and upstream swimming. *Physical Review Letters*, 104(25):1–4, 2010.

[81] National Center for Health Statistics (NCHS). *National Health and Nutrition Examination Survey Data*, 2009–2014. Centers for Disease Control and Prevention (CDC). `https://www.cdc.gov/nchs/nhanes/INDEX.htm` [Accessed 27 March 2023].

[82] L. E. Nicolle. Catheter associated urinary tract infections. *Antimicrobial Resistance and Infection Control*, 3(23), 2014.

[83] G. R. Nielubowicz and H. L. T. Mobley. Host-pathogen interactions in urinary tract infection. *Nature Reviews Urology*, 7:430–441, 2010.

[84] J. Y. Noh, D. H. Han, J. A. Yoon, M. H. Kim, S. E. Kim, I. G. Ko, K. H. Kim, C. J. Kim, and S. Cho. Circadian rhythms in urinary functions:

Possible roles of circadian clocks? *International Neurourology Journal*, 15 (2):64–73, 2011.

[85] S. Noimark, C. W. Dunnill, M. Wilson, and I. P. Parkin. The role of surfaces in catheter-associated infections. *Chemical Society Reviews*, 38(12):3435–3448, 2009.

[86] H. Okano, R. Hermsen, K. Kochanowski, and T. Hwa. Regulation underlying hierarchical and simultaneous utilization of carbon substrates by flux sensors in Escherichia coli. *Nature Microbiology*, 5(1):206–215, 2020.

[87] H. Okano, R. Hermsen, and T. Hwa. Hierarchical and simultaneous utilization of carbon substrates: mechanistic insights, physiological roles, and ecological consequences. *Current Opinion in Microbiology*, 63:172–178, 2021.

[88] Oxford University Press. *Oxford English Dictionary*. Oxford University Press, July 2023.

[89] J. Petersen and S. McLaughlin. *Introduction Growth Media*, 2021. `https://bio.libretexts.org/Courses/North_Carolina_State_University/MB352_General_Microbiology_Laboratory_2021_(Lee)/02%3A_Cultivation_of_Microbes/2.01%3A_Introduction_Growth_Media` [Accessed 16 August 2023].

[90] R. Pickard, T. Lam, G. MacLennan, K. Starr, M. Kilonzo, G. McPherson, K. Gillies, A. McDonald, K. Walton, B. Buckley, C. Glazener, C. Boachie, J. Burr, J. Norrie, L. Vale, A. Grant, and J. N'Dow. Antimicrobial catheters for reduction of symptomatic urinary tract infection in adults requiring short-term catheterisation in hospital: A multicentre randomised controlled trial. *The Lancet*, 380(9857):1927–1935, 2012.

[91] R. Pickard, T. Lam, G. MacLennan, K. Starr, M. Kilonzo, G. McPherson, K. Gillies, A. McDonald, K. Walton, B. Buckley, C. Glazener, C. Boachie, J. Burr, J. Norrie, L. Vale, A. Grant, and J. N'Dow. Types of urethral catheter for reducing symptomatic urinary tract infections in hospitalised adults requiring short-term catheterisation: Multicentre randomised controlled trial and economic evaluation of antimicrobial- and antisepticimpregnated urethral . *Health Technology Assessment*, 16(47), 2012.

[92] S. J. Pirt. *Principles of Microbe and Cell Cultivation*. Blackwell Scientific Publications, Oxford, 1975.

[93] R. Platt, B. F. Polk, B. Murdock, and B. Rosner. Risk factors for nosocomial urinary tract infection. *American Journal of Epidemiology*, 124 (6):977–985, 1986.

[94] A. Pomian, W. Majkusiak, J. Kociszewski, P. Tomasik, E. Horosz, A. Zwierzchowska, W. Lisik, and E. Barcz. Demographic features of female urethra length. *Neurourology and Urodynamics*, 37(5):1751–1756, 2018.

[95] S. Prinjha and A. Chapple. Living with an indwelling urinary catheter. *Nursing Times*, 109(44):12–14, 2013.

[96] I. Raad, W. Costerton, U. Shi Sabharwal, M. Sacilowski, E. Anaissie, and G. P. Bodey. Ultrastructural Analysis of Indwelling Vascular Catheters: A Quantitative Relationship between Luminal Colonization and Duration of Placement. *Journal of Infectious Diseases*, 168(2):400–407, 1993.

[97] M. Ramstedt, I. A. Ribeiro, H. Bujdakova, F. J. Mergulhão, L. Jordao, P. Thomsen, M. Alm, M. Burmølle, T. Vladkova, F. Can, M. Reches, M. Riool, A. Barros, R. L. Reis, E. Meaurio, J. Kikhney, A. Moter, S. A. Zaat, and J. Sjollema. Evaluating Efficacy of Antimicrobial and Antifouling Materials for Urinary Tract Medical Devices: Challenges and Recommendations. *Macromolecular Bioscience*, 19(5):1800384, 2019.

[98] E. Riches. The methods and results of treatment in cases of paralysis of the bladder following spinal injury. *British Journal of Surgery*, 31:135–146, 1943.

[99] S. Saint and B. A. Lipsky. Preventing Catheter-Related Bacteriuria. *Arch Intern Med*, 159(8):800–808, 1999.

[100] J. Saragosti, P. Silberzan, and A. Buguin. Modeling E. coli Tumbles by Rotational Diffusion. Implications for Chemotaxis. *PloS one*, 7(4), 2012.

[101] K. Schumm and T. B. Lam. Types of urethral catheters for management of short-term voiding problems in hospitalised adults: A short version Cochrane review. *Neurourology and Urodynamics*, 27:738–746, 2008.

[102] A. M. Scott, J. Clark, C. Del Mar, and P. Glasziou. Increased fluid intake to prevent urinary tract infections. *British Journal of General Practice*, 70 (692):E200–E207, 2020.

[103] G. Sezonov, D. Joseleau-Petit, and R. D'Ari. Escherichia coli physiology in Luria-Bertani broth. *Journal of Bacteriology*, 189(23):8746–8749, 2007.

[104] Y. Shen, A. Siryaporn, S. Lecuyer, Z. Gitai, and H. A. Stone. Flow directs surface-attached bacteria to twitch upstream. *Biophysical Journal*, 103(1): 146–151, 2012.

[105] D. M. Sievert, P. Ricks, J. R. Edwards, A. Schneider, J. Patel, A. Srinivasan, A. Kallen, B. Limbago, and S. K. Fridkin. Antimicrobial-Resistant Pathogens Associated with Healthcare-Associated Infections Summary of Data Reported to the National Healthcare Safety Network at the Centers for Disease Control and Prevention, 2009–2010. *Infection Control & Hospital Epidemiology*, 34(1):1–14, 2013.

[106] U. Simunič, P. Pipp, M. Dular, and D. Stopar. The limitations of hydrodynamic removal of biofilms from the dead-ends in a model drinking water distribution system. *Water Research*, 178:115838, 2020.

[107] P. Singha, J. Locklin, and H. Handa. A review of the recent advances in antimicrobial coatings for urinary catheters. *Acta Biomaterialia*, 50:20–40, 2017.

[108] S. W. Smye. The physics of physik. *Journal of the Royal College of Physicians of Edinburgh*, 48(1):3–8, 2018.

[109] S. E. Spagnolie and E. Lauga. Hydrodynamics of self-propulsion near a boundary: predictions and accuracy of far-field approximations. *Journal of Fluid Mechanics*, 700:105–147, 2012.

[110] W. E. Stamm. Catheter-associated urinary tract infections: Epidemiology, pathogenesis, and prevention. *The American Journal of Medicine*, 91(3B): S65–S71, 1991.

[111] D. J. Stickler. Bacterial biofilms in patients with indwelling urinary catheters. *Nature Clinical Practice Urology*, 5(11):598–608, 2008.

[112] G. I. Taylor. Dispersion of soluble matter in solvent flowing slowly through a tube. *Proceedings of the Royal Society of London. Series A. Mathematical and Physical Sciences*, 219(1137):186–203, 1953.

[113] S. Tenny and S. W. Boktor. *Incidence*. StatPearls Publishing, 2023. `https://www.ncbi.nlm.nih.gov/books/NBK430746/` [Accessed 17 August 2023].

[114] B. W. Trautner and L. Grigoryan. Approach to a positive urine culture in a patient without urinary symptoms. *Infectious Disease Clinics of North America*, 28(1):15–31, 2014.

[115] C. A. Umscheid, M. D. Mitchell, J. A. Doshi, R. K. Agarwal, K. Williams, and P. J. Brennan. Estimating the Proportion of Healthcare-Associated Infections That Are Reasonably Preventable and the Related Mortality and Costs. *Infection Control & Hospital Epidemiology*, 32(2):101–114, 2011.

[116] F. V. van Daalen, J. M. Prins, B. C. Opmeer, M. A. Boermeester, C. E. Visser, R. M. van Hest, J. Branger, E. Mattsson, M. F. van de Broek, T. C. Roeleveld, A. A. Karimbeg, E. A. Haak, H. C. van den Hout, M. A. van Agtmael, M. E. Hulscher, and S. E. Geerlings. Effect of an antibiotic checklist on length of hospital stay and appropriate antibiotic use in adult patients treated with intravenous antibiotics: a stepped wedge cluster randomized trial. *Clinical Microbiology and Infection*, 23(7):485.e1–485.e8, 2017.

[117] W. van Saarloos. Front propagation into unstable states. *Physics Reports*, 386:29–222, 2003.

[118] S. Vogel. *Life in Moving Fluids*. Princeton University Press, Princeton, 2nd edition, 1994.

[119] M. Von Smoluchowski. Versucheiner Mathematischen Theorie der Koagulations Kinetic Kolloider Lousungen. *Z. Phys. Chem.*, 92:129–168, 1917.

[120] J. N. Walker, A. L. Flores-Mireles, C. L. Pinkner, H. L. Schreiber, M. S. Joens, A. M. Park, A. M. Potretzke, T. M. Bauman, J. S. Pinkner, J. A. Fitzpatrick, A. Desai, M. G. Caparon, and S. J. Hultgren. Catheterization alters bladder ecology to potentiate Staphylococcus aureus infection of the urinary tract. *Proceedings of the National Academy of Sciences of the United States of America*, 114(41):E8721–E8730, 2017.

[121] L. Wang, S. Zhang, R. Keatch, G. Corner, G. Nabi, S. Murdoch, F. Davidson, and Q. Zhao. In-vitro antibacterial and anti-encrustation performance of silver-polytetrafluoroethylene nanocomposite coated urinary catheters. *Journal of Hospital Infection*, 103(1):55–63, 2019.

[122] X. Wang, K. Xia, X. Yang, and C. Tang. Growth strategy of microbes on mixed carbon sources. *Nature Communications*, 10(1):1–7, 2019.

[123] J. W. Warren. Catheter-Associated Urinary Tract Infections. *International Journal of Antimicrobial Agents*, 17:299–303, 2001.

[124] S. A. Wilks, M. J. Fader, and C. W. Keevil. Novel insights into the proteus mirabilis crystalline biofilm using real-time imaging. *PLoS ONE*, 10(10): 1–13, 2015.

[125] S. A. Wilks, V. V. Koerfer, J. A. Prieto, M. Fader, and C. W. Keevil. Biofilm Development on Urinary Catheters Promotes the Appearance of Viable but Nonculturable Bacteria. *mBio*, 12(2):03584–20, 2021.

[126] O. Witt-Hansen. *Solution to the diffusion equation*, 2018. `http://www.olewitthansen.dk/Physics/The_diffusion_equation.pdf` [Accessed 13 January 2020].

[127] S. Zhang, L. Wang, X. Liang, J. Vorstius, R. Keatch, G. Corner, G. Nabi, F. Davidson, G. M. Gadd, and Q. Zhao. Enhanced Antibacterial and Antiadhesive Activities of Silver-PTFE Nanocomposite Coating for Urinary Catheters. *ACS Biomaterials Science and Engineering*, 5:2804–2814, 2019.

[128] E. Zimlichman, D. Henderson, O. Tamir, C. Franz, P. Song, C. K. Yamin, C. Keohane, C. R. Denham, and D. W. Bates. Health care-associated infections: A Meta-analysis of costs and financial impact on the US health care system. *JAMA Internal Medicine*, 173(22):2039–2046, 2013.